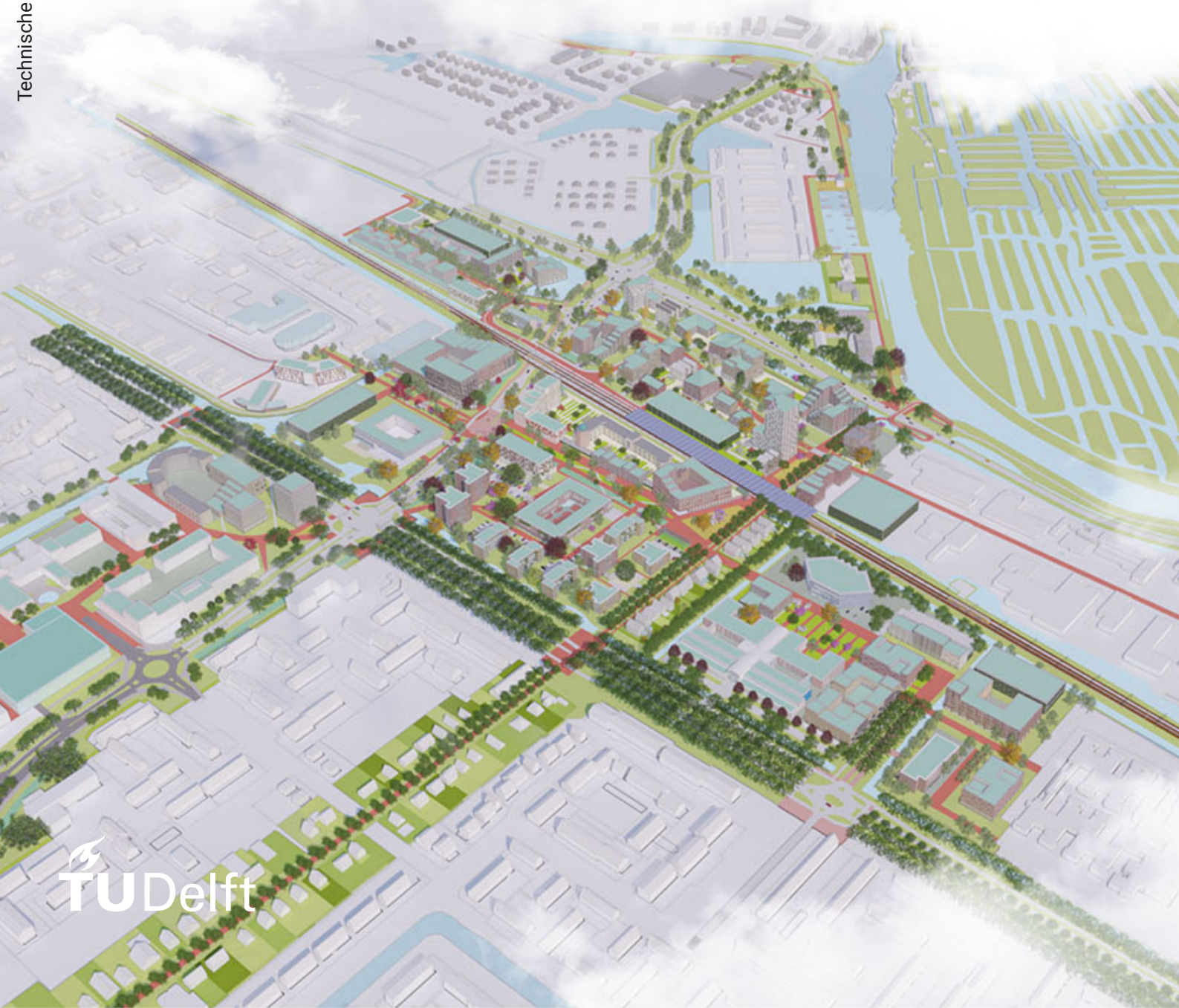# Thermal Energy Storage for District Heating

Feasibility assessment for the implementation of TES systems in various DHN cases

R.G.M. Perik

TUDelft

Thermal Energy Storage for District Heating

Feasibility assessment for the implementation of TES systems in various DHN cases

by

R.G.M. Perik

in partial fulfillment of the requirements for the degree of

Master of Science
in Mechanical Engineering

at the Delft University of Technology,
to be defended publicly on 27 May 2021 2:30 PM

Student number: 4331540
Thesis committee: Dr. ir. C. A. Infante Ferreira   TU Delft, supervisor
                   Dr. ir. I. W. M. Pothof   TU Delft
                   Prof. dr. ir. T. J. H. Vlugt   TU Delft
                   Ir. A. Ganesan   Resourcefully, supervisor

An electronic version of this thesis is available at `http://repository.tudelft.nl/`.

TUDelft

Abstract

Of the global energy demand, 20% can be allocated to residential energy demand. Most of this energy is produced by fossil fuels, which raises the importance of energy production in a more sustainable way. In order to do this on the level of residential heating applications, the Dutch government aims to make its residential neighborhoods natural gas-free.

An often considered solution is making residential areas all-electric. However, when considering the heating of these households based on electricity, high peaks may occur in the electricity grid due to simultaneous heating at times of high demand. This could cause problems regarding the capacity of the electricity grid. Subsequently, the generation of electricity is nowadays associated with relatively high CO_2 emissions, raising the awareness for alternative methods of heating. One of these methods is district heating coupled to (more) sustainable energy sources. A problem occurring with this combination is a possible discrepancy between the supply and demand of energy. Therefore, it could be beneficial to implement thermal energy storage in district heating.

This research assesses the feasibility of different configurations of thermal energy storage integrated into district heating. For this research, a case study is conducted in which district heating for a residential area coupled with thermal energy storage is modeled. The model is based on the thermodynamic equilibrium of the network and is able to compute the required characteristics and key performance indicators of the district heating network. For the case study, multiple scenarios have been created which assess different distribution characteristics and heat sources. For reference, an all-electric scenario has been designed as well.

The results of the case study show that the implementation of thermal energy storage in district heating is able to lower peak loads on the heat source by two-thirds. This implementation goes paired with an increase in levelized cost of energy of 10-16% and 8-73% higher CO_2 emissions, compared to district heating without storage and depending on the characteristics of the district heating net and its heat source. However, for certain heat sources, the advantages of thermal energy storage outweigh the drawbacks or thermal energy storage might even be considered to be inevitable. This is especially the case for renewable heat sources, of which its share in the future energy market is considered to be substantial. Also, the results show that every scenario considering district heating performs better on levelized cost of energy and CO_2 emissions than the all-electric scenario. When designing new DH projects, it is key that different available heat sources will be considered and that an accurate trade-off is made between the advantages and drawbacks of thermal energy storage.

This research is based on the comparison of various scenarios for a case study. Therefore, it does not focus on finding the optimal parameters for either district heating or thermal energy storage. For finding these optimal parameters, future research must be conducted.

Acknowledgements

I would like to express my gratitude to my supervisor, Carlos Infante Ferreira, for his support during the process of writing this thesis. You helped me remain focused, while granting me the freedom to work independently and manage my project autonomously. I am particularly grateful for the way in which you allowed me to 'check in' when needed, to discuss various issues and topics.

Also, I would like to thank everyone at Resourcefully for their input and cooperation, as well as for the open and positive environment that was made present in which I could write my thesis. Special thanks go out to Hugo Niesing for the opportunity of conducting my research at Resourcefully and Avi Ganesan for his supervision and support.

Finally, I would like to thank my friends, family and my girlfriend, whose support, feedback and positivity could not have been missed during the time spent on this thesis.

R.G.M. Perik
Delft, May 2020

Contents

Nomenclature

Roman Symbols

A	Area	(m^2)
A_c	Cross section area	(m^2)
C	Costs	$(€)$
c_p	Specific heat capacity	$\left(\frac{J}{kgK}\right)$
d	Diameter	(m)
E_p	Electrical pumping energy	(Wh/m^3)
f	Darcy-Weisbach friction factor	$(-)$
G_c	Gas consumption	(kg)
G	Irradiance	(W/m^2)
g	Gravity constant	(m/s^2)
g_{sol}	Thermal transmittance	$(-)$
H	Pressure head	(m)
h	Height	(m)
K_L	Minor loss coefficient	$(-)$
L	Length	(m)
m	Mass	(kg)
$\dot{m}$	Mass flow	$\left(\frac{kg}{s}\right)$
n	Number, Lifetime	$(-),(yr.)$
P	Power	(J/s)
p	Pressure	(Pa)
Q	Heat, Energy	$(J),(kWh)$
$\dot{Q}$	Heat flow	(W)
r	Radius, Discount rate	$(m),(-)$
Re	Reynolds number	$(-)$
T	Temperature	(K)
t	Time	(s)
U	Heat transfer coefficient	$\left(\frac{W}{m^2K}\right)$
v	Velocity	$\left(\frac{m}{s}\right)$
V	Volume	(m^3)
$\dot{V}$	Volume flow	$\left(\frac{m^3}{s}\right)$
W_c	Electric power consumption	(kWh)
z	Axial coordinate	(m)

Greek Symbols

α	Thermal diffusivity	$\left(\frac{m^2}{s}\right)$
Δ	Difference	$(-)$
ϵ	Wall roughness	(m)
η	Efficiency	$(-)$
κ	Thermal conductivity	$\left(\frac{W}{mK}\right)$
μ	Dynamic viscosity	$\left(\frac{Ns}{m^2}\right)$
ϕ	Porosity	$(-)$
ρ	Density	$\left(\frac{kg}{m^3}\right)$
σ	Deviation	$(-)$

Subscripts

aq	Aquifer
b	Direct
C	Cold
calc	Calculated
cond	Condenser
cons	Consumer
cool	Cooling
d	Diffuse
dem	Demand
el	Electric
emotor	Electric Motor
est	Estimated
evap	Evaporator
ext	External
f	Final
H	Hot
heat	Heating
hl	Heat losses
i	Initial
in	Inlet
max	Maximum
melt	Melting
min	Minimum
out	Outlet
po	Pore
prim	Primary
rel	Relative
ret	Return
s	Soil
sec	Secondary
sim	Simulink
sol	Solar
sup	Supply
t	At time t
th	Thermal
tot	Total
w	Water

Superscripts

E	East
N	North
S	South
W	West

Acronyms

ATES	Aquifer Thermal Energy Storage
BTES	Borehole Thermal Energy Storage
CAPEX	Capital Expenditures
COP	Coefficient of Performance
DC	District Cooling
DH	District Heating
DHC	District Heating and Cooling Systems
DHN	District Heating Network

DHW   Domestic Hot Water
DN   Diameter Nominal
HDD   Heating Degree Day
HEX   Heat Exchanger
HHV   Higher Heating Value
HP   Heat Pump
HTF   Heat Transfer Fluid
HTS   Heat Transfer Station
KPI   Key Performance Indicator
LCOE   Levelized Cost of Energy
MT   Medium Temperature
MTDH   Medium Temperature District Heating
OPEX   Operating Expenditures
P&ID   Process & Instrumentation Diagram
PCM   Phase Change Material
PE   Polyethylene
PTES   Pit Thermal Energy Storage
PUR   Polyurethane
PVGIS   Photovoltaic Geographical Information System
RES   Renewable Energy Sources
RMS   Root-mean-square
TES   Thermal Energy Storage
TRL   Technology Readiness Level
TTES   Tank Thermal Energy Storage
ULT   Ultra Low Temperature
ULTDH   Ultra Low Temperature District Heating
WGTES   Water-Gravel Thermal Energy Storage

1

Introduction

1.1. Background

One of the biggest challenges of this century is addressing climate change. Due to strong economic growth, urbanization and rapid population growth, the global energy demand is ever-growing. This demand can be distinguished into four sectors: industrial, transportation, commercial and residential. In 2017 the global residential energy demand accounted for 20% of the total global energy demand. The major share of the global residential energy demand is taken up by district heating and cooling systems (DHC), which accounted for 52% [34]. Because of this high contribution, DHC is a most promising field where a lot of improvement can be gained regarding sustainability.
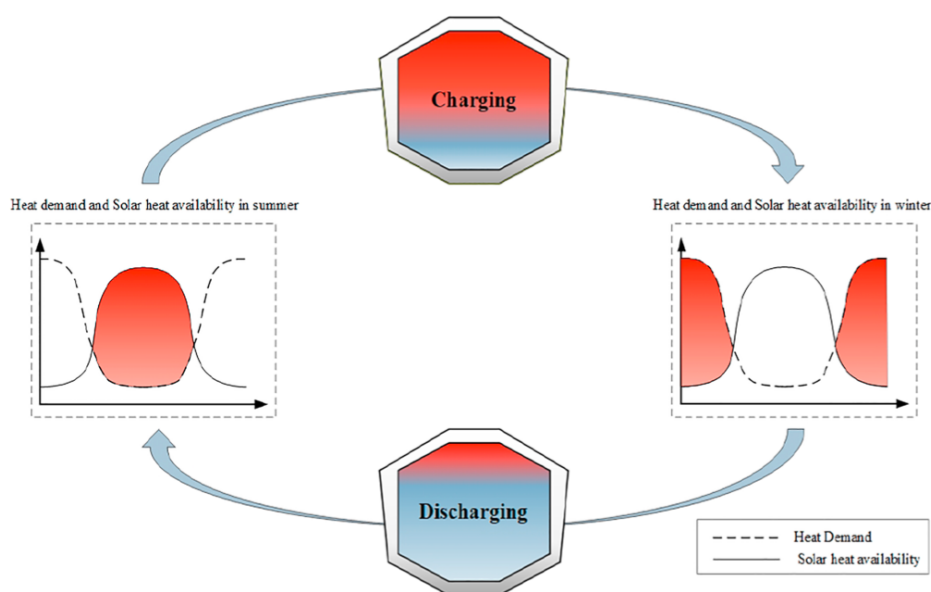
Figure 1.1: The role and cycle of a seasonal thermal energy storage in a solar-assisted district heating system with exemplary load duration curves [20]

As the global energy demand is growing and most of the energy is produced by fossil fuels, it is of utmost importance that energy production is performed in a more sustainable way. A way to do this, is by implementing renewable energy sources such as solar, wind and tidal energy. An issue that accompanies these renewable energy sources, is a discrepancy between the demand and supply of energy, particularly when district heating (DH) is considered. An example in which the disparities on a seasonal basis are clearly illustrated is shown in Figure 1.1. Here, solar energy is used for the production of heat for DH. During summer, a lot of solar energy can be obtained, but the demand for heat is low. During winter, the opposite occurs and there is a lot of de-

mand for heat but not enough solar energy. The same kind of discrepancy occurs on a daily basis. An energy storage system could align these disparities in time and could be the key to the efficient usage of renewable energy. Such a storage system could consist of a short and long (seasonal) term storage, depending on the situation. Well known types of storing energy are mechanical, electrical, (electro)chemical and thermal energy storage (TES). For DHC applications, TES, which temporarily stores energy in the form of heat, is particularly advantageous due to its high storage capacity, (dis)charging flexibility and relatively easy conversion of energy [27]. If storage is done in a sufficient way, the surplus and deficit problem can be averted due to charging and discharging the storage system at the right time, as can be seen for seasonal thermal energy storage in Figure 1.1.

1.2. Relevance

In order to comply to the Paris Agreement, the Dutch government aims to make its residential neighbourhoods natural gas free. An often considered solution is making residential areas all-electric. However, when considering the heating of these households based on electricity, high peaks may occur in the electricity grid due to simultaneous heating and/or cooling at certain times. This could cause problems regarding the capacity of the electricity grid. Therefore, it is favourable to consider an alternative energy source for DHC.

A possible solution to this problem could be DH with integrated TES. Guelpa and Verda [27] assess the implementation of TES in DHC. They argue that it is not possible to identify unique best solutions for thermal storage related to DHC, because DHC may be characterized by a variety of configurations. Therefore, they advise that further research activities should be conducted in different directions for various storage technologies. They also state that future studies should focus on making long-term (seasonal) TES more suited for installations in residential areas in order to increase the feasibility of installing them combined with DHC.

1.3. Research objectives

The aim of this research is to asses the feasibility of different configurations of a TES system integrated in DH. For this research, a case study will be done, in which a model will be designed, capable of computing the required characteristics and key performance indicators of TES integrated DH for (semi)detached houses and apartment buildings in an area of the municipality Heerhugowaard in the Netherlands. A visualisation of the case study area is shown on the cover page, adapted from Kuiper Compagnons [39]. This residential area is going to be connected to medium and/or ultra low temperature heat networks and may have several HPs installed. To find out what setup is most feasible for specific situations, the model has to be capable of defining pros and cons of various configurations of the implementation of a TES system in DH. With the outcome of the case study, a conclusion can be drawn for the implementation of TES systems for the use of DH. For comparison, a reference solution will be used where no DH is present in the case study, but where the heat demand of the households will be met by individual HPs.

The main objective of this research, which covers the scope for the case study and its model, is formulated as follows:

> ***"What is the influence of TES systems on the feasibility of new DH projects for residential heating applications?"***

To answer the main research objective, above mentioned case study will be conducted. During this case study, various sub-research objectives must be accounted for to ensure a coherent framework. These sub-research objectives are:

- What are important characteristics of DH and how can this be modeled?
- What are important characteristics of TES and how can this be modeled?
- How can TES be implemented in DH in dense urban areas, and what influences can this have?
- What is the influence of TES integrated DH on the levelized cost of energy, CO_2 emissions and the surrounding infrastructure of residential heating applications, and how does it compare to other solutions?

1.4. Methodology

To be able to answer the research question, a model was designed for the case study, which is able to assess the feasibility of the different heating scenarios.

In order to develop this model, a literature study was conducted to find out the most important characteristics and modeling techniques of DH and TES, as well as its key performance indicators (KPIs). Subsequently, the characteristics of the case study area were assessed, which led to the design of various DH scenarios, as well as a reference scenario.

Thereafter, the model was built in Matlab & Simulink [64], in which it was able to simulate the thermodynamic behaviour of the different case study scenarios on an hourly basis. The model was designed as a modular model, where each component of the scenario is modeled as a stand-alone component. This way, changes in the grid can easily be administered. After the model has simulated the different scenarios, the influence of TES systems on the feasibility of new DH projects for residential heating applications was determined through a comparison of the found results.

1.5. Thesis outline

- Chapter 2 contains a literature review, providing an overview of the related theory about DH and TES

- Chapter 3 contains information about the case study area and the different scenarios employed in the study

- Chapter 4 contains the framework of the model, explaining how the model is designed and which equations have been used

- Chapter 5 presents the main results of the simulations together with its discussion

- Chapter 6 presents the conclusions and recommendations of this study

2

State of the art

In this chapter the state of the art of DHC and TES will be discussed, as well as various ways on how to model these systems. Also, the implementation of TES in DHC applications and its KPI's will be treated. Finally, a reference solution of the research question, to which the KPIs can be compared, will be clarified.

2.1. District heating and cooling systems

DHC provide efficient heating and cooling, mostly in urban areas, by using a heat distribution network of pipes. DH is effective for CO_2 reduction and district cooling (DC) is becoming more relevant due to a rising cooling demand as a result of global warming. In working principles, there is not much difference between DH and DC. The only main difference is the temperature of the distribution medium, which for DC applications is under 10°C, while that of DH is much higher. District heating networks (DHNs) have been commercially used since 1880. Over the years, a lot has changed regarding DHC. The evolution of DHC can be classified in different generations, which are addressed in Section 2.1.2.

2.1.1. Working principles of DHC

DHC can be seen as a thermal distribution network of pipes filled with a heat transfer fluid, which is often water. In this network, mass flow is being controlled by pumps and valves, while extraction or supply of heat is maintained by the use of so-called agents. Agents use heat exchangers (HEXs) to extract or supply heat to the system. According to Sommer et al. [58], these agents can be divided into the following categories:

- Consumer (demand side): the main task of a consumer is to cover the heating or cooling demand in the network. Examples of consumers are: buildings with a heating demand in winter and cooling demand in summer and data centers with a cooling demand. When energy is supplied to the network due to a cooling demand, this is described as waste heat.

- Plant (supply side): the main task of a plant is to balance energy flows, often responsible for the supply of heat in the system. A plant has no demand itself, but equalises the energy balance of the network. For example, when a network is dominated by a demand for heat, the heat is supplied by a plant and vice versa.

- Storage: the main task of a storage agent is to comply with the mismatch between heat supply and demand over time, while not contributing to the energy balance itself. In other words, the energy contained in a storage agent is considered inside of the network. An example of a storage agent is a TES system.

2.1.2. Generations of DHC

The evolution of DHC can be categorised in different generations. This section addresses the different generations and its characteristics, provided by Lund et al. [42] and Sommer et al. [58]. Figure 2.1 shows an illustration of the evolution of these generations. To ensure a good design of the DHN in the case study, it is key to understand the previous, current and future challenges and characteristics.
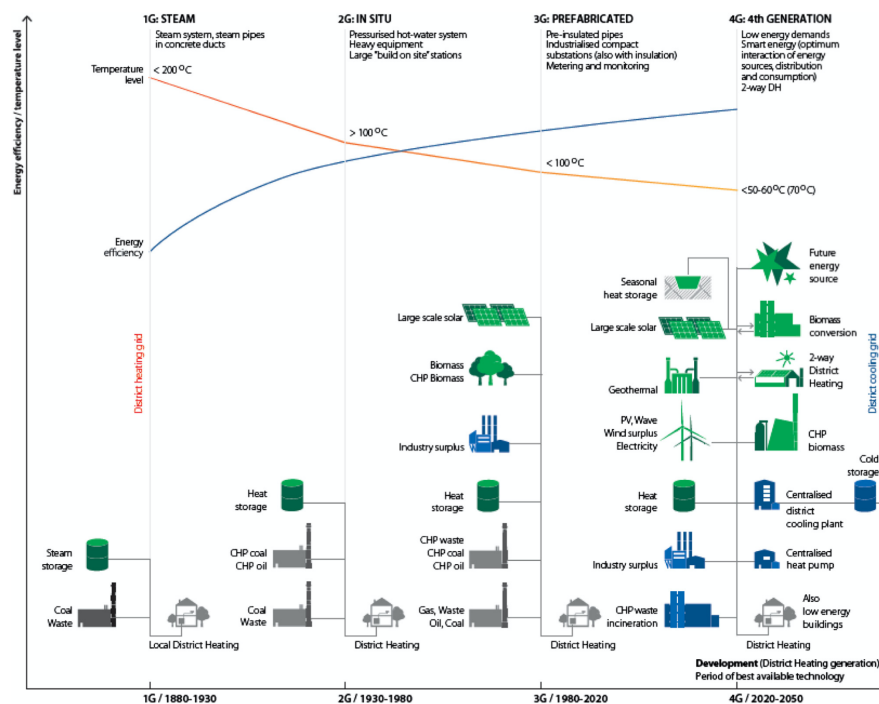
5

Figure 2.1: Illustration of the evolution of different generations of DHC [42]

In 1880, the first commercial DHN was introduced in the USA. This commenced the first generation of DH, which used steam as a heat carrier. These DHNs often consisted of steam pipes embedded in concrete ducts, steam traps and compensators. The distribution of steam was done at very high temperatures ($T > 200°C$), which was accompanied by high heat losses and dangerous, occasionally deadly, steam explosions. Even though after 1930 a new generation of DH arose, steam is still used as a heat carrier in some old parts in the center of New York and Paris.

The second generation of DH emerged in the 1930's and dominated until 1970. This new generation employed pressurised hot water ($T > 100°C$) as a distribution medium instead of steam. Although it was less dangerous, high heat losses still occurred. These DHNs often consisted of water pipes embedded in concrete ducts, large tube-and-shell HEXs and large control valves.

After 1970, in an attempt to reduce heat losses, the third generation of DH dominated the market. In these DHNs, pressurised hot water was still used as the distribution medium, but at a lower temperature ($T < 100°C$). The distribution pipes were typically pre-fabricated and insulated to reduce heat losses and manpower requirements at construction sites. Other components used, typical for this generation of DH, are substations using plate stainless steel HEXs. Also, a focus was brought on lean material components.

Since 2014, a shift is occurring, in which the fourth generation of DH is being applied. This generation is characterised by its search for sustainable heat sources and smart thermal grid. Water is still used as the distribution medium, but again at a lower temperature ($35 < T < 70°C$). The domestic hot water (DHW) is kept around 65°C to minimise legionella. The rest of the network is quite similar to the third generation of DH, in which the same kind of pipes and HEXs are used.

Because the demand for cooling is rising, the next, fifth, generation of DH must also account directly for cooling, identifying this generation as DHC. Some of these thermal grids have already been built. In this new generation, water is still the basis of the heat distribution. The operational temperature of the grid is lowered again, preferably close to the ground temperature. In combination with HPs, the heat demand is still matched as well as keeping the possibility for cooling. Another characteristic of this generation is the use of bidirectional networks or reservoir networks, with storage units applied.

2.2. Modeling of DH

The modeling of DH is based on the hydraulic and thermal balance of the system. This section will appoint the aspects of the hydraulic and thermal equilibrium, provided by Sarbu et al. [57], as well as modeling methods and numerical approaches which can be used, provided by Talebi et al. [62] and Arsene et al. [3].

2.2.1. Hydraulic equilibrium

DH relies on the principle of distributing a heated fluid in a district network. This network can be described by different nodes and branches, which represent the network. For each node in this system, mass conservation can be composed as shown in Equation 2.1. Here, ρ_{in} [kg/m^3] and ρ_{out} [kg/m^3] are the densities of the water and $\dot{V}_{in}$ [m^3/s] and $\dot{V}_{out}$ [m^3/s] are the volume flows entering and exiting the node from upstream and downstream branches respectively. Because the transported water in the DHN can be seen as an incompressible fluid, the density remains the same. Therefore, the mass conservation can be written as in Equation 2.2. Here, $\dot{V}_{ext}$ [m^3/s] is the volume flow that exits or enters the network through the node. When a closed system is taken into account, $\dot{V}_{ext}$ is considered to be zero. However, in the case for open networks such as district heating, $\dot{V}_{ext}$ is defined as positive when a volume flow enters the system and negative when a volume flow exits the system.

$$\sum \rho_{in}\dot{V}_{in} = \sum \rho_{out}\dot{V}_{out} \tag{2.1}$$

$$\sum \dot{V}_{in} - \sum \dot{V}_{out} - \sum \dot{V}_{ext} = 0 \tag{2.2}$$

The pressure balance between any two nodes is shown in Equation 2.3. Here, p_i [Pa] and p_j [Pa] are the up- and downstream pressures at nodes i and j respectively and Δp_{ij} [Pa] is the pressure drop in between.

$$\Delta p_{ij} - (p_i - p_j) = 0 \tag{2.3}$$

The pressure drop Δp_{ij} can be caused by various types of pressure losses. Frictional losses generally play a big part, which occur when friction between the moving fluid and the pipes is present. Another type of losses is called minor losses and occur due to pipe fittings and appurtenances which affect the streamlines of the moving fluid. Other losses that might occur are gravitational losses and acceleration losses. The pressure drop Δp_{ij} can be described as Equation 2.4. Here, ρ [kg/m^3] is the moving fluids density, f_{ij} [-] is the Darcy-Weisbach friction factor, L_{ij} [m] is length of the pipe, d_{ij} [m] the inner diameter of the pipe, K_L [-] is the minor loss coefficient of the pipe and $\dot{V}_{ij}$ [m^3/s] is the volume flow through the pipe.

$$\Delta p_{ij} = \frac{8\rho}{\pi^2}\left(\frac{f_{ij}L_{ij}}{d_{ij}} + K_L\right)\frac{\dot{V}_{ij}^2}{d_{ij}^4} \tag{2.4}$$

With the hydraulic equilibrium approach, it is possible to determine the water pressure losses, the pressure and flow distribution in the network and the design criteria needed for pumping equipment. Figure 2.2 shows a visualisation for this approach for a small part of a pipe network, consisting of three branches connected by four nodes, $i-1, i, i+1$ and j, each with its hydraulic and thermal parameters. The heat loss to the surroundings $\dot{Q}_{hl}$ is also shown. This heat loss and the thermal balance will be addressed in the next section.
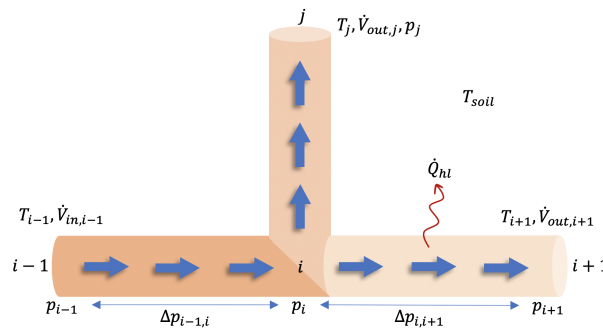

Figure 2.2: Hydraulic equilibrium in a small part of a pipe network

2.2.2. Thermal equilibrium

The thermal equilibrium of a DHN relies on the following heat balance equations. The first equation, shown in Equation 2.5, describes the energy supplied to the DHN. Here, $\dot{Q}_{sup}$ [W] is the required heat rate that must be supplied to the system to meet the demand heat rate $\dot{Q}_{dem}$ [W], while also accounting for heat losses $\dot{Q}_{hl,prim}$ [W] and $\dot{Q}_{hl,sec}$ [W] in the primary and secondary networks respectively.

$$\dot{Q}_{sup} = \dot{Q}_{dem} + \dot{Q}_{hl,prim} + \dot{Q}_{hl,sec} \tag{2.5}$$

To minimize heat losses, the distribution pipes of DHN often consist of three layers. According to van Miltenburg [68], the most commonly used pipe consists of an inner pipe made of steel, covered in a layer of polyurethane (PUR) to minimise heat loss, which in turn is covered in a layer of polyethylene (PE) for protection. A cross-section of this pipe lay-out can be seen in Figure 2.3, where $d_{i,steel}$ [m], $d_{i,PUR}$ [m] and $d_{i,PE}$ [m] are the respective inner diameters of the layers, $U_{overall}$ [W/m^{2}K] is the overall heat transfer coefficient of the pipe and T_w [K] and T_{soil} [K] are the temperatures of the distributed water and soil, respectively. The heat losses $\dot{Q}_{hl}$ [W] from the distributed water to the surrounding soil can be estimated by Equation 2.6.

$$\dot{Q}_{hl} = U_{overall} A (T_w - T_{soil}) \tag{2.6}$$
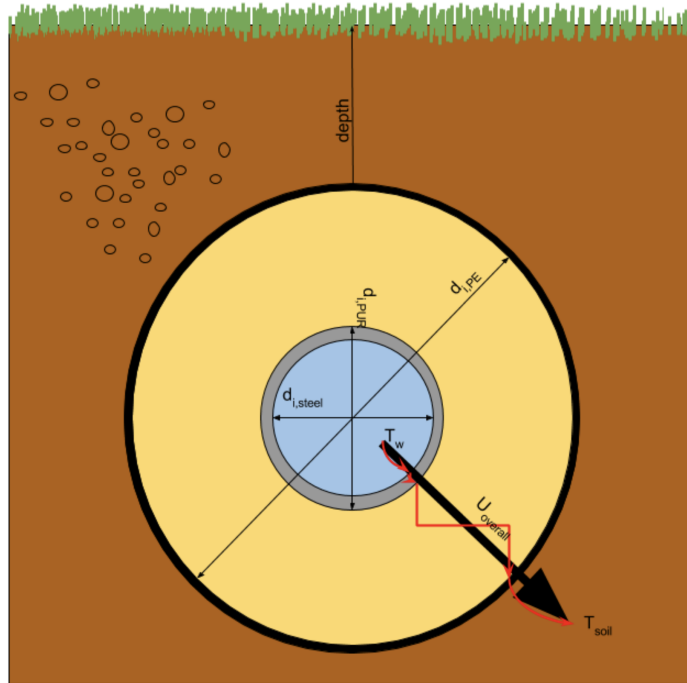
Figure 2.3: Cross section of a Steel-PUR-PE pipe, with its respective diameters, overall heat transfer coefficient U and temperatures of the water and soil [68]

Alternatively, flexible pipes can be used instead of steel. According to ISSO Publication 7 [35], flexible plastic pipes permit higher flow velocities and are particularly suitable for medium to lower temperatures due to the lifetime of the plastic, which makes them interesting for new generations of DHC. The inner pipe often consists of either PE or polybutene, enclosed by an insulation layer and in turn covered in a layer of PE for protection. Thermaflex [66], a supplier of these kind of pipes, provides heat loss factors per unit length in regard to the supply temperature of medium. Using these heat loss factors simplifies the calculation of the heat loss to the surroundings.

2.2.3. Modeling methods

According to Talebi et al. [62], holistic modeling of DHNs can either be done in physical or black-box models. In black-box models, the network is seen as one unit, where specific aspects of components are not considered but the whole system is approached by the use of a transfer function or an artificial neural network. In a physical model, each component of the DHN is approached independently and a set of equations is used to describe the flows and pressure losses in that component.

Arsene et al. [3] categorized physical modeling of looped heating networks in four methods:

1. *Link flow method*, where the unknowns of the method are the pipe flow rates ($\dot{V}$).
2. *Loop corrective flow method*, where the unknowns are the loop corrective flow rates ($\Delta\dot{V}$).
3. *Nodal heads method*, where the unknown are the pressure heads in the nodes (H).
4. *Mixed node-loop method*, where the unknowns are a mix of the above mentioned parameters.

Physical modeling of DH takes a lot of elements into consideration, which makes it computationally hard to solve. To decrease the workload in this kind of modeling, iterative numerical methods have been developed. Arsene et al. [3] listed the following methods:

1. *Numerical minimization methods*, which find the minimum value of the non-linear function subjected to linear equality and in-equality constraints.
2. *The Hardy-Cross method*, which solves a system of non-linear equations based on systematic approximations and subsequent corrections.
3. *The Newton-Raphson method*, which solves a system of non-linear equations by finding roots of a real-valued function, with increasingly better approximations.
4. *The linear theory method*, which solves a system of non-linear equations by successively linearizing the solution until the true solution is found.

Bhave [5] compared the Hardy-Cross method, Newton-Raphson method and linear theory method on various items, which can be seen in Figure 2.4. The Hardy-Cross method is considered to be less complex, but might need a lot of iterations before it is able to converge. Although the Newton-Raphson method is able to converge within fewer iterations, the iterations are more complex to solve due to more calculations per iteration and thus uses a lot more computational power. Moosavian and Jaefarzadeh [46] state that, depending on the size and complexity of the system of non-linear equations, the Hardy-Cross method may even require too much iterations to converge. According to Nielsen [48], the Newton-Raphson method requires a good initial vector for fast convergence, while the linear theory method oscillates near the true solution. A good solution can be a combination of both, where the linear theory method is used for the first iteration step, after which the Newton-Raphson method is used to converge to adequate accuracy within few iterations.

Sl. No.	Item	Hardy Cross method based on		Newton-Raphson method based on		Linear theory method based on	
		Balancing heads	Balancing flows	Nodal heads	Loops	Pipe discharges	Nodal heads (finite element method)
1.	Unknown parameters and equations used	$\Delta\dot{V}$	ΔH	H	$\Delta\dot{V}$	$\dot{V}$	H
2.	Number of unknowns	Minimum	Medium	Medium	Minimum	Maximum	Medium
3.	Initialisation	Necessary				Not Necessary	
4.	Mode of analysis	Analysis in parts, considers one loop or node at a time.		Analysis as a whole, all loops or nodes are considered simultaneously.			
5.	Suitability for hand calculation	Suitable, networks with several nodes can be analysed if sufficient time and manpower are available.		Not suitable except for small networks.			
6.	Number of iterations	Usually large.		Small and usually not more than 10			
7.	Effect of network size on the number of iterations	Increases as the size of the network increases.		Generally independent of the size of the network.			
8.	Time per iteration	Small		Large			
9.	Effect of network size on time per iteration	Increase gradually as the size of the network increases.		Increases rapidly as the size of the network increases.			
10.	Problem of convergence	May be present.			Reported to be absent.		
11.	Computer storage capacity requirement	Small and increases gradually with the size of the network.		Large and increases rapidly with the size of the network.			

Note : $\Delta\dot{V}$ - Correction to flow
ΔH - Correction to pressure head

Figure 2.4: Comparison of numerical methods for network analysis [5]

Talebi et al. [62] suggest the combination of the Newton-Raphson method and nodal heads method, due to the simplicity of the input data, the number of equations and accurate results. However, when using the nodal heads method for networks with a low volume flow, weak convergence is a problem. Therefore, Arsene et al. [3] suggest using the Newton-Raphson method together with the loop corrective flow method in this case.

In order to optimize DH, different methods can be used to minimize heat losses, construction costs and operation costs. These optimization methods can be distinguished in two categories: deterministic optimization methods, based on the analytical computation of a function gradient and/or its assessments, and heuristic optimization methods, which are based on investigative research and/or on artificial intelligence. Deterministic optimization methods are able to identify the accurate optimal solution, but often converge to local optimal solutions. However, this optimisation method can be complicated due to the dependence on the computation of derivatives. Heuristic methods often include genetic algorithms which do not depend on linearity, convexity and derivatives of the objective function. However, these kind of algorithms can be characterised by very long calculation times.

2.3. Thermal energy storage

TES systems are used to store energy in thermal form, that can later be used under varying conditions. According to Cabeza [9], TES is mainly used to overcome the mismatch between energy generation and energy use. In TES, a complete storage cycle is characterized by three steps: charge, storage and discharge. Cabeza [9] also states that in practical systems, the mentioned steps may occur simultaneously and can happen more than once in each storage cycle. According to Pilkington Solar International GmbH [52], TES can be classified by concepts and mechanisms. The following sections will address these concepts and mechanisms.

2.3.1. Storage concepts

Cabeza et al. [10] explain that TES systems can be classified as either active or passive systems. An active TES system is characterized by forced convection heat transfer into the storage material. This can be in the form of a direct system, where a heat transfer fluid (HTF) serves as a storage medium, or in the form of an indirect system, where another medium is used for storage. A passive TES system is usually a dual-medium store, where the HTF passes through the store to carry energy to and from a storage medium. A scheme of this classification is illustrated in Figure 2.5.
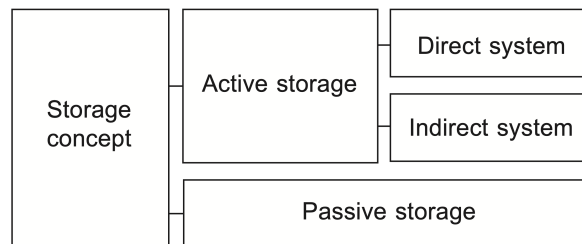

Figure 2.5: Scheme of classification of different storage systems according to the storage concept [10]

2.3.2. Storage mechanisms

TES can be distinguished in three mechanisms: chemical (sorption), latent heat and sensible heat storage. The working principles of chemical, latent and sensible storage systems are shown below in Figure 2.6. Chemical storage uses chemical reactions to store heat. Latent heat storage uses the phase transition of a medium at a specific temperature to store heat, for example at T_{melt} [K] in Figure 2.6. In sensible heat storage, energy is stored in a medium as heat by changing the temperature of the medium. As can be seen in Figure 2.6, the stored heat Q [J] rises with respect to a rising temperature and vice versa [73].
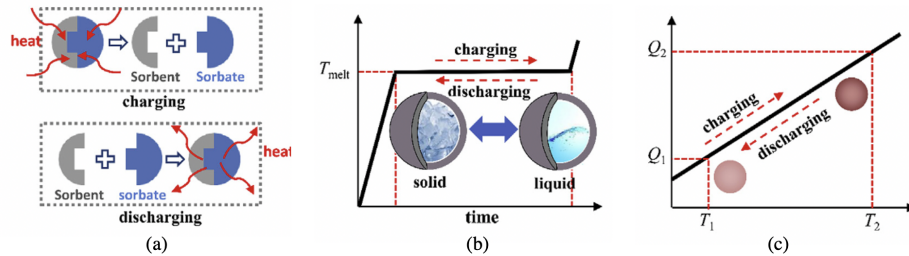
Figure 2.6: Visualization of the working principles of (a) a chemical (sorption) heat storage system, (b) a latent heat storage system and (c) a sensible heat storage system, adapted from [73]

Guelpa and Verda [27] proposed an overview of TES principles with their corresponding technology readiness level (TRL), which can be seen in Figure 2.7. For sensible heat storage, which has a TRL of at least 7, some configurations have been shown. The TRL approach was developed by NASA during the 1970s to evaluate technologies at their maturity level, which facilitates the transition of a technology from the technology development to engineering development [47]. The current NASA TRL classification scales from TRL 1 to TRL 9, where TRL 1 corresponds with basic technology research and TRL 9 with actual proven operations [24].

Figure 2.7: Classification of TES with their corresponding TRL, adapted from [27]

From Figure 2.7, it can be seen that sensible heat storage is in a more mature state of development than latent heat and chemical storage. However, this does not necessarily mean that latent and chemical storage are not promising techniques. In order to assess the differences between these TES mechanisms, their characteristics and (dis)advantages are addressed below.

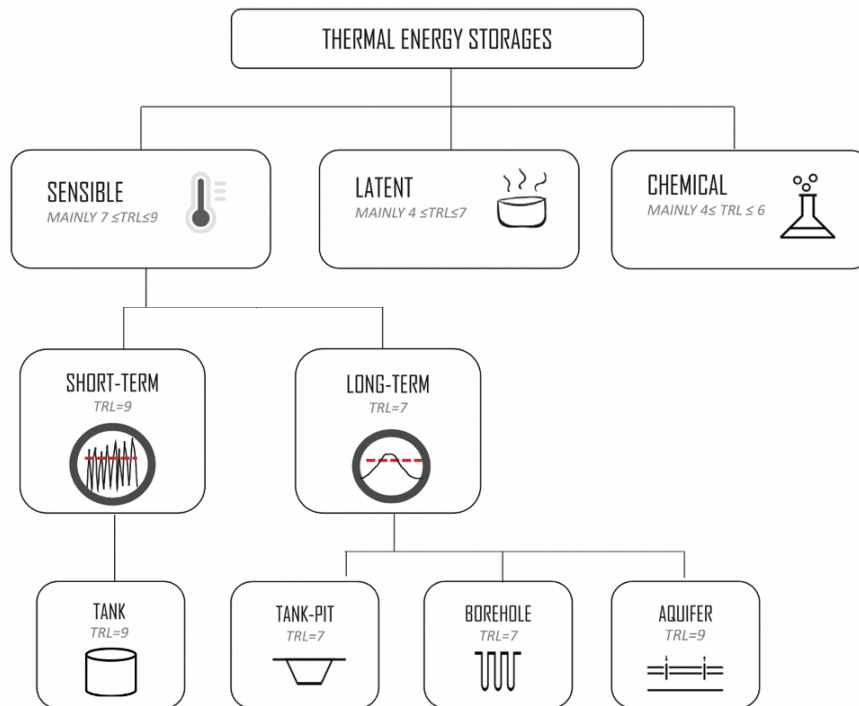Chemical storage can be classified into chemical reactions and sorption processes. Pinel et al. [53] explain that in chemical reaction storage, heat is stored by exciting a reversible endothermic chemical reaction. The stored heat can be recuperated by reversing the reaction, sometimes by adding a catalyst. Sorption storage systems make use of a charging and discharging process based on the reversible reactions between a sorbent and sorbate. During the charging fase, heat is added to break the bond between sorbent and sorbate. In the discharging fase, sorbent and sorbate are bonded again, releasing the stored heat [73]. Pinel et al. [53] also state that although chemical storage has a high potential of allowing TES, due to no long-term self discharge, much research remains before it becomes practical and economical viable.

Latent heat storage employs a phase change material (PCM) as the storage medium. Energy is absorbed or released during a change of phase, mostly solid-liquid, at the corresponding temperature. Examples of PCMs are water/ice, salt hydrates and wax [18]. According to Pinel et al. [53], this kind of TES has a relatively high energy density and the advantage of constant temperature discharge. However, the IEA SHC Task 32 [61] concludes that the improvement of using PCM in heat stores is very limited compared to (sensible) water stores. The only concept that is believed to achieve significant improvement is long term storage using subcooling, but the system would be excessively complex. Also, the investment costs may not be justified. Besides all these disadvantages, they recommend pursuing more research regarding better PCM materials.

Every material stores heat as its temperature rises and releases heat when its temperature decreases. This concept can be seen as sensible storage. According to Pinel et al. [53], sensible storage systems are usually simpler and cheaper than latent and chemical storage mechanisms and sensible storage systems are well understood, proven, reliable and have been used for centuries. Because of the need of pursuing much further research in chemical and latent heat storage technology, before they can be used for reliable and feasible storage applications, and the fact that sensible storage is proven to be reliable, the rest of this study will pursue the use of sensible TES systems for DH .

2.4. Designing sensible TES systems

When designing a sensible TES system, certain aspects have to be taken into account. This section will provide more information about these aspects. Furthermore, the following important characteristics of a sensible TES system, which have been put together by Hariri and Ward [28], limit the variety of choices of these aspects and must be taken into regard.

- The energy density or specific energy (energy capacity per unit weight);
- The operational temperature range;
- The properties of the energy transport medium, such as toxicity, corrosiveness, and heat capacitance;
- The thermal stratification in the storage unit;
- The power needed for the charging or discharging;
- The material container associated with the storage system;
- The means of controlling thermal losses from the storage system;
- The overall costs of the system.

2.4.1. Storage media

The amount of energy stored in a sensible TES system is for a large part dependent on the storage medium. Therefore, it is important to consider thermal properties of the medium. Specific heat capacity, which is one of the most important properties in TES design, accounts for the ability of a material to store heat. The amount of heat stored in a material, over a certain temperature range, can be expressed by Equation 2.7, where Q [J] is the total amount of heat stored in the material, c_p [J/kgK] is the specific heat capacity of the material, T_i [K] and T_f [K] are the initial and final temperature, and m [kg] is the mass of the material which is heated.

$$Q = m c_p (T_f - T_i) \qquad (2.7)$$

An interesting way to view the specific heat of a material is its volumetric heat capacity. The volumetric heat capacity of a material is defined by its density multiplied by its specific heat: ρc_p [J/m^{3}K]. This property gives insight in how much energy can be contained by different materials in the same volume.

Another important ability for a sensible storage medium is its ability of convenient adding or extracting heat, this ability is characterised by the medium its thermal conductivity κ [W/mK]. A high thermal conductivity means it is easy to conduct heat. However, while high thermal conductivity is preferred, it is convenient to have low thermal diffusivity α [m^2/s]. This is better for the thermal stratification of the medium, which will be elaborated in Section 2.4.4. The equation for thermal diffusivity, which relates with thermal conductivity and volumetric heat capacity, is given below.

$$\alpha = \frac{\kappa}{\rho c_p} \tag{2.8}$$

The respective volumetric heat capacity and thermal diffusivity of commonly used materials as a medium for sensible heat storage are compared in Figure 2.8.
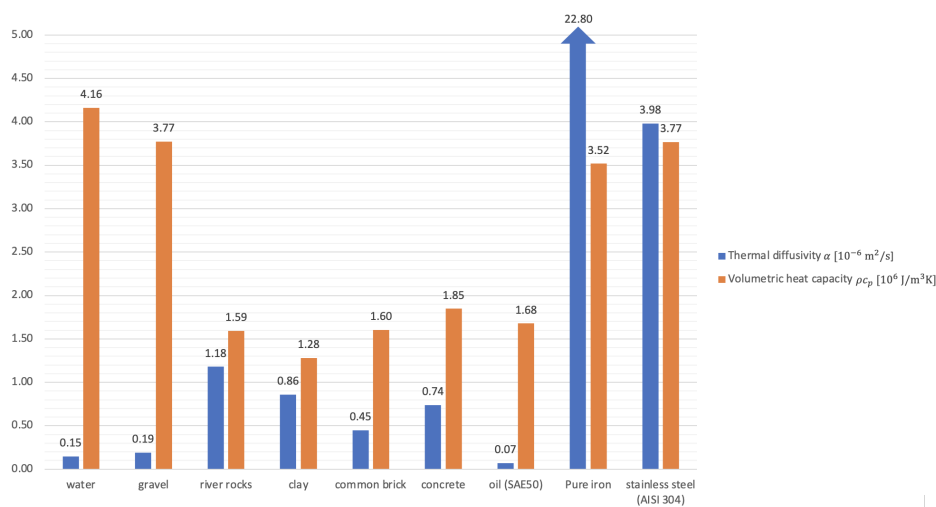

Figure 2.8: Comparison of volumetric heat capacity and thermal diffusivity of commonly used materials for sensible heat storage at 300 K [44], [1]

According to the thermal properties shown in Figure 2.8, water is the most promising storage medium of the list. It has the highest volumetric heat capacity and one of the lowest thermal diffusivities. Another advantage of water as a medium is its low cost. However, an inconvenience of water is the fact that it has a limited temperature range due to its freezing and boiling point. Nevertheless, Pinel et al. [53] explain that this is not a problem for residential applications, as water its boiling and freezing temperatures will not be reached in modern day DHC. Because of water its leading position as a storage medium, its thermal properties will be used for reference for the following materials.

Gravel has a slightly lower volumetric heat capacity and a slightly higher thermal diffusivity than water. Nevertheless, higher temperatures can be obtained in gravel than in water. River rocks used in rock beds are also capable of operating at much higher temperatures, but suffer from a low energy density, due to spacing between the rocks, and high thermal diffusivity. The spacing between the rocks is required due to the fact that a fluid, such as water or air, must be present to transport heat. Such a fluid is also needed for gravel systems. When water is used as a heat transport fluid, it becomes part of the storage medium and the system is considered a hybrid active/passive system [53]. The use of a gravel or rock bed system can be advantageous when a high operational temperature is needed. If this is not the case, gravel and rock bed systems take up more space than water systems, and is therefore not preferred due to higher installation costs and potentially limited space available. Bricks are quite similar to a rock bed when used as a storage medium and therefore can be considered with the same characteristics.

Oil is another commonly used medium for sensible heat storage. Although oil is much more expensive than water, it is capable of operating at much higher temperatures. Therefore, oil is only feasible as a storage medium when in need of high operating temperatures. Concrete slabs and iron/steel balls or pellets have also been used as a medium for sensible storage. While being able to handle very high temperatures, the cost of these media are much higher than those of water, rocks and gravel. Furthermore, oil, iron, steel and concrete have a big negative environmental impact compared to the other media discussed in this section. Therefore, only when the stability and capacity of these materials is in need, it is better to employ these materials instead of water.

2.4.2. Short- and long-term storage

TES systems can be divided into short- and long-term storage. Short-term storage is mostly used for matching the discrepancy between daily production and demand. Long-term storage is employed for matching the discrepancy between monthly/seasonal production and demand, as shown in Figure 1.1. Guelpa and Verda [27] constructed an overview with various characteristics regarding short- and long-term storage, which can be seen in Table 2.1.

Table 2.1: Main characteristics of short-term and long-term localized TESs [27]

	SHORT-TERM	LONG-TERM
Benefits	Storing energy available during the daily/weekly consumption valley to make this available during peaks	Storing energy available during the season it is largely available in order to make this available in other seasons
Energy stored in a TES unit	10-50 MWh	50-1000 MWh
Installation space (area)	Space requirements 10-100 m^2	Space requirements $10^3 - 10^4$ m^2 for tank-pit, about 100 m^2 for aquifer
More diffuse types	Water tank	Tank, pit and aquifer
Thermal losses	Lower than 5%	About 30%
Most widespread combinations	With combined heat and power plants	With solar source (largely available in summer)

Available space for placing a TES system is an important criterion. Since DHNs are mostly present in residential areas which are densely populated, and available space is often rare in those places, primarily short-term storage is used in order to distribute the daily production to reach the demand. Although long-term storage usually requires larger spaces, this is not the case for aquifer and borehole systems. The space required for these configurations is in the same order as that of short-term storage. Long-term TES systems are on average more difficult to make than short-term TES systems because they suffer from larger thermal losses, must be capable of containing enormous quantities of storage media and have a longer storage duration. However, even though long-term storage is more expensive than short-term, it is stated that the lifetime of such a system can be up to 20-30 years [27].

Long-term TES is mostly used to store energy from solar plants during summer to make solar energy available during winter. Also, heat from biomass plants is stored on a weekly basis and waste heat is also stored on a seasonal basis. When implementing long-term TES with DH, systems can be divided into two categories: direct and indirect usage.

In direct usage systems, the HTF of the network is also used as a storage medium. For example, a water-based TES directly connected to DH. Direct usage TES systems are mostly high temperature stores. In indirect usage systems, a supplementary system is often needed to transfer the heat from the storage medium to the network. In many cases, this system is an HP. This HP allows the temperature of the heat store to increase before it is supplied to the network. Due to this advantage and to keep external heat losses low, indirect usage systems are mainly low temperature stores.

2.4.3. Sensible TES configurations

Different storage principles can be employed for the use of thermal energy storage. Dahash et al. [20] constructed an overview of the most common TES configurations, with its (dis)advantages included, which can be seen in Figure 2.9. This section elaborates on these TES configurations, as well as less commonly used configuration.

Tank TES (water)
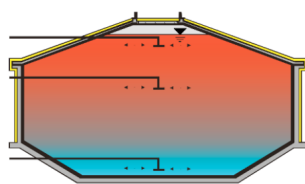
+ high thermal capacity (water)
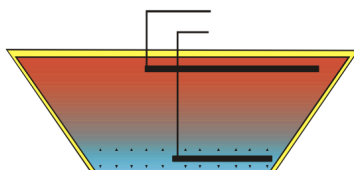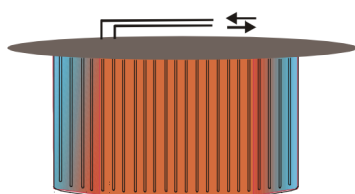+ good operation characteristics (high (dis-) charging power, usable as buffer store)
+ freedom of design (geometry)
+ thermal stratification
(+) maintenance/repair
(-) limited size (< 100,000 m³)
(-) primary energy demand
- high construction costs

Pit TES (gravel-water or water)

+ reasonable construction costs
+ medium (gravel-water) to high (water) thermal capacity
+ nearly unlimited store dimensions
(+) operation characteristics (medium charging power in case of gravel-water)
(-) complex and costly cover (in case of water)
- limited freedom of design (slope angle)
- maintenance repair difficult/not possible

BTES (soil)

+ low construction costs
+ easily extendable
- low thermal capacity
- operation characteristics (low (dis-)charging power, buffer required, heat pump recommended)
- limited choice of locations
- no thermal insulation at side and bottom possible
- maintenance repair difficult/not possible

ATES (saturated sand-water)
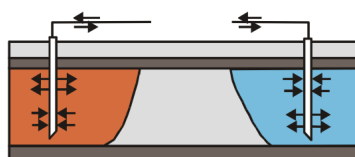
+ very low construction costs
(+) medium thermal capacity
(-) operation characteristics (low/medium (dis-) charging power, buffer and heat pump recommended)
- very limited choice of locations
- no thermal insulation possible, relatively high thermal losses

Figure 2.9: Construction concepts for (underground) thermal energy storage systems with their advantages and disadvantages [20]

Tank TES (TTES) is one of the most common configurations of TES. In TTES a concrete or steel container is filled with a storage medium, which is most often water. These tanks can either be installed above ground, half-buried or fully buried. Fully buried systems wield the advantage of a better insulation. However, excavation costs are quite high. Besides burying, storage tanks are frequently heavily insulated to prevent large thermal losses. In TTES, water is usually the preferred storage medium, but other media can also be used. The storing capacity of a TTES can be obtained by Equation 2.7 from Section 2.4.1. In this approximation m [kg] stands for the total mass inside the tank. The temperature difference used in the equation should be the range in which the TTES operates.

Pit TES (PTES) is quite similar to TTES when considering the operational side. Instead of a tank, excavated pits, which are coated with a watertight layer, are used as the storage unit. When water is used as a storage medium, the same energy density as TTES is applicable. Water-gravel mixtures are also commonly used, then the pit TES is referred to as water-gravel TES (WGTES). However, when employing WGTES, a lower energy density is present, which leads to an increase of volume of 50% compared to TTES [60]. When approximating the storage capacity of a PTES, done in the same manner as for TTES, it is important to note that the distribution of the storage media must be taken into regard, in order to achieve an accurate result.

Aquifer TES (ATES) consists of multiple wells and underground water reservoirs, which can be used to extract and inject groundwater. The groundwater can be used for heating and cooling purposes, after which it is injected back into the respective well. In these wells, the storage medium is the water-soil formation of the water reservoir, while the water also acts as the heat transfer fluid. An important specification, while searching for proper placement for an ATES, is the geologic condition. The aquifer must be embedded in-between two impermeable layers of clay, leaving enough room for a reservoir, while no significant mass flow of the groundwater is present. If the groundwater mass flow through the aquifer is too big, it could cause significant dissipation of storage media and thus excessive heat losses.

Another important criterion for the aquifer is the porosity of its soil. The porosity ϕ [-] is described in Equation 2.9, as the ratio of the volume of pore space V_{po} [m^3], to the total volume of the medium V_{tot} [m^3]. Aquifer porosities range from 10 to 45%, with a range of 20 to 30% to be suitable for ATES. In a saturated aquifer, the pore space is filled with water. Accordingly, the density of the aquifer ρ_{aq} [kg/m^3] can be found by Equation 2.10. With this density, the storage capacity of the aquifer can be found in the same manner as explained for BTES and TTES.

$$\phi = \frac{V_{po}}{V_{tot}} \tag{2.9}$$

$$\rho_{aq} = \phi \rho_w + \rho_s (1 - \phi) \tag{2.10}$$

Borehole TES (BTES) is quite similar to the working principle of ATES. However, instead of using water reservoirs underground, soil and/or rock is utilized to store heat. Multiple vertical boreholes, usually U-pipes, are installed in the ground, in which water is used as the heat transport fluid. This type of storage needs insulation on the top to reduce heat losses. However, BTES is still very susceptible to seasonal changes. Besides that, BTES has a much lower energy density than other TES with water as a storage medium. With the total volume of the boreholes, the storage capacity can be obtained in the same way as discussed for TTES.

A less common configuration for TES is cavern TES, where large underground rock caverns are used as storage unit. According to Dahash et al. [20], cavern TES is often used in gas turbine plants to store compressed air. These systems are likely to operate at temperatures above 200 °C. However, another option is to use water as a storage medium. In that way, the characteristics are quite similar to that of a PTES system with water as a storage medium. Therefore, cavern TES can be considered with the same (dis)advantages as PTES. Unfortunately, large underground rock caverns must exist in order to transform them into suitable TES system, because it would be too expensive to excavate similar caverns. Therefore, it would often be more feasible to build one of the aforementioned sensible TES systems [50].

Fleuchaus et al. [23] compared above mentioned TES configurations with each other, with an exception for cavern TES, on various feasibility parameters. This comparison is shown in Table 2.2. From this comparison, it can be seen that ATES is a promising configuration due to its ability to ensure high storage capacity while keeping the space requirements and costs low. A drawback for ATES is its need for subsurface requirements, preliminary investigation, maintenance, its interaction with its environment and legislation.

Table 2.2: Comparison of common TES configurations [23]

	TTES/PTES	BTES	ATES
Storage medium	Water, water/gravel	Groundwater/sediments	Groundwater/sediments
Subsurface requirements	low	medium	high
Required pre-investigation	low	medium	high
Maximum storage capacity [kWh/m^3]	high	low	medium
Storage volumes [m^3]	low	medium	high
Space requirement [m^2]	high	low	low
Investment costs	high	medium	low
Maintenance	low	low	high
Environmental interaction	low	medium	high

In many countries, ATES is still in an emerging market phase, where investment costs and risks are quite high. Nonetheless, ATES is very often employed in the Netherlands, which is the market leader in ATES applications, as can be seen in Figure 2.10 and Figure 2.11. Because ATES applications in the Netherlands are in the maturity phase, the limiting market barriers for development are shortage of subsurface space, size of the applications and legislation. If these barriers are overcome, the application of ATES in the Netherlands can be a feasible option for TES.
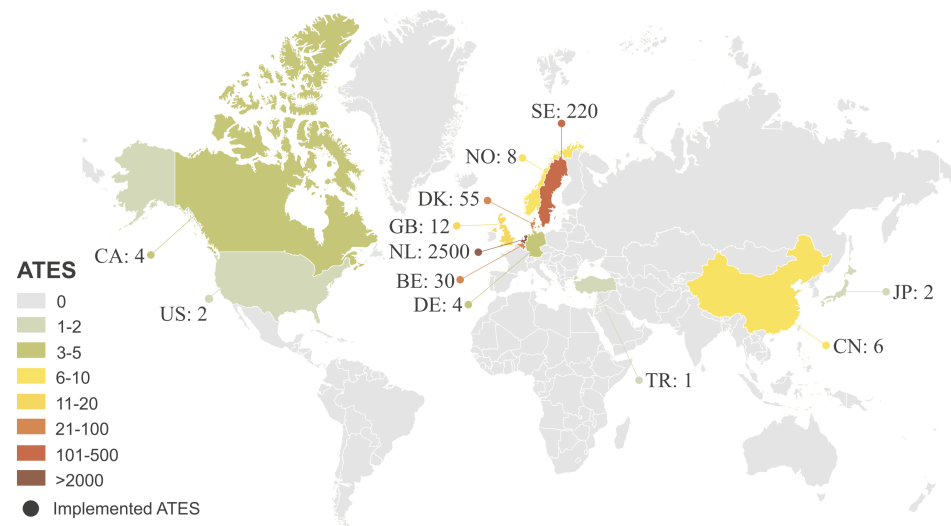
Figure 2.10: Global distribution of ATES systems [23]
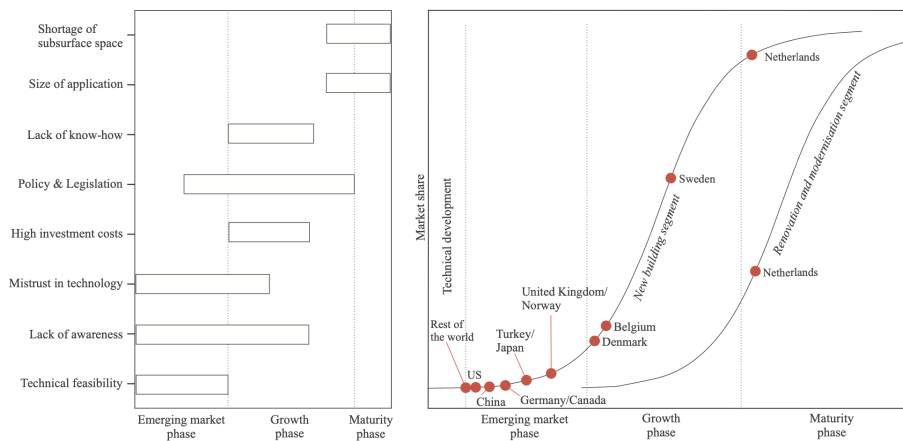
Figure 2.11: Left: limiting market barriers in the development of ATES as a function of the market development level. Right: market development of ATES in all relevant countries considering new building and renovation segments [23]

2.4.4. Stratification

According to Li [40], when using water or air as the storage medium, thermal stratification is a meaningful aspect of the storage performance. Thermal stratification is caused by natural convection, which divides the hot and cold water due to their difference in density: the hot water will rise to the top of the tank, while the cold water will descend to the bottom. In between the hot and cold water a thermocline, a mixing layer with a temperature gradient, will form, acting as a natural barrier that maintains the separation of hot and cold water. To keep the hot and cold water separated as much as possible to minimize mixing losses, the

thermocline must be kept as small as possible, concerning to the height of the storage unit. Stratification exists in different orders. These orders are defined by the temperature gradient ($\frac{\delta T}{\delta z}$) between the hot and cold regions. In Figure 2.12 different levels of stratification are shown. In case (a), a large temperature gradient is present, which indicates a small thermocline region. This is a good example of a highly stratified store with two big regions of the store respectively at a hot and cold temperature. In case (b), the temperature gradient is smaller, which indicates a bigger thermocline region. Therefore, case (b) is a good example of a less stratified store than case (a), where the hot and cold regions of the store are smaller, which indicates more mixing between hot and cold water, and thus more thermal losses. Case (c) shows a perfectly mixed storage unit, this means it has a uniform temperature, thus no thermocline. In other words, this is unstratified storage. Even though Li [40] talks mostly about water and air, stratification also occurs with other fluids. However, the scale of stratification is highly dependent on the storage medium.
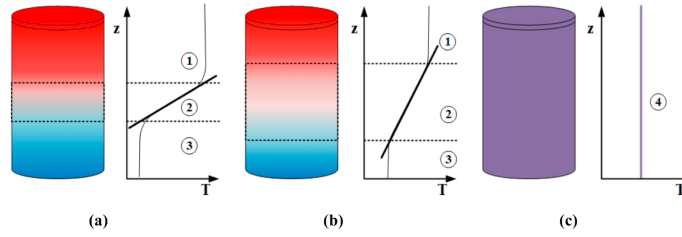

Figure 2.12: Different levels of stratification for same amount of stored heat, (a) highly stratified, (b) moderately stratified, (c) fully mixed storage, (1) hot region, (2) thermocline, (3) cold region, and (4) uniform temperature) [20]

In Figure 2.9, stratification in different TES configurations is also depicted, where the red color represents the hot part and the blue color the colder part. In the case of ATES and BTES, stratification works differently because of the separation of the hot and cold storage unit and the configuration of and the flow direction in the boreholes.

2.4.5. Geometry of the storage unit

By optimizing the geometry of the storage unit of a TES system, thermal losses can be decreased. For example, by minimizing the surface-to-volume ratio $\left(\frac{A}{V}\right)$ of the storage unit and adding insulation layers to the storage unit, external thermal losses are minimized. Other thermal losses that occur frequently are internal exergetic losses, which originate due to decreasing stratification in the storage unit [20]. Even though stratification relies on the storage medium, it can be substantially influenced by the position of the in- and outlet ports, and the aspect ratio $\left(\frac{h}{d}\right)$, where h [m] is the height and d [m] the diameter of the storage unit. Furthermore, Dahash et al. [20] also state that an aspect ratio of 1 should be pursued to minimize thermal losses. Note that this aspect ratio is defined for tank storage.

When using PTES or BTES, the aspect ratio must be approached somewhat differently. For ATES the aspect and the surface-to-volume ratio are non-applicable due to the result of the design of the overall system. An aspect that should be concerned when addressing the geometry of the storage unit of ATES is the distance between the wells. When wells are placed too close to each other, thermal interference occurs and the performance goes down. To prevent thermal interference, the distance between the hot and cold wells is based on the thermal radius r_{th} [m]. The approximation for the thermal radius, given by Bloemendal and Hartog [6], is shown in Equation 2.11. Here, $c_{p,w}$ [J/kgK] and $c_{p,aq}$ [J/kgK] are the specific heat of water and the aquifer respectively, V [m³] is the volume of pumped groundwater and L [m] is the screen length of the well. Due to Dutch regulations, a distance of three times the thermal radius must be held for the installation of ATES systems in the Netherlands.

$$r_{th} = \sqrt{\frac{c_{p,w} V}{c_{p,aq} \pi L}} \tag{2.11}$$

2.4.6. Insulation

Another important factor for storage performance is the insulation of the storage unit. Bott et al. [8] present some cases where high thermal losses occur due to insufficient insulation. For example, measurements were taken at a seasonal TES facility in Stuttgart, where thermal losses of 40% were detected because the storage unit was only insulated at the top. To ensure fewer thermal losses, it is best to insulate the storage unit sufficiently. Bott et al. [8] listed the following important requirements for insulation material properties:

- Uniform and continuous application of insulation
- Durability
- Insensitivity to thermal stress or external natural influences
- Good drying abilities

According to Dahash et al. [20], common materials used for insulation are polyurethane, expanded and extruded polystyrene and glass wool. Other used materials are polyethylene foam, foam glass and glass granulates. The latter two are recycled materials from waste glass.

Because the cost increases as the insulation is applied to all the sides of a storage unit, a cost-benefit analysis must be done to ensure economical feasibility. For example, TTES are usually insulated at all sides because it is relatively easy to apply during construction, while many PTES and WGTES are not insulated at the side walls. The thermal losses that occur in those cases are often compensated by making larger storage volumes. Another concept that may be applied is an inhomogeneous pattern of insulation. An example is shown in Figure 2.13, in which at the top, where the hot water accumulates, the insulation is relatively thick. As the temperature of the medium decreases downwards, also the insulation thickness decreases, while maintaining an acceptable thickness of insulation at all times.
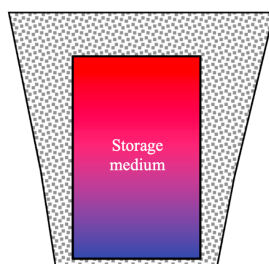
Figure 2.13: Inhomogeneous distribution of insulation with consideration of economic feasibility and technical performance to maintain stratification [20]

A well-known problem with water-based storage is water leaking into surroundings and insulation layers, which causes high heat losses. To prevent leakage, liners are often applied. In TTES these liners are usually made of (stainless) steel. In PTES and WGTES, plastic liners are often used. The advantage of steel liners over plastic liners is its long lifetime, diffusion resistance and the maximum storage temperature, which for steel liners is well above 95°C, while for plastic liners it is below 90°C. On the other hand, steel liners are susceptible to corrosion, demand more complex installation procedures than plastic liners, and are much more expensive than plastic liners. Often used materials for plastic liners are ethylene propylene diene monomer, high-density polyethylene, low-density polyethylene, polypropylene and butyl rubber, of which high-density polyethylene is most widely used [8].

In the case of BTES, where the surrounding soil of the boreholes acts as the storage medium, only the top of the store is insulated. For ATES, insulation is not applied at all, because the storage medium is embedded between impermeable layers of clay.

2.5. Modeling of TES

Modeling the thermo-hydraulics of large-scale underground TES systems tends to be complicated due to its many components and temperature-dependent behavior. Dahash et al. [20] state that a wide range of tools is used for modeling TES systems, which can be divided into the following categories:

1. *Energy system simulation*, such as Dymola, TRNSYS, Matlab/Simulink
2. *Building physics envelope heat and mass transfer tools*, such as WUFI Pro, Delphin
3. *Computational fluid dynamics*, such as ANSYS Fluent, OpenFOAM and COMSOL Multiphysics

According to Pinel et al. [53], commercial numerical calculation codes are sometimes used to assess the performance of TES. These codes offer very detailed results about the thermo-hydraulics in the TES systems but do not account easily for interacting with their surroundings. Above mentioned simulation tools, on the other hand, allow models to reproduce transient dynamic interactions between systems and their surroundings while offering a cheap and fast way to do so.

TTES and PTES have been represented by rudimentary plug-flow models as well as sophisticated models, which account for full Navier-Stokes equations. The basis for these models often are complete Navier-Stokes and energy balance equations and/or their simplifications, provided by fluid textbooks such as White [72]. The so-called plug-flow models are characterized by their assumption of a flow direction and velocity, which only require the solution of an energy balance equation. Less simplified TTES/PTES models are often based on one-dimensional numerical solutions and assume perfectly insulated storage tanks by only accounting for temperature gradients in the longitudinal direction. According to Cruickshank and Harrison [19], when accounting for low flow rates, the performance of stratified storage tanks is appropriately simulated in these approaches. Additionally, most models only assume pure heat conduction in the soil and neglect humidity diffusion, while humidity diffusion plays a big part in heat transfer around TTES/PTES.

Many BTES models also only assume heat transfer by pure conduction in the soil, neglecting humidity diffusion. Subsequently, older BTES models only account for the evaluation of heat transfer around the buried tubes, while newer BTES models are often numerically solved or composed of a hybrid form, combining numerical and analytical solving. These newer models include energy system simulation and building physics envelope heat and mass transfer tools. Other newer, more complete, models also include the influence of humidity diffusion on heat transfer. Even though this enables more accurate results, the extra complexity of the model must be considered.

ATES modeling is often based on heat and mass transfer and includes the continuity equation based on Darcy's law and an energy balance equation. Some models have been designed for ATES, both analytical and numerical. Simplified analytical models, which are generally only applicable to the simplest cases and preliminary design phases, provide fast and, for some specific conditions, satisfactory results. More comprehensive numerical models are used for qualitative calculations and offer more detailed results, but require more attention and time.

When designing a model for TES, a trade-off must be made between the simplicity and detail of the result. Depending on the requirements of the model, the modeling of TES systems can be done on component level, TES level and system level. Various approaches are used for modeling on these levels and combining them. Depending on these levels, various parameters must be taken into account for producing a correct model. Required parameters can be the thermal capacity, geometry and insulation of the storage unit itself, positions of in- and outlet ports, stratification, storage media properties and surrounding conditions.

Due to its lower computation efforts, energy system simulation tools are often employed for modeling on system level. Subsequently, multiphysics tools are often used for modeling on component level, due to their focus on detail. Co-simulation of these tools can be an option of coupling system level and component level modeling.

2.6. Implementation of TES in DH

When DHNs are dependent on renewable energy sources (RES), TES can be implemented to manage the discrepancy between supply and demand. This section will first state the benefits and drawbacks of pairing TES with DH. Subsequently, the performance of various TES systems coupled with DH will be discussed.

2.6.1. (Dis)advantages of pairing TES with DH

Coupling DH systems with TES can generate certain benefits and drawbacks regarding technical, economical and environmental context. Various effects, and their benefits, of combined use of TES and DH, given by Guelpa and Verda [27], are listed below:

- Reducing generation unit size, avoiding additional investment costs and reducing system complexity
- Thermal peak shaving made possible, increasing system performance, decreasing costs, maximizing profits in electricity selling, reducing emissions
- Relieving irregularities of RES, reducing primary energy needs by increasing RES exploitation, reducing operating costs and allowing zero-emission energy plants
- Smaller pipe size in the distribution network, reducing investment costs and the impact on the urban layout
- Allowing connection of more buildings to the DHN, increasing the overall efficiency of an urban energy system, while decreasing emissions
- Network management flexibility, reducing pumping costs and related emissions
- Avoiding installation of pressurization vessels, reducing investment costs and the systems complexity
- Avoiding installing of combustion chambers in buildings, reducing maintenance costs and explosion risks for users

Besides above-mentioned benefits, drawbacks can occur when implementing TES in DH applications. Guelpa and Verda [27] also listed the following possible drawbacks:

- Increased investment costs
- More space is required
- Significant thermal losses
- Challenging design of the systems and its connection
- Lack of suitable supportive legislation

2.6.2. Performances of TES systems connected to DH

The (dis)advantages of combined use of TES and DH, mentioned in Section 2.6.1, are universal. However, when TES is implemented in DH, the performances of the various system may differ. This section addresses (dis)advantages and other characteristics of TTES, PTES, ATES and BTES when employed in combination with DH, reviewed by Guelpa and Verda [27].

Because TTES and PTES are quite similar on the operational side, they will be considered to have the same relationship with DH when coupled. Although studies have shown that the implementation of long-term TTES/PTES in DH is technically feasible, available space for the storage unit in urban areas remains a substantial drawback. Other obstacles are high construction costs and high thermal losses. To optimize the capacity of the TES system, it is important to note its dependence on the DHN its temperature, thermal losses and stratification. Also, the return temperature of the DHC must be selected accordingly in regard to the volume of the TES unit, or the other way around. Finally, the TES system can be combined with HPs in order to increase the supply temperature to the DHN.

Coupling ATES with DH has the advantage that specific capital costs decrease when increasing the storage size, enabling big affordable DHN with TES. However, in dense urban areas, ATES systems might be placed nearby each other. This could cause complications because of the thermal interference between hot and cold wells. As discussed in Section 2.4.5, thermal interference can be averted by following Equation 2.11. Other technologies that exploit groundwater must be considered as well. Nevertheless, ATES has the advantage of occupying less space than TTES, which is in turn very convenient for dense urban areas. Due to national regulations, ATES systems in the Netherlands usually operate at relatively low temperatures. Therefore, it is recommended to implement HPs into the DHN and/or ATES.

Although BTES systems in DH are easy to place in urban areas, due to the low space requirements, the energy density of BTES is relatively low and the construction costs are high. Also, high thermal losses occur when employing long-term storage. As for ATES, HPs can be used to boost the performance of BTES. However, due to the low economic feasibility BTES are not often implemented in DH.

2.7. Key performance indicators
To assess the feasibility of TES and DH systems, KPIs must be assigned which give insight in TES and DH systems, regarding sustainability, performance and costs. This section addresses two interesting KPIs, which can be used in the case study to compare different approaches.

2.7.1. Levelized cost of energy
The levelized cost of energy (LCOE), shown in Equation 2.12, describes the cost per unit of energy delivered over the lifetime of a system [€/kWh] [16]. Here, n [yr.] is the lifetime of the system in years, C_{tot} [€] and Q_{tot} [kWh] are the total costs and energy delivered of year t respectively. Furthermore, r [-] represents the discount rate of the investment, which accounts for the discount of future values against today's and the riskiness of the investment. In terms of financial feasibility, the LCOE can be seen as the minimum selling point of the delivered energy to make the project break even or make profit.

$$LCOE = \frac{\sum\limits_{t=1}^{n} \frac{C_{tot}}{(1+r)^t}}{\sum\limits_{t=1}^{n} \frac{Q_{tot}}{(1+r)^t}} \tag{2.12}$$

2.7.2. CO$_2$ emissions
The main reason why this study is conducted is that more sustainable heating must be implemented in district areas due to the threat of increasing global warming. Therefore, it is key that the sustainability of new heating scenarios is taken into regard when designing those. To assess the sustainability of the different scenarios, their yearly CO$_2$ emissions can be compared.

2.8. Reference solution
To assess the feasibility of employing a TES integrated DHN, a reference solution will be used concerning the heat supply for the residential area in the case study. The reference solution must be able to be assessed by the KPIs discussed in Section 2.7. The reference solution will comply with the approach of the Dutch government to make residential neighborhoods natural gas-free, but will not include DH or TES.

A possible solution for meeting the heat demand of households, without using natural gas and avoiding the use of DH or TES, covered by Planbureau voor de Leefomgeving [54], is the use of an individual HP per household. HPs exist in various types, of which the Heat Pump Association UK [29] listed the following as the most common types, as well as the characteristics discussed below:

1. Air-source HP
2. Water-source HP
3. Ground-source HP

Air-source HPs extract heat from ambient air. This kind of HP is frequently employed due to the relatively low installation costs. The performance of air-source HPs depends on diurnal and seasonal fluctuations in the ambient temperature. Therefore, air-source HPs function best in moderate climates. Water-source HPs extract heat from water in either a closed loop, submerged in a water basin or an open loop, where water is extracted directly from a water source. The diurnal and seasonal temperature fluctuations of water are less than that of ambient air. Therefore, water-source HPs can provide a more steady operation efficiency than air-source HPs. However, due to the need for access to a water source, water-source HPs are less common. For ground-source HPs, a closed network of pipes is buried in the ground, where an HTF is used to extract heat from the soil. Due to a quite constant temperature of the soil, ground-source HPs offer an efficient operation. The installation costs of ground-source HPs are higher than that of water- and air-source HPs, because of the required excavation and installation of underground components. To minimize the costs in the reference solution, it is assumed that all the buildings will have air-source HPs employed.

To make the reference solution independent of external factors, the following assumptions are made concerning the electricity source of the HPs:

1. The provided electricity is abundant, thus high electricity peaks caused by the HPs can be met.
2. The electricity grid is able to deliver the high electricity demands.

3

Case study

In this chapter, the different aspects of the case study will be elaborated. First, the area of the case study and its buildings will be illustrated. After which, the different scenarios for meeting the heat demand will be explained.

3.1. Stationsplein Heerhugowaard

The area on which the case study is performed is the area around the 'stationsplein' in Heerhugowaard in the Netherlands. Part of the area will be newly constructed in the near future while some buildings will remain the same. Figure 3.1 shows the distribution of buildings in this area, categorized in color by their energy labels, which are shown in the bottom right-hand corner. All the blue buildings will be newly constructed. For the properties of these buildings, a given estimate will be used in the model. For the properties of the other buildings, the known building properties will be used. Most of the buildings in this area are residential buildings. However, some (parts) of these buildings are commercial. These different types of buildings will have a different approach later on, in which slightly different heat demand profiles will be composed.

Figure 3.1: Buildings in the case study area in Heerhugowaard in the Netherlands, categorized in color by their energy label

The case study area, shown in Figure 3.1, consists of a heterogeneous distribution of 89 buildings. Of every building in the area, specific characteristics are known, such as the ground area, the number of levels, the energy label, the number of households and residents per building. These characteristics will later be used as a basis to model the consumer heat demand on building level.

As stated previously, part of the buildings will be newly built and an estimate of the respective characteristics of these buildings have been provided by Resourcefully, together with the characteristics of the remaining buildings. Of all the 89 buildings, 47 buildings will be newly built and are mostly apartment buildings. These apartment buildings consist of at least 5 levels with a maximum of 10, with an exception for the few (semi)detached houses near the water in the north. Of the remaining 42 buildings, around half are also apartment buildings, while the other half are (semi)detached houses. The (semi)detached houses consist of 1-2 households per house and the apartment buildings in the case study mostly consist of an average amount of 32 households per building. The total number of households in the case study area equals 1971. Also, it is assumed that a total number of residents of 4731 inhabit the case study area, which adds up to an average number of residents per household of 2.4. Table 3.1 gives an overview of the distribution and characteristics of the buildings in the case study area.

Table 3.1: Distribution and characteristics of buildings in the case study area in Heerhugowaard

Case study area characteristics	Value	Unit
Total number of buildings	89	-
Number of apartment buildings	62	-
Number of (semi)detached houses	27	-
Total number of households	1971	-
Average number of households per apartment building	32	-
Average apartment size	80	m^2
Average number of households per (semi)detached house	2	-
Average (semi)detached house size	115	m^2
Total number of residents	4731	-
Average number of residents per household	2.4	-

In the case study area, a section of a medium temperature (MT) heat net of 70 to 90°C is available [32],[30]. The heat of this heat net originates from a biomass plant and a waste incineration plant. the MT heat net is depicted in Figure 3.1 as the glowing red line which travels from the bottom left to the top right-hand corner. This section of the available MT heat net can be employed as a heat source for the DHN of the case study area, operating at an MT supply level of 70 to 90°C.

Another option for a heat source in the area is the presence of a collective ultra low temperature (ULT) waste heat net operating at 25 to 30°C, which might be placed in the case study area in the near future [38]. This collective waste heat net is already available nearby the case study area but not directly in the case study area as of today. However, this waste heat net can be connected where preferred when renovating the area.

Because the ULT source in this area will result in a DHN of a much lower supply temperature than with the MT source, the DHN will endure fewer heat losses to the surroundings. However, due to the low temperature, an HP must be employed to raise the temperature at household level. This is assumed to be quite efficient for well-insulated buildings, but for the older buildings in the area, it may not be a feasible solution. Therefore, it is also possible to implement a combination of the MT and ULT heat source for the DHN, depending on its layout and the insulation of the connected buildings. An overview of the possible heat sources with their characteristics can be seen in Table 3.2.

Table 3.2: Possible heat sources in the case study area, together with their temperature range [32],[38]

Possible heat source	Temperature range
MT heat net from a biomass and waste incineration plant	$70 - 90$°C
ULT collective waste heat net	$25 - 30$°C

3.2. Case study scenarios

The heat demand in the case study area can be met by multiple DHN scenarios. The chosen scenarios for this case study are shown in Table 3.3 and are discussed below. Different scenarios are designed for the separate use of each possible heat source mentioned in Section 3.1, as well as for the combined use of the two heat sources. Subsequently, each scenario is expanded with an additional scenario, which employs a collective storage system. This collective storage system facilitates long- and short-term storage. Also, a reference scenario is added, which supplies the case study area with an alternative way of all-electric heating.

Table 3.3: Characteristics of the different DHN scenarios and the reference scenario

Scenario	Heat supply	Supply temperature [°C]	Storage	Supply method
1a	MTDH	70	-	HEX
1b	MTDH	70	ATES/TTES	HEX
2a	ULTDH	25	-	Water-to-water HP
2b	ULTDH	25	ATES/TTES	Water-to-water HP
3a	Combined ULT/MTDH	25/70	-	Water-to-water HP / HEX
3b	Combined ULT/MTDH	25/70	ATES/TTES	Water-to-water HP / HEX
4	All-electric	-	-	Air-to-water HP

3.2.1. Scenario 1: MTDH

The first scenario relies entirely on the MT heat net as a heat source, making the first scenario MTDH with a supply temperature of 70°C. Due to the relatively high supply temperature, the heat for both space heating and DHW can be delivered to all the buildings by use of a supply set with an HEX, as shown in Figure 3.2. It is assumed that the HEX cools the supply mass flow by 30 K, bringing the return line to a temperature of around 40°C, without accounting for additional heat losses. Furthermore, the scenario is expanded with an additional scenario, in which a collective storage facility is employed. Here, an ATES system is used for seasonal storage, while daily fluctuations are absorbed in a buffer TTES.

Table 3.4: Characteristics of the different first scenarios

Scenario	Heat supply	Supply temperature [°C]	Storage	Supply method
1a	MTDH	70	-	HEX
1b	MTDH	70	ATES/TTES	HEX
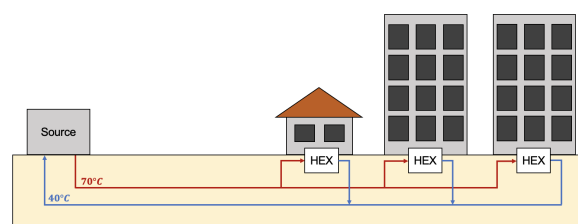
(a) Scenario 1a: MTDH
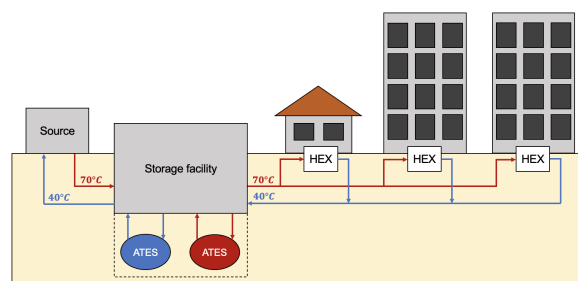
(b) Scenario 1b: MTDH with collective storage

Figure 3.2: Schematic view of scenario 1a and 1b

### 3.2.2. Scenario 2: ULTDH

The second scenario relies entirely on the ULT collective waste heat net as a heat source, classifying the second scenario as ULTDH with a supply temperature of 25°C. Due to the relatively low supply temperature, the heat for both space heating and DHW must be delivered to all the buildings by use of a supply set accompanied by a water-to-water HP, as shown in Figure 3.3. This HP upgrades the delivered heat to the required temperature for space heating and DHW, which can differ per building due to their utilization of underfloor heating or radiators. It is assumed that the HP cools the supply mass flow by 13 K, bringing the return line to a temperature of around 12°C, without accounting for additional heat losses. Furthermore, the scenario is again expanded with an additional scenario, in which the same collective storage facility is employed. Here, an ATES system is used for seasonal storage, while daily fluctuations are absorbed in a buffer TTES, as shown in Figure 3.3

Table 3.5: Characteristics of the second scenario

Scenario	Heat supply	Supply temperature [°C]	Storage	Supply method
2a	ULTDH	25	-	Water-to-water HP
2b	ULTDH	25	ATES/TTES	Water-to-water HP
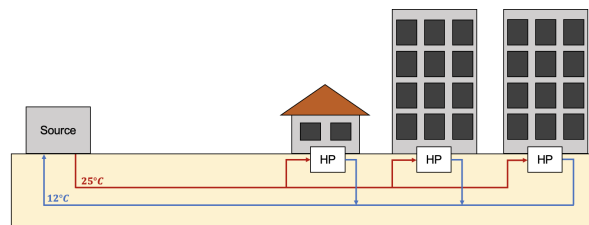
(a) Scenario 2a: ULTDH
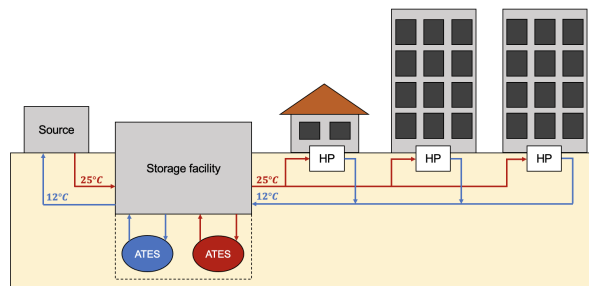
(b) Scenario 2b: ULTDH with collective storage

Figure 3.3: Schematic view of scenario 1a and 1b

3.2.3. Scenario 3: combined ULT/MTDH

The third scenario which is assessed relies on the combined use of the ULT collective waste heat net and the MT heat net as heat sources. To keep heat losses in the DHN low, all the buildings which can use underfloor heating will be connected to the ULTDH. For all the buildings which cannot use underfloor heating due to their insufficient insulation, an MTDH is used to provide heat. This division of buildings connected to the different DHNs is shown in Figure 3.4. Here, the red buildings will rely on MTDH, while the purple buildings will be supplied by ULTDH combined with individual HPs. Furthermore, the scenario is again expanded with an additional scenario, in which the same collective storage facility is employed. Here, an ATES system is used for seasonal storage, while daily fluctuations are absorbed in a buffer TTES. The schematics of the DHNs will be the same as the MTDH network in scenario 1 and the ULDH network 2 respectively, shown in Figures 3.2 and 3.3.

Table 3.6: Characteristics of the third scenario

Scenario	Heat supply	Supply temperature [°C]	Storage	Supply method
3a	Combined ULT/MTDH	25/70	-	Water-to-water HP / HEX
3b	Combined ULT/MTDH	25/70	ATES/TTES	Water-to-water HP / HEX
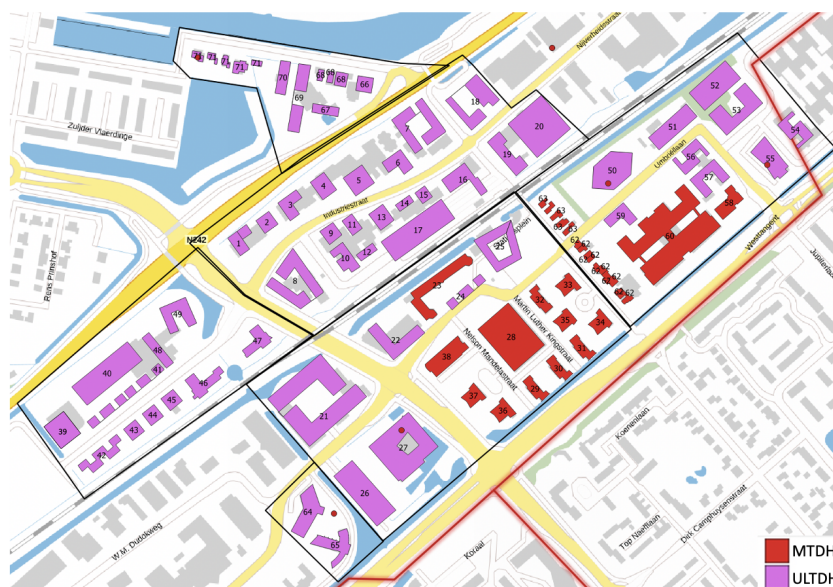
Figure 3.4: Distribution of the ULTDH and MTDH connected buildings for scenario 3

3.2.4. Scenario 4: all-electric

The last scenario is used as a reference scenario to compare the previous DHN scenarios with an alternative way of gas-free heating. This scenario is based on an all-electric approach, in which the heating demand will be covered by individual air-to-water HPs for each household, which utilize the outside air as a heat source. Using this kind of HPs eliminates the need for a DHN.

4

Framework of the model

In this chapter, the framework of the model will be treated. First, the structure of the model will be explained. Next, the characteristics of the consumer heat demand will be discussed and implemented in a Simulink model, which is validated with various data. Subsequently, the modeling of the DHN will be discussed, as well as the implementation and modeling of an ATES system integrated into the DHN. Finally, the implementation of costs and the KPIs of the DHN scenarios will be discussed. It must be noted that the consumer heat demand is highly dependent on weather conditions and consumer behavior. The conditions in this case study are chosen to simulate the future heat demand, in which warmer years are more common due to climate change. For this reason, the year 2014 has been chosen as a reference year, because this is the hottest year on record of which all the required data for this study was easily available.

4.1. Structure of the model

To assess the feasibility of the implementation of TES in the DHN scenarios of the case study, a model is designed which performs thermodynamic calculations of the DHN scenarios on an hourly basis. The model consists of a Simulink model, supported by multiple Matlab scripts, which either provide input data or process the output data provided by the Simulink model. The Simulink model is designed with a bottom-up approach, where the ends of the DHN piping are taken as a starting point. Subsequently, the calculations follow the DHN, through all of the consumers, all the way towards the heat source. Figure 4.1 shows a visualization of the calculation order of the model. Here, the model starts with initial conditions at the end of the piping, as shown on the left. Subsequently, the model calculates from the left to the right, through all the consumers and ending at the heat source.
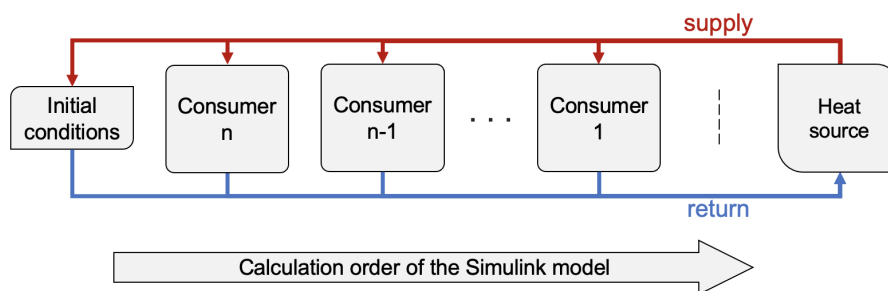

Figure 4.1: Visualization of the calculation order of the Simulink model

31

Figure 4.2 shows a flowchart of the structure of the whole model. In the first place, an input for the Simulink model is made in a Matlab start-up file. Subsequently, the Simulink model computes the DHN scenarios. Finally, a Matlab end file will process the exported data and run a storage model before providing the required results for the evaluation of the KPIs.

In the Matlab start-up file, weather and consumer data are provided to create the required input for the Simulink model. Next, the Simulink model will perform further calculations with this input. The Simulink model can be divided into three main sections. The first one contains the consumer heat demand. This section combines the Matlab input and initial conditions for the DHN and calculates the respective consumer's heat demand. Next, a part of the district heating network is composed. Here, the dimensions of the piping, as well as its heat and pressure losses, are calculated until the next consumer is met in the network. Now, the initial conditions are replaced by the conditions of the network at the place of the consumer. Subsequently, the respective consumer's heat demand and its influence on the network are calculated and the next part of the network is composed again. This will be repeated until the whole network is covered. At last, the required heat supply of the heat source is found by evaluating the needs of the network. A version of this Simulink model is made for each scenario of the case study.

The Simulink model exports its results to the Matlab end file, which processes the calculated data regarding the required KPIs. Before the data processing is done, a storage model assesses the implementation of a storage system in each scenario. Because this storage model is used to evaluate the required magnitude of the systems, it is designed in Matlab after the Simulink model has computed all of the required data. Finally, with all the results from the Simulink and Matlab model, the KPIs of the different scenarios can be evaluated.
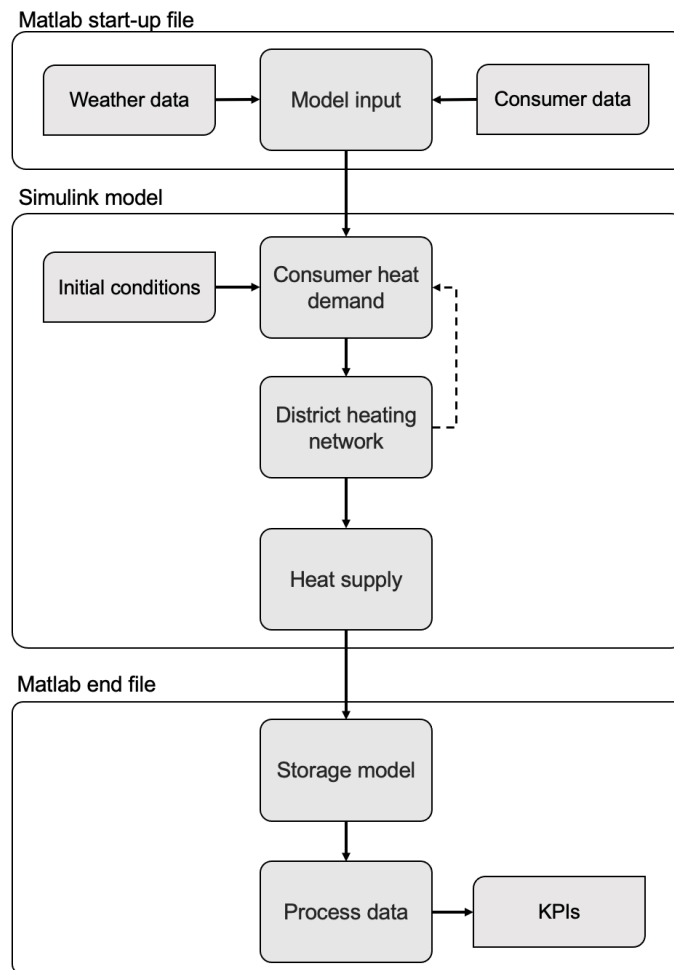

Figure 4.2: Flowchart of the structure of the model used for the case study

4.2. Consumer heat demand

The first important component of the Simulink model is the heat demand of the consumers in the DHN. The heat demand of a consumer can be described by two significant parts. The first one is the heat needed for space heating due to envelope losses of the building to the surroundings. The other part is the demand for DHW usage by the consumers that must be met. This section addresses the ways how both of these demands are modeled.

4.2.1. DHW demand

Friedel et al. [25] approached the DHW demand of multiple households in the Netherlands with different heat technologies and concluded that on average 1.3 kWh of heat is required for DHW per day per resident. Because DHW is not used constantly throughout the day, a profile is needed to simulate the DHW heat demand. Ahmed et al. [2] derived hourly DHW profiles for various apartments with different groups of people. From this study, the fraction-based profile of the total daily DHW heat demand, which can be seen in Figure 4.3 as the blue line, is constructed for one person. Dependent on the number of residents in a building, the hourly profile will be multiplied by the total daily DHW heat demand to simulate the dynamic demands. For commercial buildings, the DHW demand is assumed to be negligible due to the absence of showers.
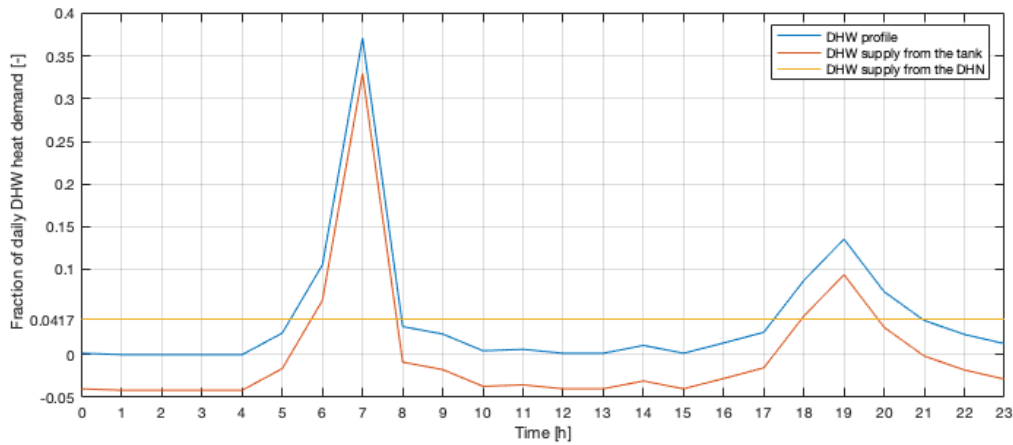

Figure 4.3: Hourly DHW heat demand profile based on percentages of the total daily heat demand (blue), together with the DHW supply from the tank (red) and from the DHN (yellow), adapted from Ahmed et al. [2]

To avoid high peaks in the DHN due to simultaneous use of DHW of various households, buffer tanks are implemented in the dwellings. Because the blue DHW profile in Figure 4.3 is fraction based on the total daily DHW demand, the buffer tank will be scaled the same way. It is assumed that the buffer tank is fully emptied and filled within 24 hours, without thermal losses. Therefore, the heat demand of the buffer tank is designed as $\dot{Q}_{DHW,tank} = \frac{1}{24} \cdot Q_{DHW,daily}$. By subtracting the filling rate of $\frac{1}{24}$ of the DHW profile of the house, the DHW profile can now be met by two supply principles. The first one being the DHW supply from the DHN, shown as the yellow line in Figure 4.3. The DHN originated DHW supply either supplies to the buffer tank or directly to the DHW, depending on the DHW demand. The second one is the DHW supply from the buffer tank, shown as the red line in Figure 4.3. When the DHW profile (blue) is lower than the DHW supply (yellow), excess heat is stored in the buffer tank (red). When the DHW profile (blue) is higher than the DHW supply (yellow), the stored heat is extracted from the buffer tank (red). When the DHW supply from the buffer tank has a negative value it means the buffer tank is being filled and when it has a positive value it supplies DHW to the house. The capacity of the buffer tank can be determined by finding the largest enclosed area between the red line and the zero line. This area represents the fraction of the total heat demand which must be stored in the buffer tank. The capacity of the buffer tank is then calculated by multiplying the area with the total heat demand.

4.2.2. Space heating demand

The space heating demand of a building is influenced by the building its properties, conditions of the surroundings and internal heat gains. Because internal heat gains are relatively small compared to the space heating demand caused by outside conditions, internal heat gains are neglected in this study. The space heating demand is mainly caused by envelope losses to the surroundings. These losses are characterized by Equation 4.1, where $\dot{Q}_{loss}$ [W] is the heat loss rate to the surroundings, U [W/m²K] and A [m²] are the heat transfer coefficient and area of segments of the buildings envelope, T_{inside} [K] is the inside temperature of the building and $T_{outside}$ [K] is the temperature of the surroundings. The inside temperature of the building is mainly influenced by a thermostat. Normally, people will not be at home the whole day. However, due to the current state of COVID-19 measures, most people are working from home. To maintain a comfortable environment it is assumed that the thermostat setting of the residential buildings equals 20.5°C at all times. For simplicity reasons, the inside temperature in the model will be equal to the corresponding temperature of the thermostat setting. Because the scope of this research is on DHN for residential applications and only a small fraction of the buildings are commercial buildings, it is assumed that the commercial buildings have the same temperature regulation as the residential buildings.

$$\dot{Q}_{loss} = \begin{cases} \sum UA \cdot (T_{inside} - T_{outside}), & T_{inside} - T_{outside} > 0 \\ 0, & T_{inside} - T_{outside} \leq 0 \end{cases} \tag{4.1}$$

Because most of the buildings in the case study area will be newly built, an estimate is made of the buildings' dimensions. This estimate contains the floor surface, number of floors and the fact that the buildings will have flat roofs. The same data is available of the buildings that have already been build. To assess the required segment areas of the buildings, the following assumptions have been made. Only flat roofs are considered, therefore is the roof area A_{roof} [m²] equal to the ground floor area A_{ground} [m²] as shown in Equation 4.2. According to the Office of the Deputy Prime Minister of the United Kingdom [51], the window area A_{window} [m²] of a building can be assumed as a quarter of the total floor area, which roughly equals to the ground area A_{ground} [m²] multiplied by the number of levels n [-] of the building, as shown in Equation 4.3. Finally, it is assumed that the external wall area A_{wall} [m²] is equal to the square root of the ground floor A_{ground} [m²], multiplied by 4 to account for all the sides of the building, multiplied by the average height of a level h [m], multiplied by the number of levels n [-] of the building, minus the window area A_{window}, as shown in Equation 4.4.

$$A_{roof} = A_{ground} \tag{4.2}$$

$$A_{window} = \frac{1}{4} n A_{ground} \tag{4.3}$$

$$A_{wall} = nh4\sqrt{A_{ground}} - A_{window} \tag{4.4}$$

Rijksdienst voor Ondernemend Nederland [55] published a document with representative building examples of the Netherlands, together with its building properties. From this document, it can be concluded that the heat transfer coefficients of different segments of the buildings depend on the buildings' energy label and type of window glazing. An overview of these heat transfer coefficients can be seen in Table 4.1 and Table 4.2. For the values corresponding with energy label A+, the minimum allowed values of 'Bouwbesluit 2012 online' of the Rijksoverheid [45] have been used for reference. The provided heat transfer coefficients can be used together with the area of the buildings segment of the case study to calculate $\sum UA$ of Equation 4.1.

Table 4.1: Overall heat transfer coefficient of building segments categorized by its energy label [55], [45]

	Energy label						
	A+	**B**	**C**	**D**	**E**	**F**	**G**
Ground floor [W/m²K]	0.29	0.36	0.64	1.28	2.33	1.72	2.44
Roof [W/m²K]	0.17	0.36	0.64	0.64	0.89	1.54	2.08
Outer wall [W/m²K]	0.22	0.36	0.64	0.64	1.45	1.61	2.22

Table 4.2: Overall heat transfer coefficient of different types of window glazing [55]

	Single-pane	Double-pane	HR++	Triple-pane
Windows [W/m^{2}K]	5.20	2.90	1.10	0.50

For heat loss to occur in a building, a temperature difference between the inside and outside of the building must be present. As stated before, the inside temperature of a building can be assumed to have a daily recurring profile influenced by the thermostat. The outside temperature, however, is highly fluctuating throughout the year. The KNMI [36] provides accurate measurements of the outside temperature at various weather stations in the Netherlands for the last 70 years. Figure 4.4 shows the temperature profile of the year 2014 measured at the weather station positioned most nearby the case study area. This data can be used to simulate an hourly temperature profile of the case study area.
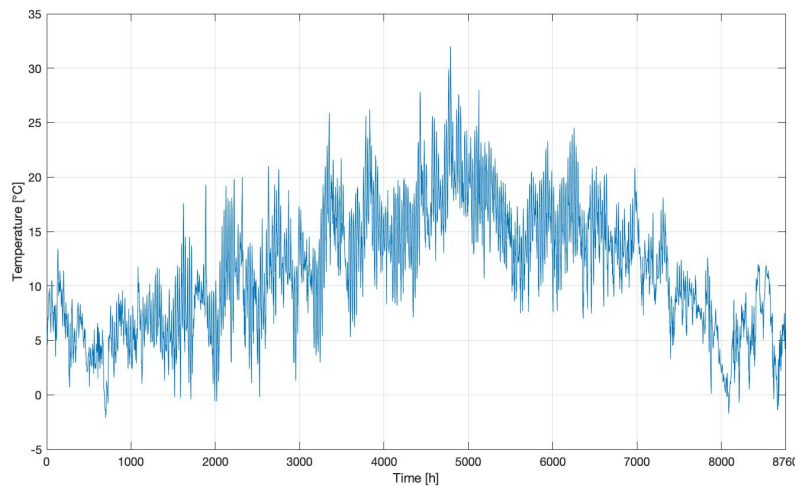

Figure 4.4: Hourly temperature profile of 2014 at weather station Berkhout, adapted from KNMI [36]

Besides envelope losses to the surroundings, also heat gains occur due to solar radiation through windows. Because these heat gains are considered to be significant, they are subtracted from the envelope losses to determine the space heating demand. To determine the solar radiation through windows, a couple of assumptions are made. The solar radiation through windows is dependent on the sun's rotation and the orientation of the windows. However, these orientations are not always known. Therefore, the windows of a building are viewed as vertical planes, of which the total window area is equally divided over the four sides of the building. It is also assumed that each side of the building faces one of the cardinal directions.

The EU Science Hub [21] has developed a photovoltaic geographical information system (PVGIS) tool, which provides full data sets of solar irradiance per hour for long periods at self-chosen locations. With this tool, the direct in-plane irradiance G_b [W/m^2] and diffuse in-plane irradiance G_d [W/m^2] on vertical planes facing certain cardinal directions can be determined. Together with the total area of the windows and the transmittance factor of the type of glazing, the solar heat gain through windows can be simulated by Equation 4.5. Here, $\dot{Q}_{sol}$ [W] is the heat flow through the window, A_{window} [m^2] is the total area of a buildings windows, g_{sol} [-] is the solar transmittance factor of the type of glazing of the window, G_b^N [W/m^2], G_b^E [W/m^2], G_b^S [W/m^2] and G_b^W [W/m^2] are the direct in-plane irradiances in the four cardinal directions and G_d^N [W/m^2], G_d^E [W/m^2], G_d^S [W/m^2] and G_d^W [W/m^2] are the diffuse in-plane irradiances in the four cardinal directions. Figure 4.5 illustrates an hourly solar heat gain profile per overall window area in the year 2014 in blue, together with its moving average with a sliding window of 24 hours in orange. Here, it can be seen that the profile is fluctuating on a daily basis, with a higher heat gain in summer than in winter.

$$\dot{Q}_{sol} = A_{window} g_{sol} \frac{1}{4} \left(G_b^N + G_b^E + G_b^S + G_b^W + G_d^N + G_d^E + G_d^S + G_d^W \right) \tag{4.5}$$
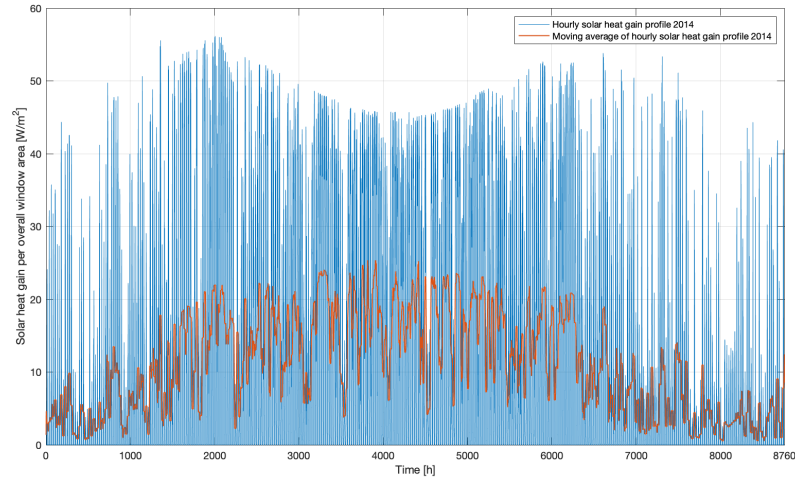
Figure 4.5: Hourly solar heat gain profile of 2014 in Heerhugowaard (blue) and its moving average (orange)

Because heating is usually not done when the outside temperature is above a certain threshold, the concept of heating degree days (HDD) is applied to assign this threshold. An HDD is the number of degrees that a day its average temperature is below a base value for the outside temperature, below which a building is assumed to need space heating. If the daily average temperature outside is above this base value, no heating is applied. According to the European Environment Agency, this base value is 15.5°C within Europe. The HDD profile of the year 2014 is shown in Figure 4.6. During the summer of 2014, the heating degree days equals zero quite some of the time. To make sure no heat demand is simulated at these moments, the condition is created where the heat demand is equal to zero when the heating degree day is zero.

Figure 4.6: Daily HDD profile of 2014 at weather station Berkhout, adapted from KNMI [37]

4.2.3. Consumer heat demand profile

The heat demand profile of the consumers can be simulated by the combined use of the DHW demand profile and space heating demand profile, discussed in Section 4.2. The heat demand of the consumer can now be calculated by Equation 4.6, where $\dot{Q}_{dem}$ [W] is the total heat demand per hour of the consumer, $\dot{Q}_{DHW}$ [W] is the DHW heat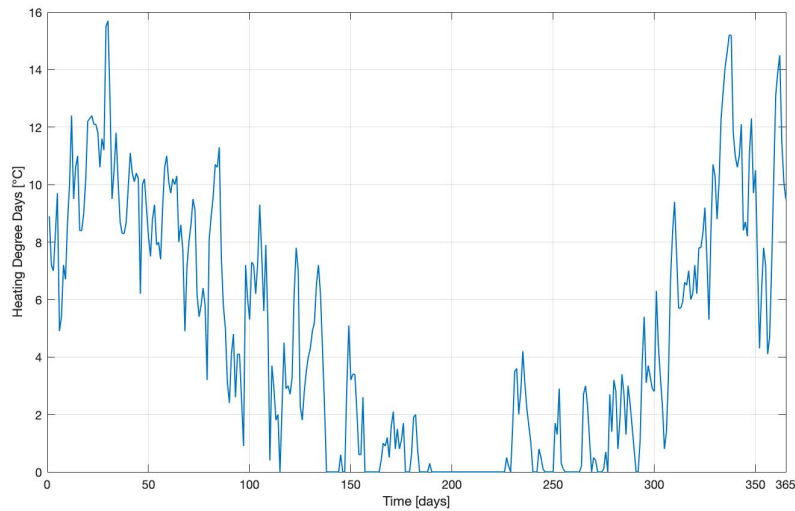 demand, $\dot{Q}_{loss}$ [W] is the heat loss to the surroundings, $\dot{Q}_{sol}$ [W] is the solar heat gain and T_{HDD} [°C] is the HDD. Figure 4.7 shows the heat demand profile of a consumer, simulated by the use of Equation 4.6 and the previously assigned profiles. Here, the blue line is the hourly heat demand profile in W and the orange line is a moving average, with a sliding window of 24 hours, computed of the hourly heat demand profile.

$$\dot{Q}_{dem} = \begin{cases} \dot{Q}_{DHW} + \dot{Q}_{loss} - \dot{Q}_{sol}, & \Delta T_{HDD} > 0 \ and \ \dot{Q}_{loss} > \dot{Q}_{sol} \\ \dot{Q}_{DHW}, & \Delta T_{HDD} = 0 \ or \ \dot{Q}_{loss} \leq \dot{Q}_{sol} \end{cases} \tag{4.6}$$
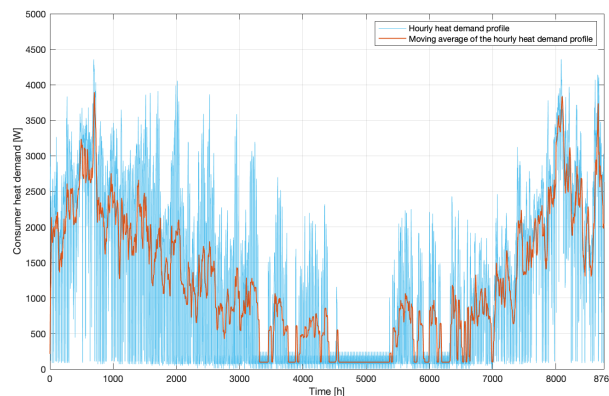

Figure 4.7: Consumer heat demand profile with the hourly heat demand of a consumer (blue) and its moving average (orange)

4.2.4. Validation

For validation of the consumer heat demand profile, a heat demand profile data set from ECN (Energieonderzoek Centrum Nederland, part of TNO) is used as a reference. This data set was provided to Resourcefully by ECN for a previous study and contains hourly heat demand data for various residential buildings with different characteristics and heating techniques. This data was generated by a heat demand profile model in which heat loss patterns and energy demand patterns for heat, gas and electricity are simulated on building level. The hourly heat demand profile concerns both space heating and raw DHW usage (without a buffer tank). By identifying the various inputs for the provided data set and using them as a baseline for the input for the Simulink model, the Simulink can be validated with regard to the model of ECN. The inputs for the chosen reference case are shown in Table 4.3.

Table 4.3: Comparison of inputs for the reference case and the Simulink model

Variables	ECN input	Model input	Model calculated
User surface [m^2]	103.1	103.1	
Roof surface [m^2]	65.4		51.9
Ground floor surface [m^2]	51.9	51.9	
External wall surface [m^2]	43.6		48.74
Window surface [m^2]	21.6		25.77
U value roof [W/m^{2}K]	0.89	0.89	
U value ground floor [W/m^{2}K]	2.33	2.33	
U value external wall [W/m^{2}K]	1.45	1.45	
U value window [W/m^{2}K]	2.9	2.9	
UA total [W/K]	305		312.5
Inside temperature	Iterative thermal mass and thermostat profile	Maintaining a comfortable 20.5°C	
Outside temperature	KNMI hourly profile of 1987	KNMI hourly profile of 1987	
Global irradiance	Irradiation 1987 on south facing vertical plane	Irradiation 2014 on south facing vertical plane	
g-value of the window [-]	0.7	0.7	-
Daily DHW demand [kWh]	4.3	-	2.99
Number of residents	-	2.3	-

The ECN model uses weighted mean values of a terraced house of 'Voorbeeldwoningen 2011 Bestaande bouw' [55] for the building its surface areas. Because these surface areas are not known for the case study area, a derivation is made for the required surface areas from the ground surface and user surface of a building, which are known values in the case study. In the last column of Table 4.3, the calculated surface areas for the reference case are shown. The inputs for the overall heat transfer coefficients of the buildings segments are the same for both the ECN model and the case study model and do also originate from 'Voorbeeldwoningen 2011 Bestaande bouw'. The inside temperature profile of the ECN model is approached by an iterative thermal mass calculation, where a fluctuating thermostat setting identifies the need for space heating. To minimize computational power, the Simulink model does not account for thermal mass because it has to be able to determine the space heating for various buildings. Also, the inside temperatures of the buildings equal a constant value of 20.5°C, as explained in Section 4.2.2. In both models, the outside temperature profile is provided by measurements of the year 1987 at KNMI's facility at 'the Bilt' [36]. This year was chosen by ECN for its model for its harsh winter to illustrate a worst-case scenario. The global irradiation profile used in the ECN model is provided by Meteonorm [43] and is based on historical data of the solar irradiation on a south-facing vertical plane in 1987 at 'the Bilt'. Because this data was not available for the Simulink model, the same kind of irradiation profile has been generated by PVGIS [21] for another year and has been scaled to meet the same annual irradiance. To compute the solar heat gain through the windows the same g-value of 0.7 for the glazing is used in both models, assuming double glazed windows. Finally, a daily DHW demand profile is used for the ECN model, which accounts for a total daily DHW demand of 4.3 kWh per building. Because the Simulink model does not account for a total daily DHW demand but for the number of residents of the building, the number of residents of the average household of 'Voorbeeldwoningen 2011 Bestaande bouw' is chosen as input.

In Figure 4.8 the hourly heat demand profiles from ECN (orange) and the Simulink model (blue) are compared. Here, it can be seen that the profile of ECN is much more fluctuating than the profile of the Simulink model. It is important to state that one very high peak and drop occur every 24 hours and only lasts for one hour. After that, the heating demand recovers to a less fluctuating profile. This behavior indicates that the ECN model probably has implemented a control system that boosts space heating demand in the morning and limits space heating demand in the evening.

Figure 4.8: Comparison of a heat demand profile for an example building generated by the Simulink model (blue) and ECN (orange)

To eliminate these two reoccurring high fluctuations in ECN's heat demand, a moving average of both of the profiles is computed. This way a better comparison can be made about the behavior of the overall profiles. These moving average profiles can be seen in Figure 4.9, where the Simulink model is again blue and the ECN model again orange. Here, it can be seen that the demand profiles have a similar fluctuating pattern. Overall the Simulink model has a slightly higher demand than the ECN model, but this can be explained by the fact that the inside temperature of the building is kept at 20.5°C at all times.
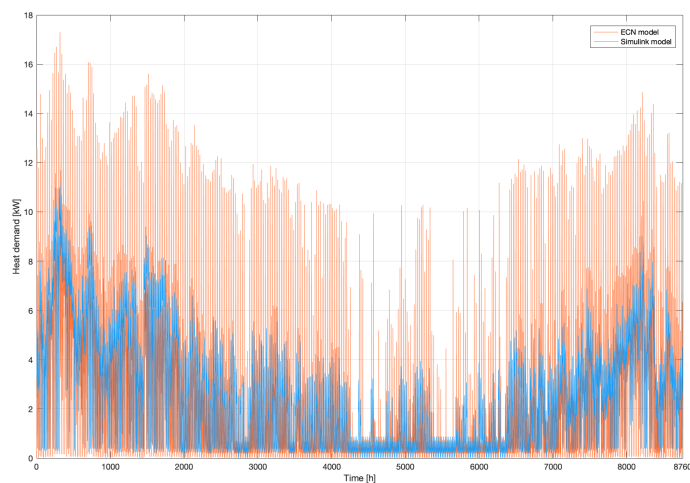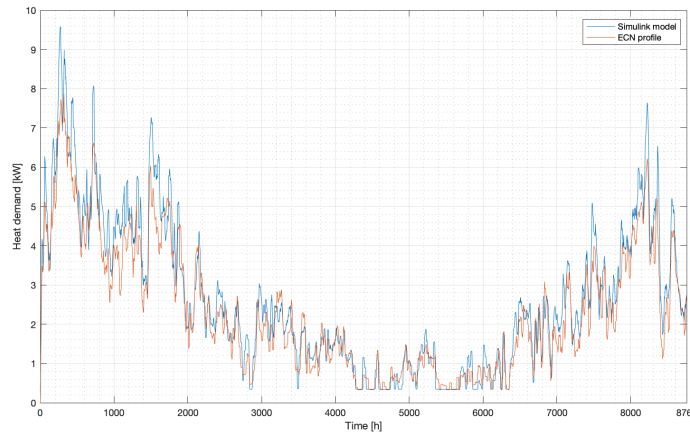
Figure 4.9: Comparison of a heat demand profile for an example building generated by the Simulink model (blue) and ECN (orange)

To assess the discrepancy between the models, its relative deviation can be calculated. This is done with both the moving average heat demand profiles and the total heat demand over the year. For the total heat demand, the relative deviation is calculated as shown in Equation 4.7, where σ_{rel} [%] is the relative deviation from the ECN model in percentages, Q_{sim} [kWh] is the total heat demand of the Simulink model and Q_{ECN} [kWh] the total heat demand of the ECN model. When assessing the relative deviation of the moving average profiles, the root-mean-square (RMS) is taken from the relative deviation to compute the deviation in one number. Also, instead of total heat demands, the heat demands per hour $\dot{Q}_{sim}$ [kW] and $\dot{Q}_{ECN}$ [kW] are used.

$$\sigma_{rel} = \frac{Q_{sim} - Q_{ECN}}{Q_{ECN}} \cdot 100 \tag{4.7}$$

Additional validation with real heat demand data can be done with 'Kleinverbruiksdata' from Liander [41], a Dutch utility company in Amsterdam. The 'kleinverbruiksdata' contains the average yearly gas usage of 2019 per postal code and its number of connections. The raw heat demand of the buildings can be deduced from the yearly gas usage as shown in Equation 4.8. Where, G_c [m^3] is the yearly gas consumption, HHV [kWh/m^3] is the higher heating value of natural gas and η_{HR107} is the HHV efficiency of an HR107 boiler, which equals 96% [7]. By replacing Q_{ECN} by Q_{gas} in Equation 4.7, the relative deviation of the total heat demand can again be computed.

$$Q_{gas} = G_c \cdot HHV \cdot \eta_{HR107} \tag{4.8}$$

Because the required data is not available for the case study area in Heerhugowaard, an area in Amsterdam called 'KNSM eiland' is used for the validation. This area is chosen because of another study done for Resourcefully which provides additional information about the buildings. The following four buildings, characterized by their different postal codes, have been chosen for their similarity with the building types in the case study area. Building 1019 LG is a tall flat with 22 stories containing a total of 112 apartments of energy label C. Building 1019 LH and building 1019 LJ are both relatively big apartment complexes with 6 stories containing a total of 52 apartments of energy label C. Building 1019 LK is a smaller apartment complex with 8 stories containing a total of 27 apartments of energy label B. The results of both validation methods can be seen in Table 4.4.

Table 4.4: Relative deviations of the model to reference data

Reference	Building	Energy label	σ_{rel} of total heat demand	RMS of σ_{rel} of moving average heat demand
ECN model	-	-	21.02%	3.67%
Liander	1019 LG	C	-15.47%	-
Liander	1019 LH	C	1.40%	-
Liander	1019 LJ	C	1.30%	-
Liander	1019 LK	B	2.75%	-

As can be seen in Table 4.4, some deviation is present between the Simulink model and its references. The behavior of the moving average heat demand seems to be matching the ECN model quite well, which indicates a reliable profile. The total heat demand of the ECN model and the Simulink model deviates a bit. However, the validation of the total heat demand of the model with the Liander data shows little deviation, which indicates that the model is working in the right magnitude. The heat demand of the buildings depends on the behavior of the residents as well, thus the outcome of models or measured data should not be taken too literally. Therefore, the fact that the Simulink model is operating in the right magnitude of the Liander data and matching the profile of the ECN model, indicates that the Simulink model gives a reliable approximation of the case study area.

4.3. District heating network

Besides the consumer heat demand, estimated in Section 4.2, the grid of the district heating and its components must be composed as well. As stated before, the model will be based on a bottom-up approach. Therefore, the ends of the DHN piping are taken as a starting point. Subsequently, the calculations follow the piping towards the heat source. Figure 4.10 shows a visualization of this approach. The calculations follow from left to right, beginning at the end of the pipe branch and updating the supply and return lines after each building, working towards a junction where other pipe branches meet. Because the calculation order is from left to right, the supply line is calculated in reverse. This is taken into account during all the calculations of the supply line. This section will address more details about this approach. The pipe end block, on the left of Figure 4.10, contains the initial conditions of the calculations. Its content is shown in Figure 4.11. Here, the initial mass flow, temperature and pressure of the supply and return lines are set. To maintain a sufficient velocity in the pipes at the end of the network, it is assumed that a small amount of mass flow bypasses the last building. This means that the end of the supply line will turn into the beginning of the return line. The bypass mass flow can be increased if the heat losses at the last consumers are too high.
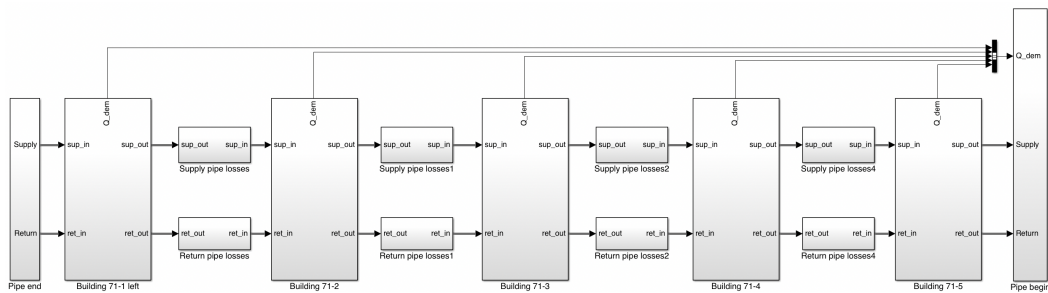

Figure 4.10: Visualization of the Simulink model approach, where the calculation order is from left to right and the supply line is calculated in reverse
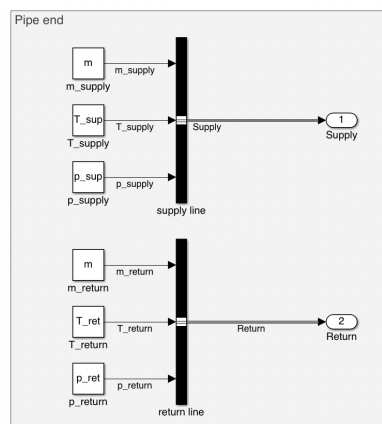

Figure 4.11: Content of the pipe end block of the Simulink model

4.3.1. Consumer supply set

In Section 4.2, the consumer heat demand is estimated. With this heat demand and the characteristics of the supply set, the heat demand that must be supplied by the network can be determined. For the MTDH scenarios, it is assumed that a counterflow plate HEX is used to supply the heat from the net to the consumer. This distribution results in the consumer supply set shown in Figure 4.12, where the grey block represents the counterflow plate HEX. It is assumed that no accumulation of mass is present in the supply set. Here Equations 4.9, 4.10 and 4.11 are identified, where $\dot{Q}_{dem}$ is the consumer's heat demand, $\dot{m}_{cons}$ [kg/s] the required mass flow to meet the consumer's heat demand, c_p [J/kgK] is the specific heat of the distributed water, ΔT [K] the temperature difference between the consumer's HEX in- and outlet, $\dot{m}_{sup,in}$ [kg/s] and $\dot{m}_{sup,out}$ [kg/s] are the in- and outlet mass flow of the supply line respectively, $\dot{m}_{ret,in}$ [kg/s] and $\dot{m}_{ret,out}$ [kg/s] are the in- and outlet mass flow of the return line respectively.

$$\dot{m}_{cons} = \frac{\dot{Q}_{dem}}{c_p \cdot \Delta T} \tag{4.9}$$

$$\dot{m}_{ret,out} = \dot{m}_{ret,in} + \dot{m}_{cons} \tag{4.10}$$

$$\dot{m}_{sup,out} = \dot{m}_{sup,in} - \dot{m}_{cons} \tag{4.11}$$
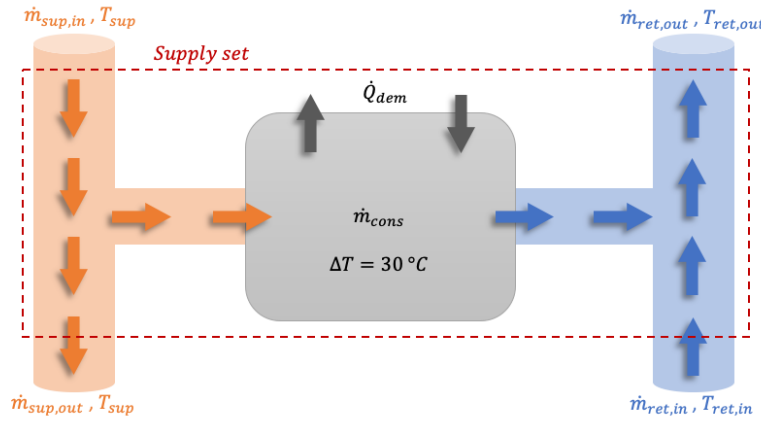
Figure 4.12: Consumer supply set connected to supply (orange) and return (blue) line of the DHN, with direction of flows

In the HEX, it is assumed that the consumer mass flow, flowing through the HEX, is cooled by 30 K, resulting in Equation 4.12, which evaluates the outlet temperature of the return line $T_{ret,out}$ [°C]. Here, $T_{ret,in}$ [°C] is the inlet temperature of the return line, T_{sup} [°C] is the temperature of the supply line, which stays constant throughout the supply set, and ΔT_{HEX} [°C] is the temperature drop across the HEX. The HEX in the model accounts for both the DHW and space heating demand.

$$T_{ret,out} = \frac{\dot{m}_{ret,in} T_{ret,in} + \dot{m}_{cons} \left(T_{sup} - \Delta T_{HEX} \right)}{\dot{m}_{ret,out}} \tag{4.12}$$

Finally, as shown in Equation 4.13, the pressure balance can be composed according to Bernoulli's principle at both the supply and the return line [72]. Here, ρ [kg/m^3] is the density of the distributed fluid, A_c [m^2] is the cross-section area of the pipes and p_{in} [Pa] and p_{out} [Pa] are the pressures, v_{in} [m/s] and v_{out} [m/s] are the velocities and $\dot{m}_{in}$ [kg/s] and $\dot{m}_{out}$ [kg/s] are the mass flows at the out and inlet of the control volume respectively.

$$p_{out} = p_{in} + \frac{1}{2}\rho \left(v_{in}^2 - v_{out}^2 \right) = p_{in} + \frac{1}{2\rho}\left(\frac{\dot{m}_{in}^2 - \dot{m}_{out}^2}{A_c^2} \right) \tag{4.13}$$

For the ULTDH scenarios, it is assumed that water-to-water heat pumps are implemented into the supply set to supply the heat from the net to the consumers. The space heating demand in the new buildings will be delivered by underfloor heating, which requires a supply temperature of 45°C and provides a return temperature of 35°C. According to the technical data sheet of Viessmann [69], when implementing a water-to-water heat pump with a supply temperature at the evaporator of 25°C and a supply temperature at the condenser of 45°C, a coefficient of performance (COP) of 6.32 can be assumed. For the DHW demand, a supply temperature of 65°C is required to prevent legionella growth [35]. Viessmann [69] assumes a COP of 3.63 for a heat pump with a supply temperature at the evaporator of 25°C and a supply temperature at the condenser of 65°C. In the case where these heat pumps are used, the required mass flow $\dot{m}_{cons}$ [kg/s] to meet the consumer's heat demand is determined by Equation 4.14. Here, $\sum \dot{Q}_{HP}$ [W] is the heat demand of the heat pumps, given by Equation 4.15, where $\dot{Q}_{dem,space}$ [W] and $\dot{Q}_{dem,DHW}$ [W] are the heat demands of space heating and DHW respectively and $COP_{45°C}$ [-] and $COP_{65°C}$ [-] are the COPs for the two different supply temperatures mentioned above. The electricity demand of the heat pumps can be determined by Equation 4.16. On the occasion where the old buildings do not have underfloor heating but are still using radiators, the heat pump will deliver a supply temperature of 65°C for space heating and both COPs should be $COP_{65°C}$.

$$\dot{m}_{cons} = \frac{\sum \dot{Q}_{HP}}{c_p \cdot \Delta T} \tag{4.14}$$

$$\sum \dot{Q}_{HP} = \dot{Q}_{dem,space} \cdot \left(\frac{COP_{45°C} - 1}{COP_{45°C}} \right) + \dot{Q}_{dem,DHW} \cdot \left(\frac{COP_{65°C} - 1}{COP_{65°C}} \right) \tag{4.15}$$

$$\sum P_{HP} = \frac{\dot{Q}_{dem,space}}{COP_{45°C}} + \frac{\dot{Q}_{dem,DHW}}{COP_{65°C}} \tag{4.16}$$

The Simulink model from Figure 4.10 contains building level blocks. The content of such a block is shown in Figure 4.13. From left to right, first the consumer heat demand is calculated as explained in Section 4.2. Then, the consumer mass flow is computed in the HEX area, according to Equation 4.9. Subsequently, in the supply set area, the inputs from the pipes and the building are acquired and translated into the required output. Here, Equations 4.10, 4.11 and 4.12 are used in the top grey subsystem to determine the outgoing flows and temperatures and Equation 4.13 is used in the bottom grey subsystem to determine the outgoing pressures. In the case of the ULTDH scenarios, not only the raw heat demand is obtained but also the electricity demand of the heat pumps.
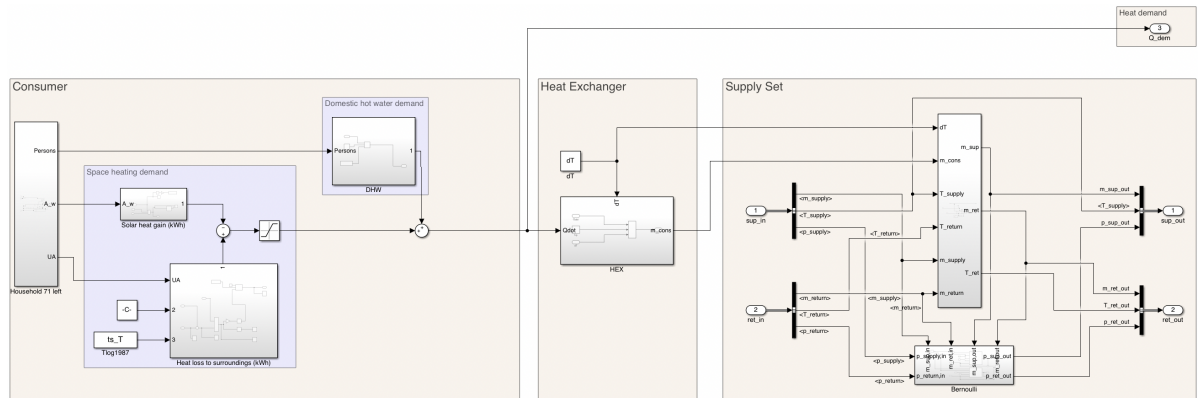
Figure 4.13: Simulink model on building level with from left to right: the consumer heat demand calculation, the required mass flow calculation and finally the supply and return pipe calculations

4.3.2. Grid

The grid of the DH network is dependent on the layout of the piping in the case study area. In Figure 4.14, the chosen layout of each scenario is shown. Here, the red lines represent the medium temperature (70°C/40°C) network originating from the MT heat source (the thick glowing red line) and the purple lines represent the ultra low temperature (25°C/12°C) network originating from the ULT heat source (the thick glowing purple line). For scenario 3, Figure 3.4 is used as a basis for the distribution of buildings connected to either the ULT or MTDH. To ensure easy installation and maintenance, the piping is mostly placed next to the street. Also, the number of connections to the existing ULT/MT heat sources have been minimized to one per heat source.

(a) Scenario 1: MTDH

(b) Scenario 2: ULTDH

(c) Scenario 3: Combined ULTDH/MTDH

Figure 4.14: Layout of the piping for the different scenario's of the case study, where the red lines represent the MTDH and the purple lines the ULTDH

The diameters of the pipes depend on the required mass flow in the grid and can be calculated with the use of Equation 4.17. Here, d [m] is the diameter of the pipe, $\dot{m}$ [kg/s] is the mass flow of water in the pipe, ρ [kg/m^3] is the density of the water and v [m/s] is the flow velocity of the water.

$$d = \sqrt{\frac{4 \cdot \dot{m}}{\rho \cdot v \cdot \pi}} \tag{4.17}$$

According to the ISSO publication 7 'Grondleidingen voor warmte- en koudetransport' [35], the flow velocity inside the pipe has a maximum allowed value of 3 m/s. Furthermore, the Plumbing Engineering Services Design Guide by the Institute of Plumbing [63] recommends a maximum allowed pressure drop per unit length of 400 Pa/m for the design of a DHN. The major pressure losses in the pipe can be approached by the Darcy-Weisbach equation shown in Equation 4.18. Here, $\frac{\Delta p_{major}}{L}$ [Pa/m] is the pressure drop per unit length in the pipe due to major losses, f [-] is the Darcy-Weisbach friction factor and ρ [kg/m^3] is the density and v [m/s] is the velocity of the distributed water. According to ISSO publication 7 [35], the minor losses in DHN can be approximated by roughly 10% of the piping's major losses. Therefore, a factor of 1.1 is implemented in Equation 4.19 for the total pressure drop per unit length $\frac{\Delta p_{tot}}{L}$ [Pa/m]. Furthermore, the flow will be assumed to always be turbulent ($Re_D > 3500$), resulting in the approximation of the Darcy-Weisbach friction factor by the Haaland equation shown in Equation 4.20. Here, ϵ [m] is the wall roughness of the pipe, d [m] is the inner diameter of the pipe and Re_D [-] is the Reynolds number of the flow. For a flow inside of a pipe, the Reynolds number can be evaluated by Equation 4.21. Here, v [m/s] is the flow speed, d [m] is the inner diameter of the pipe, ρ [kg/m^3] is the density and μ [kg/ms] is the dynamic viscosity of the fluid respectively.

$$\frac{\Delta p_{major}}{L} = \frac{f}{d} \cdot \frac{1}{2} \rho \cdot v^2 \tag{4.18}$$

$$\frac{\Delta p_{tot}}{L} = 1.1 \cdot \frac{\Delta p_{major}}{L} \tag{4.19}$$

$$\frac{1}{\sqrt{f}} \approx -1.8 \log \left[\frac{6.9}{Re_D} + \left(\frac{\epsilon/d}{3.7} \right)^{1.11} \right] \tag{4.20}$$

$$Re_D = \frac{v \cdot d \cdot \rho}{\mu} \tag{4.21}$$

Thermaflex, a supplier specialized in pipe systems for heating and sanitary applications, provides insulated pipes in various diameters. These pipes are made of a polybutene inner pipe, with a wall roughness of 0.01 mm, surrounded by a layer of polyolefin foam enclosed by an outer casing of polyethylene [66]. With the previously mentioned approach for finding the diameter for a pipe, a choice can be made out of Table 4.5, which contains the nominal diameters (DN) in which Thermaflex provides pipes. This table also contains the heat loss per unit length of the pipe for different diameters and distribution temperatures, which are used to estimate the heat loss in the model. The temperature drop in the pipes can be approximated by Equation 4.22. Here, ΔT_{loss} [K] is the temperature drop over the length of the pipe, $\frac{\dot{Q}}{L}$ [W/m] is the heat loss per unit length from Table 4.5, L [m] is the length of the pipe, c_p [J/kgK] is the specific heat of the medium and $\dot{m}$ [kg/s] is the mass flow of the medium.

$$\Delta T_{loss} = \frac{\frac{\dot{Q}}{L} \cdot L}{c_p \cdot \dot{m}} \tag{4.22}$$

Table 4.5: Heat loss per unit length in W/m for different inner diameters and distribution temperatures of pipings, adapted from 'Technical Data Sheet: Flexalen 600' [66]

DN [mm]	Heat loss per unit length [W/m]						
	Average distribution temperature [°C]						
	20	30	40	50	60	70	80
20	1.390	2.824	4.302	5.822	7.385	8.990	10.638
25	1.713	3.479	5.297	7.167	9.088	11.061	13.084
32	2.168	4.401	6.698	8.641	10.947	13.311	15.732
40	2.072	4.203	6.393	8.641	10.947	13.311	15.732
50	2.754	5.583	8.488	11.468	14.521	17.647	20.846
65	3.673	7.443	11.307	15.265	19.315	23.458	27.690
80	3.204	6.489	9.855	13.299	16.823	20.425	24.104
100-1	3.386	6.850	10.393	14.012	17.708	21.479	25.326
100-2	4.114	8.323	12.624	17.018	21.503	26.078	30.743

In Figure 4.10, the grid sections are represented by the pipe losses blocks. For both the supply and return lines, one of these blocks is implemented between consumers to simulate the losses in the grid. The content of a pipe loss block of the supply line is shown in Figure 4.15. The pipe losses block consists of an input section, seen on the left in yellow, and an output section, seen on the right in blue, and two sections that approach the temperature and pressure losses inside the pipe section. Because the direction of calculation of the Simulink model is upstream for the supply line, the temperature and pressure losses are added to the supply line. For the return line, the direction of calculation is downstream and the temperature and pressure losses are subtracted from the return line. The orange area calculates the temperature loss through the pipe section according to Equation 4.22. The purple area calculates the pressure drop across the pipe section, where four Matlab functions are implemented according to Equations 4.17, 4.18, 4.20 and 4.21. To assess the limits of the velocity and pressure drop of the supply and return line a control block is implemented. The control block asserts that the input signal is less than a static upper bound, which is equal to either the maximum velocity or the maximum pressure drop. If the upper bound is exceeded the block produces a warning signal to indicate a larger pipe diameter is needed.
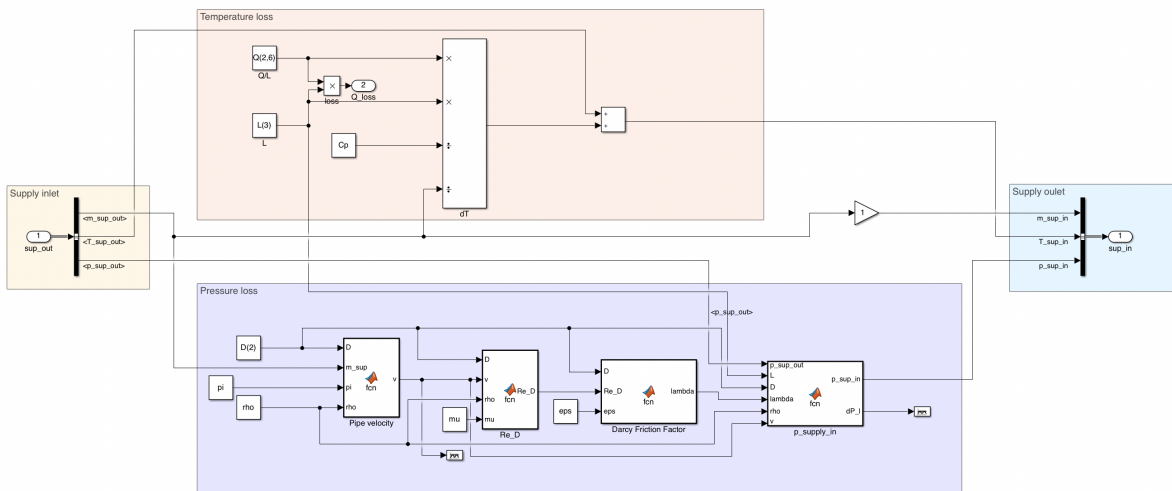

Figure 4.15: Content of a pipe losses block for the supply line in the Simulink model

4.4. Circulation pump

To transport the fluid in the DHN, centrifugal pumps are implemented between the heat source and the consumers. The pumps bring the supply line to the required pressure while receiving the return line. Centrifugal pumps are often used for these kinds of purposes because they can reach high flow rate capabilities with minimal maintenance. Because the required pump characteristics depend on the required pressure head and flow rate, different circulation pumps may be chosen for the different scenarios. First, the required delivery head is determined by the maximum difference between the pressure of the supply and return line in the scenario. Subsequently, with the maximum flow rate in the DHN of the scenario, the required pump capacity can be determined. With these two required characteristics determined, a choice is made according to the Cost Engineering manual of DACE [49]. This document contains multiple centrifugal pumps listed by their characteristics. The shaft power of the circulation pump P_{shaft} [W] can be calculated according to Equations 4.23 and 4.24. Here, $\dot{V}_{pump}$ [m^3/s] is the pumping capacity, p_{sup} [Pa] and p_{ret} [Pa] are the discharge and suction pressures respectively, η_{pump} [-] is the efficiency of the centrifugal pump, $\dot{m}_{sup}$ [kg/s] is the mass flow of the pumped medium and ρ [kg/m^3] is its density. According to the DACE manual, the default efficiency η_{pump} [-] for a centrifugal pump is assumed to be 0.75.

$$P_{shaft} = \frac{\dot{V}_{pump} \cdot \left(p_{sup} - p_{ret}\right)}{\eta_{pump}} \tag{4.23}$$

$$\dot{V}_{pump} = \frac{\dot{m}_{sup}}{\rho} \tag{4.24}$$

With the calculated shaft power and Equation 4.25, an electric motor can be chosen from the manual which will be used as the power supply for the pump. In Equation 4.25, P_{shaft} [W] is the required shaft power that must be provided, P_{el} [W] is the required electric power that must be supplied to the electric motor and η_{emotor} [-] is the efficiency of the electric motor. According to the DACE manual [49], the default efficiency η_{emotor} [-] is assumed to be 0.8 for an electric motor .

$$P_{el} = \frac{P_{shaft}}{\eta_{emotor}} \tag{4.25}$$

When the decision for the pump and the electric motor has been made, the manual can be used to provide the price of the required pumps and electric motors. Also, Equations 4.23 and 4.25 can later be used to determine the electricity demand of the motor for the yearly pumping profile, after accounting for the efficiency of the electric motor. This gives an estimate of the operation costs of the pump.

4.5. Heat source

As mentioned in Section 3, two types of heat sources are available in the case study area. For the MTDH scenarios, an MT heat net can be used as the source of heat. This heat net can supply heat at a temperature of 70 to 90°C at the place of connection shown in Figure 4.14. The heat of this MT heat net is generated by a biomass and waste incineration plant, corresponding to a CO_2 emission of 10.5 kg/GJ, according to its supplier [31]. It is assumed that this heat source can easily supply the required peak loads of the case study. However, to minimize peak loads in the MT heat net and its sources, it may be beneficial to implement storage to absorb the fluctuating demand of the end-user. This way an almost constant baseload can be provided by the heat source.

The other option for the heat source of the DHN can be the use of a collective ultra low temperature waste heat net which can supply heat at a temperature of 25 to 30°C. This collective waste heat net connects industrial and residential complexes, is able to transfer the surplus of heat between different participants and is currently under development from a small to bigger scale [38]. It is possible to connect this collective waste heat net to the ULTDH scenarios as a source. Because this heat net depends on the fluctuating surplus of its users and a small number of storage principles are employed, it is assumed it is required to implement an ATES in the ULTDH scenarios. An exception will be made for the scenarios without any ATES, where for simplicity reasons it is assumed that the peak loads can be delivered by the collective heat net. This is done to illustrate the difference in peak loads on the heat source. However, it is probably not realistic for the collective heat net to supply the highly fluctuating end-user demand in the case study. According to CE Delft [12], the CO_2 emissions related to (industrial) waste heat, without co-firing, are assumed to be 8.8 kg/GJ.

4.6. Storage

In order to flatten the load on the heat sources and to store heat during low demand periods, storage facilities are applied in the scenarios. The location of the storage facility will always be between the heat source and the first consumer of the DHN. This way, the heat source can benefit from the dampening behavior of the storage facility on the heat demand of all the consumers. The storage facility consists of an ATES system with an HP and a buffer TTES. The ATES system operates with multiple well pumps, pumping in the desired direction. Due to startup time and increased risk of clogging in the wells, it is not efficient to switch between pumping directions. For that reason, a buffer TTES will be implemented in the storage facility to absorb the short-term fluctuation in the heat demand, while the ATES system is employed to absorb the long-term fluctuation. Two process and instrumentation diagrams (P&ID), for the MT scenario, of the connection of the storage facility to the DHN and heat source, as well as their mass flows, are given in Figure 4.16. Here, the red arrows represent the supply lines and the blue arrows the return lines from the DHN. Figure 4.16 shows (a) the P&ID during peak moments, where the ATES system and buffer TTES are both discharging and (b) the P&ID during moments of low demand, where the ATES system and buffer TTES are both charging. It is also possible for the ATES system and buffer TTES to (dis)charge separately from each other.
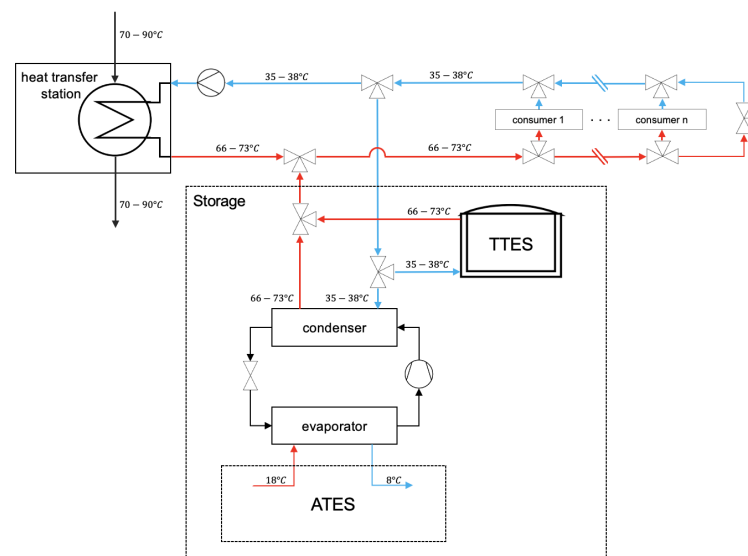
(a) Storage discharging
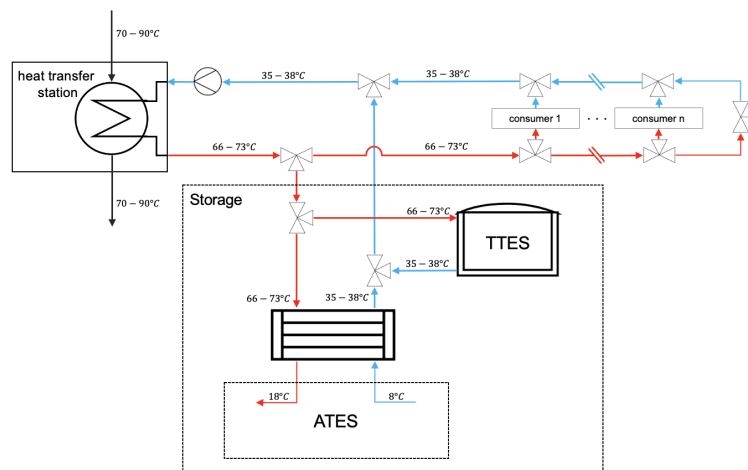
(b) Storage charging

Figure 4.16: P&ID for the MT scenarios, with (a) the storage discharging phase and (b) the storage charging phase

4.6.1. Method of calculation

Because the DHN demand profile is fluctuating on a daily and seasonal basis, the related total storage profile is expected to behave in the same manner. To be able to apply the buffer TTES for short-term storage and the ATES system for long-term storage, it is key to determine the two different types of fluctuation. For this application, a method is used which employs a filter technique. This filtering technique is used to separate the short- from the long-term fluctuations in the storage profile. Before this technique can be used, an estimation must be made for the storage profile, which is based on an estimated constant source profile that originates from the mean of the demand profile. A flowchart of this method can be seen in Figure 4.17, which will be further explained below. Following this method, the power profiles of the short- and long-term storage systems can be calculated, as well as an updated source profile that accounts for the characteristics of the storage facility.
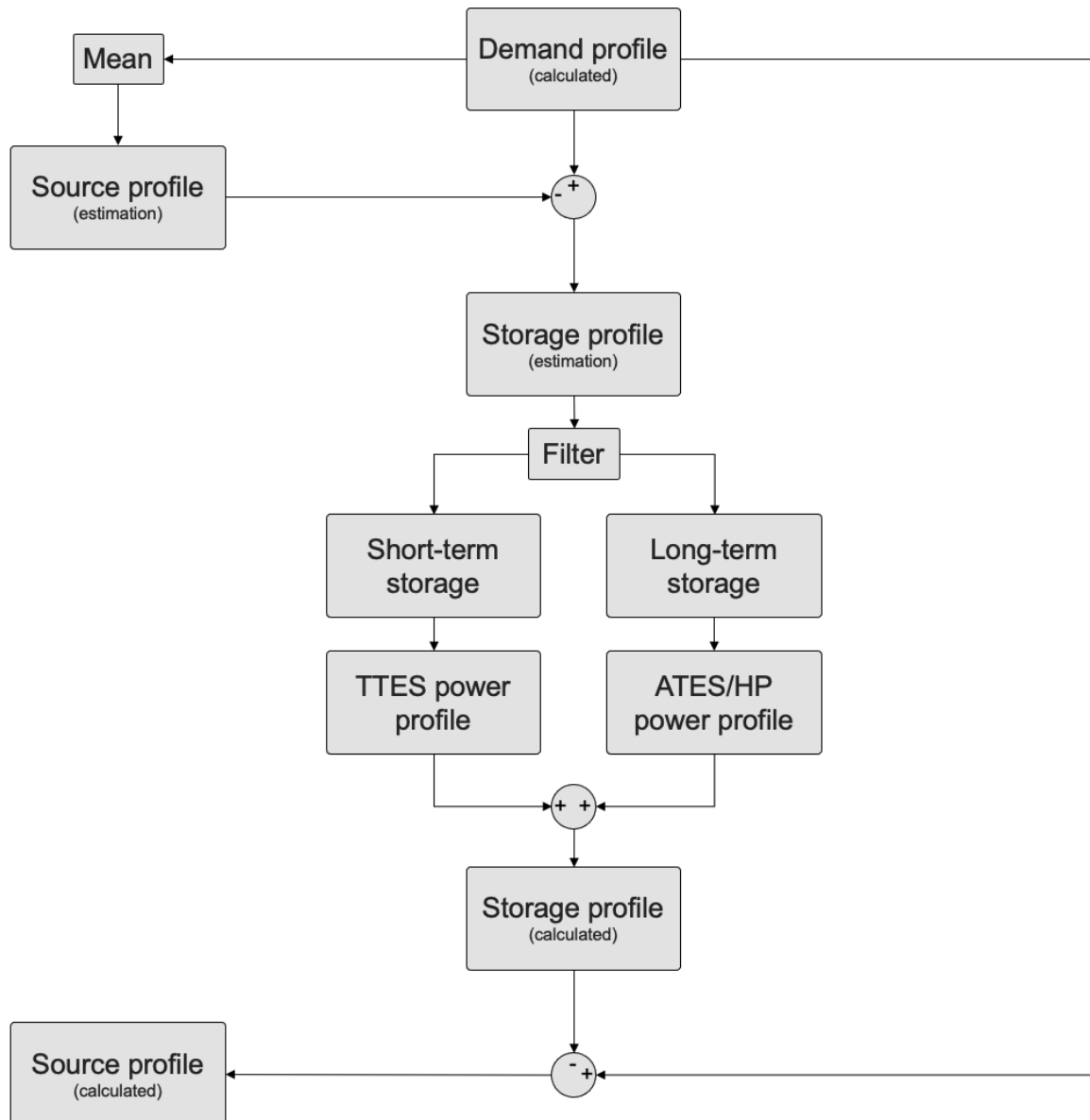

Figure 4.17: Flowchart of the method for the storage technique used in the case study

Foremost, the demand profile of the DHN $\dot{Q}_{dem,calc}$ [W] is calculated by the Simulink model. In the scenarios where storage is applied, the power of the source is initially estimated to be constant throughout the year, while meeting the total heating demand. This is done by assuming the initially estimated source profile $\dot{Q}_{source,est}$ [W] to be equal to the mean of $\dot{Q}_{dem,calc}$ [W], shown in Equation 4.26. In real life, the total yearly heat demand of the case study area is assumed to be predicted in the right magnitude, facilitating this approach. By subtracting the source profile $\dot{Q}_{source,est}$ [W] from the demand profile $\dot{Q}_{dem,calc}$ [W], the potential storage profile $\dot{Q}_{storage,est}$ [W] is found, shown in Equation 4.27.

$$\dot{Q}_{source,est} = mean\left(\dot{Q}_{dem,calc}\right) \tag{4.26}$$

$$\dot{Q}_{storage,est} = \dot{Q}_{dem,calc} - \dot{Q}_{source,est} \tag{4.27}$$

As mentioned before, the storage profile is fluctuating on both a daily and seasonal basis. To improve the performance of the storage techniques, it is beneficial to separate the short- from long-term fluctuations in the storage profile. This way, the right storage technique can be used for the right type of storage. For this application, a filter technique is used which dampens the short-term fluctuation by calculating a centered moving average of the storage profile, with a sliding window of the previous 12 and the next 12 hours, resulting in the remaining long-term fluctuating storage profile, as shown by Equation 4.28. This method assumes a perfect prediction of the network behavior for the upcoming 12 hours. This perfect prediction would be difficult to obtain in a real system, but such predictions are currently already made quite accurately. Therefore, to identify the short- and long-term storage profiles, according to which an estimate can be made for the required characteristics of the storage units, this method is assumed to be realistic and gives a close to perfect estimate. Furthermore, it is assumed that a control system is employed, which is responsible for the implementation of the predicted consumer heat demand in the (dis)charging behavior of the storage facility. By calculating the difference between the storage potential and the long-term storage profile, the short-term storage profile is found, as shown by Equation 4.29. A representation of this filter technique for a sample profile is shown in Figure 4.18.
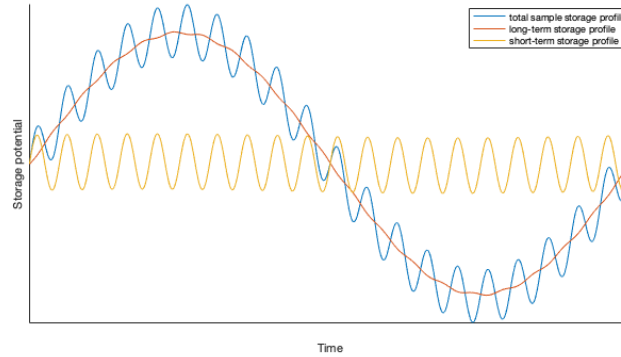
Figure 4.18: Visualization of the filter technique used to separate short-term fluctuation (yellow) and long-term fluctuation (red) for a sample storage profile (blue)

In Figure 4.18, the blue line represents a sample storage profile, which possesses both short- and long-term fluctuation. By applying a moving average of the sample profile, as mentioned earlier, the red line is found. The red line represents the long-term fluctuation segment of the sample profile, where the short-term fluctuation has been dampened. Subsequently, the difference between the sample profile (blue) and the long-term fluctuation segment (red) is calculated, resulting in the remaining short-term fluctuation segment of the sample profile shown in the figure as the yellow line. By applying this filter technique in the case study, with Equations 4.28 and 4.29, the short- and long-term segments of the storage potential can be distinguished from each other.

$$\dot{Q}_{storage,long-term} = movmean\left(\dot{Q}_{storage,est}, 24\right) \tag{4.28}$$

$$\dot{Q}_{storage,short-term} = \dot{Q}_{storage,est} - \dot{Q}_{storage,long-term} \tag{4.29}$$

With the calculated short- and long-term storage profile, the power profile of the buffer TTES $\dot{Q}_{TTES}$ [W] and ATES/HP system $\dot{Q}_{ATES/HP}$ [W] can be determined respectively. This approach will be discussed in the following section. After the power profiles of the buffer TTES and the ATES/HP system have been determined correctly, they can be added together to create an updated storage profile $\dot{Q}_{storage,calc}$ [W], shown by Equation 4.30. By subtracting this updated storage profile from the calculated demand profile of the DHN, the calculated source profile $\dot{Q}_{source,calc}$ [W] is found, which accounts for the buffer TTES and ATES/HP characteristics, as described by Equation 4.31.

$$\dot{Q}_{storage,calc} = \dot{Q}_{ATES/HP} + \dot{Q}_{TTES} \tag{4.30}$$

$$\dot{Q}_{source,calc} = \dot{Q}_{dem,calc} - \dot{Q}_{storage,calc} \tag{4.31}$$

4.6.2. Storage profiles of the TTES and ATES

After identifying the short- and long-term components of the storage profile, as explained in the previous section, they can be used together with the characteristics of the respective storage unit to determine the power profiles of both the buffer TTES and the ATES/HP system.

It is assumed that the TTES will support perfect stratification and insulation, maintaining a gradual increase of the water temperature from its bottom to the top, as shown in Figure 4.22, without heat losses to the surroundings. To simplify the model significantly, it is also assumed that the buffer TTES is able to deliver in the required temperature ranges given in Figure 4.16. As a result of these assumptions, the power profile of the TTES $\dot{Q}_{TTES}$ [W] is equal to the short-term segment of the storage profile, as shown in Equation 4.32 and explained in Section 4.6.1. Because the TTES can either be operated in charging or discharging mode, its power is either negative for charging and positive for discharging, which is illustrated in Figure 4.20c.

$$\dot{Q}_{TTES} = \dot{Q}_{storage,short-term} \tag{4.32}$$

When computing the power profile of the ATES/HP system, the characteristics of the components of the system have to be taken into regard. As shown in Figure 4.16, the heat is transferred from the DHN to the ATES directly via an HEX during the charging phase. This is in contrast to the discharging phase, where the heat is transferred from the ATES to the DHN via an HP. The HP employs the ATES as a heat source and heats the return line of the DHN to the required temperature of the supply line when necessary. The temperature of the cold well of the ATES $T_{well,cold}$ is assumed to be 8°C and the temperature of the hot well $T_{well,hot}$ is assumed to be 18°C. Moreover, the temperature difference of the evaporator ΔT_{evap} [K] and the source temperature of the HP T_C [K] are shown by Equations 4.33 and 4.35. For the condenser, the in- and outlet temperatures are equal to the return and supply temperatures T_{ret} and T_{sup}, which fluctuate slightly during the year. The HP sink temperature T_H [K] and the condenser temperature difference ΔT_{cond} [K] are given by Equations 4.34 and 4.36. Subsequently, the theoretical maximum efficiency COP_{carnot} [-] and the COP [-] of the heat pump can be calculated with Equation 4.37. Here, η_{HP} [-] is the system efficiency, which equals around 40% for water-to-water HPs with refrigerant R410A, according to technical data from Viessmann [69]. As the COP is dependent on the fluctuating T_{ret} and T_{sup}, the COP will be fluctuating as well.

$$\Delta T_{evap} = T_{well,hot} - T_{well,cold} \tag{4.33}$$

$$\Delta T_{cond} = T_{sup} - T_{ret} \tag{4.34}$$

$$T_C = \frac{T_{well,hot} + T_{well,cold}}{2} \tag{4.35}$$

$$T_H = \frac{T_{sup} + T_{ret}}{2} \tag{4.36}$$

$$COP = \eta_{HP} \cdot COP_{carnot} = \eta_{HP} \cdot \frac{T_H}{T_H - T_C} \tag{4.37}$$

Figure 4.19 shows a flowchart of the ATES/HP system and its power profile, which is dependent on the long-term segment of the previously determined storage profile. Here, it can be seen that the power profile of the ATES/HP system is divided into a discharge and charge phase. First, the (dis)charging profiles will be determined, after which the power profile of the ATES/HP system is calculated. Because the (dis)charging phases are dependent on the previously calculated long-term storage profile and the ATES system must be able to deliver according to this profile, the power of the discharge phase of the ATES system $\dot{Q}_{discharge}$ [W] equals the positive parts of the long-term storage profile $\dot{Q}_{storage,long-term}$ [W], as shown in Equation 4.38. Subsequently, the ATES system must be able to deliver the positive part of the previously calculated long-term storage profile but suffers from thermal losses and the influence of the HP. For the ATES system to be able to deliver the calculated discharge phase, the ATES system must be charged properly, taking into account these thermal losses and the influence of the HP. This results in the power of the charge phase of the ATES system $\dot{Q}_{charge}$ [W] shown in Equation 4.39, where, the power of the charge phase is determined by the negative values of the long-term storage profile $\dot{Q}_{storage,long-term}$ [W], the thermal recovery factor of the ATES system η_{ATES} [-] and the COP [-] of the HP. For the ATES in the case study a thermal recovery factor of $\eta_{ATES} = 0.8$ is assumed, because this is considered to be a common factor for low temperature ATES in the Netherlands according to Bakr et al.[4]. By combining the power of the charging $\dot{Q}_{charge}$ and discharging phase $\dot{Q}_{discharge}$ of the ATES/HP system, the total power profile of the ATES/HP system $\dot{Q}_{ATES/HP}$ [W] can be determined, as shown by Equation 4.40. This power profile of the ATES/HP system is either positive or negative, depending on its (dis)charging mode, which is illustrated in Figure 4.20b. Additionally, the electricity consumption of the employed HP can be determined by Equation 4.41.

$$\dot{Q}_{discharge} = \begin{cases} \dot{Q}_{storage,long-term}, & \dot{Q}_{storage,long-term} > 0 \\ 0, & \dot{Q}_{storage,long-term} \le 0 \end{cases} \tag{4.38}$$

$$\dot{Q}_{charge} = \begin{cases} \frac{\dot{Q}_{storage,long-term}}{\eta_{ATES}}\left(1 - \frac{1}{COP}\right), & \dot{Q}_{storage,long-term} < 0 \\ 0, & \dot{Q}_{storage,long-term} \ge 0 \end{cases} \tag{4.39}$$

$$\dot{Q}_{ATES/HP} = \dot{Q}_{discharge} + \dot{Q}_{charge} \tag{4.40}$$

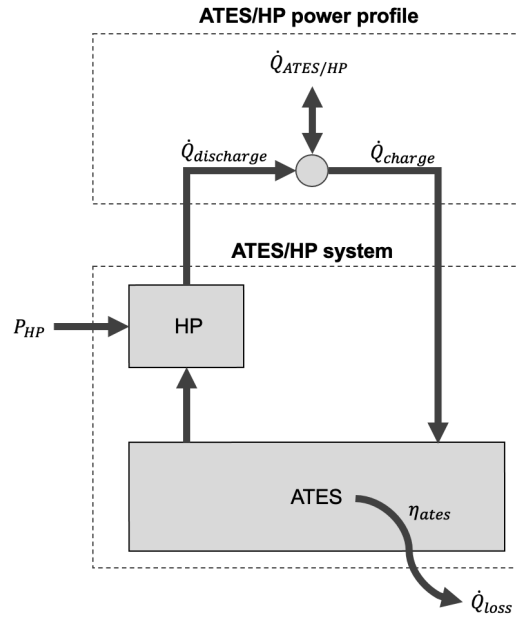$$P_{HP} = \frac{\dot{Q}_{discharge}}{COP} \tag{4.41}$$

Figure 4.19: Flowchart of the ATES/HP system with in- and outgoing flows

Figure 4.20 gives an illustration of the applied filter technique, explained in Section 4.6.1, applied to the MTDH scenario 1b. In the figure, the top graph (a) depicts the power profile of the total storage facility $\dot{Q}_{storage,calc}$ [W], which is determined by the difference of the estimated supply of the heat source and the heat demand of the DHN. Here, the short- and long-term fluctuations are both still present and must be separated. The middle graph (b) depicts the power profile of the ATES/HP system $\dot{Q}_{ATES/HP}$ [W], which accounts for the long-term fluctuations. Here, the filter technique and the ATES/HP characteristics explained in Section 4.6.1 and 4.6.2 are applied and accounted for to predict the long-term storage behavior for the upcoming 12 hours. Subsequently, the same is done but for the short-term fluctuation and the TTES, resulting in the power profile of the buffer TTES $\dot{Q}_{TTES}$ [W] depicted in Figure 4.20c, which accounts for the short-term fluctuations. In the three profiles of the figure, the charging phase is occurring when the power is negative and the discharging phase when the power is positive. The total storage power profile contains a very high daily fluctuation and the respective TTES power profile must account for these peaks. Therefore, the TTES must be able to collect and deliver relatively high loads. However, because these fluctuations occur a couple of times a day and cancel each other out, the amount of stored heat is not unreasonably high and the TTES is assumed to be able to handle these high fluctuations. Alternatively, the ATES only accounts for the long-term fluctuation and possesses a much more constant power. Therefore, an enormous amount of heat can accumulate during the charging phase and be slowly discharged when needed. During autumn and spring, problems can occur when the ATES is on the boundary of (dis)charging. In practice, control systems may be implemented which prevent this behavior. However, because the ATES only switches between its (dis)charge phase a few times a year with plenty of time in between and to simplify the model, it is assumed that this behavior does not cause any major problems and that the ATES functions appropriately.
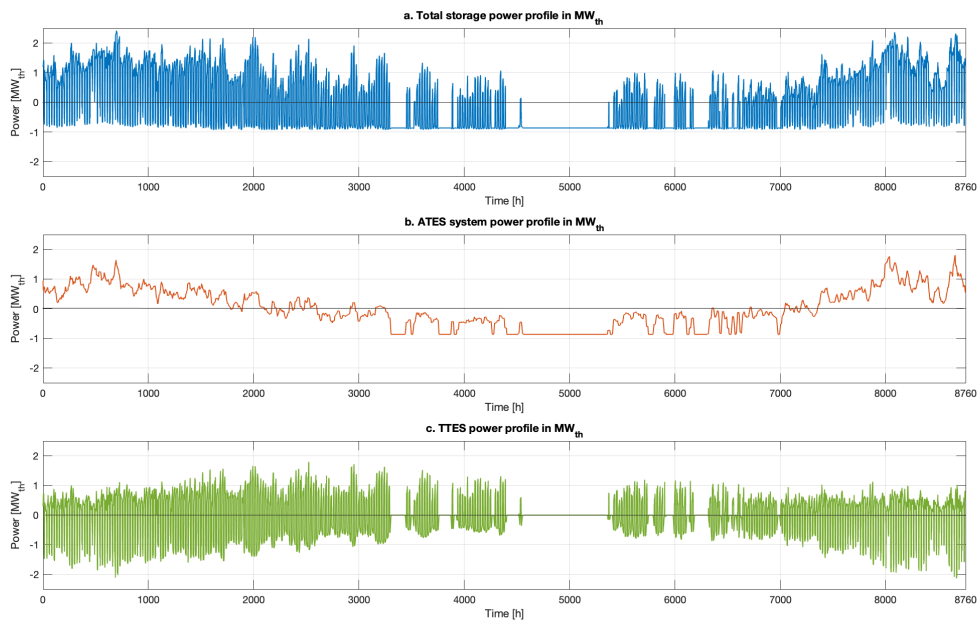

Figure 4.20: Power profiles for the total storage facility (a), the ATES system (b) and the buffer TTES (c) for the MT scenario 1b during one year

4.6.3. Storage capacities of the TTES and ATES

By performing a cumulative sum of the power profile of the buffer TTES and the power profile of the ATES, the storage capacity profiles Q_{TTES} [Wh] and Q_{ATES} [Wh] are calculated. These profiles represent the amount of energy stored in the respective storage unit. The total required storage capacity for the buffer tank $Q_{TTES,tot}$ [Wh] or the ATES $Q_{ATES,tot}$ [Wh] can be determined by finding the difference between the minimum and the maximum value of the storage capacity profile Q_{TTES} or Q_{ATES}. Both the storage capacity profiles will be adjusted in such a way that the storage unit is filled for 50% of its capacity at the beginning of the year, which is illustrated in Figure 4.21. During summer, when the demand for heat is low, the TTES is not used and the stored heat remains constant. In reality, this stored heat would be discharged before summer because it would otherwise slowly dissipate. However, to significantly simplify the model and because the amount of stored heat is very small compared to the yearly heat supply, it is assumed that a full discharge is not necessary.
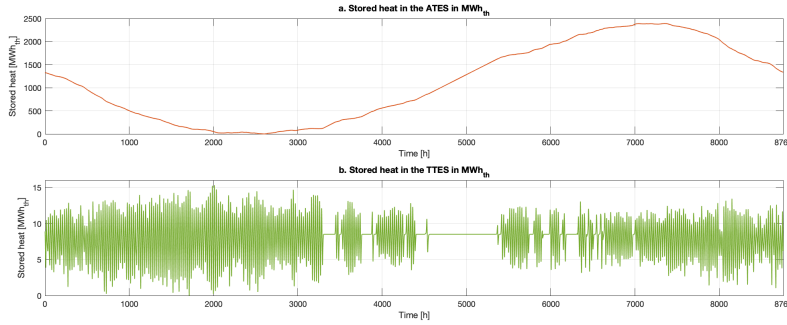
Figure 4.21: Storage capacity profiles for the ATES system (a) and the buffer TTES (b) for the MT scenario 1b during one year

With the required storage capacity profile of the buffer tank, the volume of the tank can be determined. Following Equation 4.42, the amount of stored water m_{TTES} [kg] can be obtained. Here, $Q_{TTES,max}$ [J] is the maximum amount of stored heat of the buffer tank, c_p [J/kgK] is the specific heat of the stored water, T_{sup} [K] and T_{ret} [K] are the temperatures of the supply and return line respectively. Subsequently, the required volume of the buffer tank V_{TTES} [m^3] can be calculated with Equation 4.43. Here, ρ_w [kg/m^3] is the density of the stored water. The buffer tank will be viewed as a cylinder with height L_{TTES} [m] and radius r_{TTES} [m]. The height L_{TTES} is assumed to be 5 m and radius r_{TTES} is calculated according to Equation 4.44.

$$m_{TTES} = \frac{Q_{TTES,max}}{c_p \cdot \left(T_{sup} - T_{ret}\right)} \tag{4.42}$$

$$V_{TTES} = \frac{m_{TTES}}{\rho_w} \tag{4.43}$$

$$r_{TTES} = \sqrt{\frac{V_{TTES}}{\pi \cdot L_{TTES}}} \tag{4.44}$$
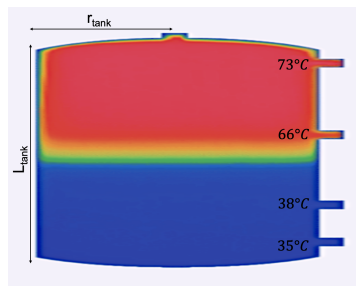
Figure 4.22: Visualization of the buffer TTES, with its dimensions and its temperature at different levels of stratification for the MT scenario, adapted from Fröling [26].

The dimensions of the ATES can be determined in the same manner. The amount of stored water m_{ATES} [kg] can be obtained by Equation 4.45. Here $Q_{ATES,tot}$ [J] is the total capacity of the ATES, c_p [J/kgK] is the specific heat of the stored water, ΔT_{ATES} [K] is the temperature difference of the hot and cold well of the ATES. Subsequently, the required storage volume of the ATES V_{ATES} can be calculated with Equation 4.46. Here, ρ_w [kg/m^3] is the density of the stored water. Finally, the ATES wells will be viewed as cylinders embedded between the two impermeable layers which confine the aquifer. Therefore, the height of the cylinder is equal to the length of the aquifer. With Equation 4.47, the hydraulic radius of the ATES wells can be calculated. Here, ϕ [-] is the porosity of the ground in the aquifer and L_{ATES} [m] is the screen length of ATES. According to Bloemendal and Hartog [6], a common value for the porosity of sandy aquifers in the Netherlands is $\phi =$ 0.3. Therefore, this is assumed to be the porosity for the ATES in the model.

$$m_{ATES} = \frac{Q_{ATES,tot}}{c_p \cdot \Delta T_{ATES}} \tag{4.45}$$

$$V_{ATES} = \frac{m_{ATES}}{\rho_w} \tag{4.46}$$

$$r_{ATES} = \sqrt{\frac{V_{ATES}}{\phi \cdot \pi \cdot L_{ATES}}} \tag{4.47}$$

The ATES employs well pumps in order to pump the stored water up and down in the wells, as shown in Figure 4.23. These well pumps use electricity to deliver pumping power in order to pump the required water around. According to Sommer et al. [59], the electric power of the well pumps of an ATES can be calculated by Equation 4.48. Here, P_{well} [W] is the required electrical power of the well pump, which accounts for pumping the groundwater from and in the well. Also, n [-] is the number of wells, $\dot{V}_{well}$ [m^3/h] is the volume displacement inside the well and E_p [Wh/m^3] is the electrical energy needed to pump one m^3 of groundwater in or out the well. The calculated electricity usage of the well pumps accounts for the total pumping power of the well pumps, including pressure losses in the HP and pipes and pressure drop through the porous aquifer. As provided by IF-Technology, an engineering consultancy firm specialized in geothermal energy, and reported by Sommer et al. [59], the E_p for an ATES in the Netherlands can be assumed to vary from 0.1 to 0.2 kWh/m^3. This electricity usage is mostly dependent on the (dis)charging behavior of the wells of the ATES system and its interaction with the aquifer and is only for a small part dependent on the frictional losses in the rest of the system. Thus, the E_p factor remains reliable, even when an ATES system employs deeper wells and/or traverses larger distances. In the case study, the characteristics of the ATES systems and their surroundings are quite similar to the system proposed by Sommer et al. Therefore, it can be assumed that the E_p in the case study is in the same range as proposed by Sommer et al. and equals an average value of 0.15 kWh/m^3. By combining the electric power of the well pumps P_{well} and the electric power of the HP P_{HP}, which is described in Equation 4.41, the total electric power of the ATES system is obtained, as shown in Equation 4.49.

$$P_{well} = n \cdot \dot{V}_{well} \cdot E_p \tag{4.48}$$
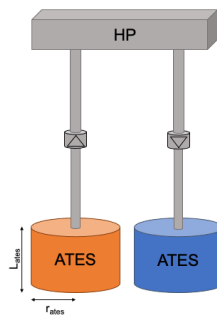
$$P_{ATES} = P_{well} + P_{HP} \tag{4.49}$$

Figure 4.23: Visualization of the ATES system with HP, well pumps and reservoirs

4.7. Air-to-water heat pumps

In the all-electric reference scenario, instead of using a DHN to supply the households with heat, air-to-water HPs are employed. Here, each household is equipped with an individual HP. Air-to-water HPs utilize the outside air as a heat source and are therefore dependent on the outside temperature. Because the outside temperature fluctuates throughout the year, the COP of these HPs is also fluctuating. According to the technical data about air-to-water HPs from Viessmann [70], shown in table 4.6, it can be assumed that COPs of equivalent HPs will be the range as displayed. In the Simulink model, the HPs are modeled in the same way as described for the ULTDH scenarios in Section 4.3.1, with the following exception. Because the all-electric scenario employs air-to-water HPs, no supply set is needed to feed the HP with hot water because the HP utilizes the outside air. Instead, the temperature of the outside air is used as an input to determine the fluctuating COP at the given time. Subsequently, the COP is determined by a 1-D lookup table in the Simulink model, which either inter- or extrapolates to calculate the specific COP corresponding to the outside temperature in regard to the given COP values in table 4.6. With the calculated COP values, the electricity demand of the air to water HP can be determined in the same manner as for the water to water HPs by Equation 4.16 in Section 4.3.1. Figure 4.24 gives a visualization of the block which executes this calculation in the Simulink model. Here, input 1 and 2 represent the DHW and space heat demand of a household respectively, input 3 represents the outside and output 1 represents the final electricity demand of the HP. The 'air-to-water HP' block replaces the 'HEX' and 'supply set' blocks in the Simulink model, which are shown in Figure 4.13 in Section 4.3.1.

Table 4.6: COP of an air to water HP for outside and supply temperatures, adapted from 'VITOCAL Ontwerphandleiding lucht/water warmtepompen' [70]

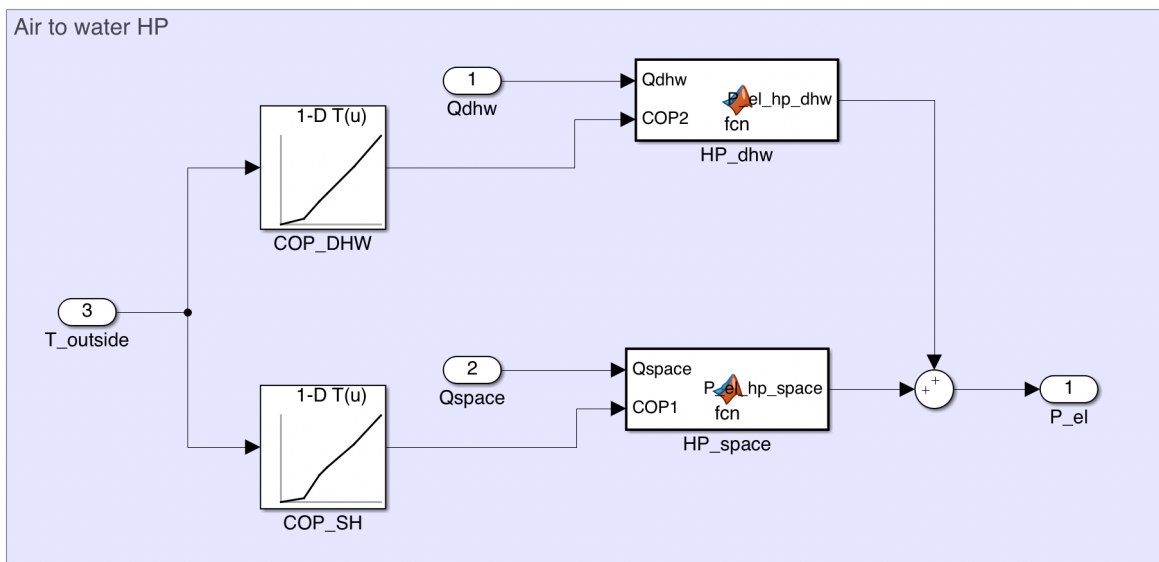| T_{sup} [°C]	COP of an air to water HP [-]					
	$T_{outside}$ [°C]					
	-7	2	7	10	20	30
45	2.36	2.54	3.49	3.79	4.75	6.06
65	1.81	1.94	2.31	2.47	3.05	3.73

Figure 4.24: Content of an air-to-water HP block in the Simulink model

4.8. Costs

With all the components of the different scenarios chosen and correctly sized, the capital expenditures (CAPEX) and operating expenditures (OPEX) of the components can be assessed by using the following methods, as well as the costs for different kinds of energy.

4.8.1. CAPEX

In this subsection, the CAPEX of the components of the DHNs in the case study scenarios will be given. First, the CAPEX of the different components and their sources will be given. Subsequently, a summary of the CAPEX of the different components can be seen in Table 4.7.

One of the first components which comes into sight when assessing the CAPEX of the DHNs of the different scenarios is the heat transfer station (HTS) which transfers heat from the heat source to the distribution network. According to the Vesta MAIS model by the CE Delft [14], CE Delft, Greenvis and Innoforte agreed that a correct assumption of the CAPEX of an HTS ranges from 125 €/kW to 145 €/kW. For the different scenarios in the case study, the average value of 132.50 €/kW will be assumed.

Subsequently, the water in the DHN will be pumped around by a circulation pump. With the maximum flow rate and required pump capacity of the pumps, covered in Section 4.4, the DACE manual [49] can be used to provide the CAPEX of the selected centrifugal pumps and electric motors.

The CAPEX of the piping consists of both the materials costs for the piping and the installation costs. According to the Vesta MAIS model by the CE Delft [14], the CAPEX can be approached by a range of investment costs, which takes the uncertainty in installation costs due to different soils into regard. This range is computed based on the maximal transferred heat in a section of the pipe for a temperature difference of 30 K. The range of costs is described in the Vesta MAIS model by Equation 4.50 and 4.51 and gives the CAPEX in €/m pipe. Here, $\dot{Q}_{pipe}$ [MW] is the maximum transferred heat in the section of the pipe in regard to a temperature difference of 30 K, $CAPEX_{min}$ [€/m] is the minimal investment cost of the pipe per unit length, based on soils that are easy to excavate, such as grass or open pavement. $CAPEX_{max}$ [€/m] is the maximum investment cost of the pipe per unit length, based on soils that are difficult to excavate, such as asphalt. Because these equations are dependent on the transferred heat of the pipe sections, which differs for the different scenarios, the CAPEX range is translated to the specific DN of the pipes used in the case study, for a temperature difference of 30 K. It is assumed that during the placing of the piping, asphalt, grass and anything in between is encountered. Therefore, it is assumed that the CAPEX of the pipes will be the average of their respective minimum and maximum CAPEX values. In Figure 4.25, the calculated average CAPEX values for the DN of the in the case study used pipes are shown. With these values, the CAPEX of the piping in all the scenarios can be determined.

$$CAPEX_{min} = 400 + 210 \cdot max\left(\dot{Q}_{pipe}\right)^{0.5} \qquad (4.50)$$

$$CAPEX_{max} = 800 + 200 \cdot max\left(\dot{Q}_{pipe}\right)^{0.6} \qquad (4.51)$$
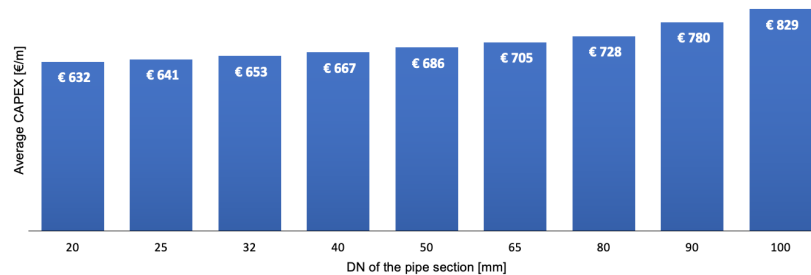

Figure 4.25: Average CAPEX values for different DN of the pipe sections in €/m, adapted from the Vesta MAIS model [14] and the Flexalen product guide [65]

In the distribution network of the DHN, multiple substations are implemented which provide tens to hundreds of households with heat. In general, a group of (semi)detached homes is connected to one substation, while apartment buildings will have their own substation. According to the Vesta MAIS model by the CE Delft [14], it is assumed that the CAPEX for substations in DHN ranges from 120 €/kW to 150 €/kW. For the different scenarios in the case study, an average CAPEX for the substations of 135 €/kW will be assumed.

Finally, the heat is transferred from the distribution network to the households by means of a supply set. The supply set makes the heat "usable" for the building by controlling the heat flow and temperature level supplied to the customer. The supply set limits the heat flow and thus distributes the heat over the connected households. According to the Vesta MAIS model from CE Delft [13], [14], supported by Innoforte and Greenvis, a reasonable assumption for the CAPEX of a supply set is 2,500 € for a detached home and 1,500 € for a household in an apartment building. Subsequently, 2,700 € must be accounted for the connecting pipes of each building to the distribution network.

Additionally, in the case of ULTDH, water-to-water HPs must be employed to increase the supplied temperature for space heating and DHW use. These HPs will be installed on top of the supply set and/or substation and include an HP boiler for DHW. In the case study, detached homes will have an individual HP, while apartment buildings will utilize collective HPs for the whole building. According to 'Prijslijst 2020 NL Decentrale energieoplossingen voor woningen' by Viesmann [71], the CAPEX for an individual water-to-water HP of 5.8 kW, including an HP boiler for DHW, is 7,885 € per system and the CAPEX for a collective water-to-water HP of 110 kW for an apartment building, with HP boilers for DHW included, is 66,506 € per system. In the case of an all-electric scenario, where no DHN is present, the heat demand of all the households will be covered by individual air-to-water HPs. According to Viessmann [71], a typical CAPEX for such an HP, with an HP boiler for DHW included, is 7,232 € per system.

In some scenarios of the case study, collective storage is applied by the use of an ATES system with a buffer TTES. The ATES system consists of an ATES doublet with well pumps, central HP and a control room and equipment. According to the Vesta MAIS model by CE Delft [13], the CAPEX of an ATES system which includes all of these components can be assumed to be 1,113 €/kW, with a minimum investment of 400,000 € per system. The ATES system is coupled with a buffer TTES to absorb daily fluctuations in the heat demand. According to a proposal for the design of a DHN in Wageningen by Royal Haskoning DHV [56], the CAPEX of a buffer TTES consists of four parts. The first one is the buffer tank itself, for which the CAPEX is assumed to be 54,000 €/100m^3 of stored volume. Secondly, there must be accounted for insulation, for which the CAPEX is assumed to be 115 €/m^2 of surface area of the tank. Subsequently, a circulation pump is added, of which the CAPEX is assumed to be 9,000 € for commonly used pumps for such applications. Finally, the installation costs are considered and assumed to be equal to the sum of the previous three parts.

The CAPEX of the different components given in this section, together with additional information and its source, are summarized in Table 4.7.

Table 4.7: CAPEX for different components of the DHN, with additional information and its sources

Component	CAPEX	Additional information	Source
HTS	132.5 €/kW	-	CE Delft [14]
Circulation pump	-	Dependent on pump characteristics	DACE manual [49]
Distribution pipes	See Figure 4.25	Dependent on DN of the pipe sections	CE Delft [14], Thermaflex [65]
Substations	135 €/kW	-	CE Delft [14]
Supply sets	1,500 €/household	Indoor costs and supply set per apartment	CE Delft [14]
	2,500 €/household	Indoor costs and supply set per detached home	CE Delft [14]
	2,700 €/building	Additional cost of building connection to the DHN	CE Delft [13]
Water tank	1,500 €	Individual DHW water tank	CE Delft [15]
Heat pumps	7,885 €	Individual water-to-water HP inc. boiler for a detached house	Viessmann [71]
	66,506 €	Collective water-to-water HP inc. boilers for an apartment building	Viessmann [71]
	7,232 €	Individual air-to-water HP inc. boiler for one household	Viessmann [71]
ATES	1,133 €/kW	Fully equipped ATES system	CE Delft [13]
Buffer TTES	54,000 €/100m^3	Buffer tank	Royal Haskoning DHV [56]
	115 €/m^2	Insulation of the buffer tank	Royal Haskoning DHV [56]
	9,000 €	Common pump costs for a buffer TTES	Royal Haskoning DHV [56]

4.8.2. OPEX

For the different components of the DHN, summarized in Table 4.7, the OPEX must be accounted for as well. According to CE Delft [13], the OPEX of a component consists of the yearly operational and maintenance costs and is related to the CAPEX of the component. Table 4.8 shows the different OPEX values as a percentage of the CAPEX values for the DHN its components, adapted from the Vesta MAIS model from CE Delft [13],[15] with recommendations from Infante Ferreira [33].

For the circulation pump, the HPs and the ATES system, the electricity consumption is significant and thus contributes to the OPEX values. This electricity consumption can be calculated as shown in Section 4.4, 4.3.1 and 4.6.2 respectively. For these components, the costs of the yearly consumed electricity must be added to the OPEX. In the OPEX of the heat transfer station, the cost of the consumed heat is also taken into regard.

Table 4.8 also contains the expected lifetime of the DHN its components. For the analysis of the case study, a duration of 30 yr. is chosen because this is also the expected lifetime of the largest components of a DHN. As can be seen in Table 4.8, some other components have an expected lifetime of 15 yr. and must be replaced after 15 yr. This results in an additional investment of the full CAPEX, shown in Table 4.7, when the lifetime has exceeded.

Table 4.8: OPEX and lifetimes for different components of the DHN, adapted from the Vesta MAIS model from CE Delft [13], [15] and discussed with Infante Ferreira [33]

Component	OPEX	Lifetime
HTS	2% of investment + heat consumption from source	30 yr.
Circulation pump	2.5% of investment + electricity consumption	15 yr.
Distribution pipes	2% of investment	30 yr.
Substations	2% of investment	30 yr.
Supply sets	2% of investment	15 yr.
Water tanks	2% of investment	15 yr.
HPs	2.5% of investment + electricity consumption	15 yr.
ATES	2.5% of investment + electricity consumption	30 yr.
Buffer TTES	2% of investment	30 yr.

4.8.3. Costs of energy

Ecofys, in collaboration with EnNatuurlijk [67], estimated the national costs of heat in the Netherlands for the coming few decades and concluded that the national costs of heat equal roughly 0.035 €/kWh. This conclusion is based on the assumption that the heat originates from a proportional share of geothermal heat, waste heat, biomass and combined heat and power plants. For the case study, it is assumed that the price of heat at the two different sources is equal to these national costs.

The costs of electricity can be divided into two different rates. The first rate is used for the electricity usage in the DHN, where the DHN operator is the electricity consumer. The second rate is used for the electricity usage of the consumer HPs, where the HPs are owned and operated by the community of owners of the connected households. According to the CBS [11], the average prices for the following two types of consumers can be assumed. For the type of residential consumers, the costs of electricity can be assumed to be 0.18 €/kWh. For the type of commercial large use consumers, of which the DHN operator belongs, the costs of electricity are assumed to be 0.072 €/kWh.

4.9. KPIs

To assess the feasibility of the different scenarios, they need to be compared to each other. The following KPIs have been chosen for this assessment due to their relation to costs, sustainability and infrastructure. The first two KPIs, which assess the costs and sustainability of the scenarios are assumed to be leading. The last KPI assesses the impact on the surrounding infrastructure of the scenarios, which must be taken into regard when discussing the previous two.

4.9.1. LCOE

The KPI which relates to the economical feasibility of the scenarios is the LCOE, shown in Equation 2.12 in Section 2.7. The LCOE is the minimum price at which the energy has to be sold to make the project profitable, which represents the financial break-even point of the project. In Equation 2.12, the LCOE is described as the cost per delivered unit of energy over the lifetime of the system [€/kWh] [16]. Here, n [yr.] is the lifetime of the system in years, C_{tot} [€] and Q_{tot} [kWh] are the total costs and energy produced of year t respectively. Furthermore, r [-] represents the discount rate of the scenario, which accounts for the discount of future values against today's and the riskiness of an investment. According to Colmenar-Santos et al. [17], it is essential that all economic evaluations of the use of DHN are carried out using an appropriate discount rate for infrastructural projects, sometimes referred to as a 'social' discount rate, which for projects that are located in Western Europe is recommended by the European Commission to be 3.5%. Therefore, this will be the discount rate used in the model. The lifetime of the scenarios is assumed to be 30 years, because this is the longest lifetime of most of the components. Some components, which have a lifetime of 15 years, have to be replaced accompanied by an additional investment of the CAPEX at year 15 of the analysis.

4.9.2. CO_2 emission

The KPI which relates to the sustainability of the different scenarios is their yearly CO_2 emission. Because the scenarios employ a lot of electricity and heat, it is assumed that the total emission of CO_2 per scenario is highly dependent on the use of these two energy carriers and the emitted CO_2 of the infrastructure is left out of scope.

As mentioned in Section 4.5, the CO_2 emissions of the consumed heat from the MTDH source and the ULTDH source are assumed as 10.5 kg/GJ and 8.8 kg/GJ respectively. According to the European Environment Agency [22], the CO_2 emission of electricity in the Netherlands is 0.390 kg/kWh, which translates to roughly 108.33 kg/GJ. Table 4.9 gives an overview of the emissions of the different kind of fuels used in the case study.

Table 4.9: CO_2 emissions of the different types of energy per kWh and GJ used in the case study, together with it sources

Energy type	kg CO_2/kWh	kg CO_2/GJ	Source
Electricity	0.390	108.33	EEA [22]
Heat (from LT heat source)	0.032	8.8	CE Delft [12]
Heat (from HT heat source)	0.038	10.5	HVC [31]

4.9.3. HTS load

The KPI which addresses the impact of the different scenarios on the infrastructure of the case study area is defined as the peak load of the HTS at the source. This KPI is chosen because of the characteristics of the heat sources in the case study. Because the heat sources consist of an MT heat net originating from a biomass and waste incineration plant and a collective waste heat net, it is key to keep the peak load of the HTS on the source low. By doing so, the underlying waste heat and/or collective heat net is influenced as little as possible and it is possible to operate it more efficiently and reliably and it can provide more consumers. To address the difference between the impact on the heat source, the peak loads of the HTS of the different scenarios will be compared to the highest peak load on the HTS regarding that heat source. The peak load of the HTS for both heat sources is observed separately.

5

Results and discussion

Using the model discussed in the previous chapter, the different scenarios of the case study are simulated and compared to each other. In this chapter, the most important results will be presented. First, the most important results regarding the parameters of the DHN of the different scenarios will be given and discussed. Subsequently, the same will be done for the most important expenses. At last, the different KPIs of the scenarios will be treated. Additionally, a full review of the model parameters, hourly energy profiles and total expenses of each scenario can be found in Appendix A, B and C, respectively.

5.1. General parameters

This section presents the most important results regarding the parameters of the DHN of the different scenarios. First, the found parameters regarding the DHN itself will be presented and compared. Next, the results of the two heat sources of the case study will be treated for the different scenarios. At last, the results of the storage units used in the case study will be given and discussed for the applicable scenarios.

5.1.1. DHNs

In Table 5.1, an overview of the parameters of the DHN can be seen for the different scenarios. The first given parameter is the total heat demand of all the consumers in the DHN, on building level. For each scenario, this is the same because the buildings and their characteristics do not change. At first glance, this total consumer heat demand seems low for 1972 households. However, the majority of dwellings are small new-build apartments, which comply with the latest insulation requirements of energy label A+, resulting in very limited heat losses to the surroundings explaining the low heat demand. Also, the climate data used in the case study year is of one of the hottest years on record, which is directly related to the consumer heat demand and explains low consumer heat demand.

Table 5.1: Comparison of the main DHN parameters for the different DH scenarios for the case study

Parameter	Scenario 1a/b	Scenario 2a/b	Scenario 3a/b	Unit
Total consumer heat demand	10.35	10.35	10.35	GWh
Heat demand covered by HPs	-	2.37	1.41	GWh
Heat demand covered by DHN	10.35	7.98	8.94	GWh
Heat demand at the HTS	11.78	8.69	10.33	GWh
Heat losses in DHN	1.43	0.71	1.39	GWh
	12.15%	8.19%	13.49%	-
Total pipe length of the DHN	5320	5000	6120	m

The second and third parameters in Table 5.1 introduce the distinction between coverage of the heat demand by either the DHN or HPs. Scenario 1 does not employ any consumer HPs, thus the total consumer heat demand is covered by the DHN. Alternatively, scenarios 2 and 3 employ water-to-water HPs at consumer level. Therefore, a portion of the heat demand is delivered as electricity by means of the HP. This results in a lower heat demand which has to be covered by the DHN, as can be seen in the table.

The DHN in the different scenarios must transport the required heat from an HTS connected to the source. During this transport, heat losses from the piping to the surroundings occur. To compensate for these losses, a larger amount of heat must be supplied to the DHN at the HTS. The heat demand at the HTS for the different scenarios can be seen in Table 5.1, together with the heat losses in the respective DHN.

As can be seen from these results, scenario 1 experiences the most heat losses, scenario 2 the least and scenario 3 in between the latter two. However, when compared to the total heat demand at the HTS, the relative heat losses for scenario 3 are the highest. These heat losses depend on multiple factors, of which the distribution temperature and the dimensions of the pipes are the most important ones. Scenario 1 and the MT part of scenario 3 employ a higher distribution temperature than scenario 2 and the ULT part of scenario 3. It is for that reason that the MT solutions are subjected to larger heat losses than the ULT solutions, illustrated by the fact that scenario 1 has double the amount of heat losses of scenario 2.

Also, the temperature difference between the supply and return lines of scenario 1 and the MT part of scenario 3 is much higher than the temperature difference for scenario 2 and the ULT part of scenario 3. This results in a higher required mass flow to achieve the same amount of delivered heat and thus larger pipes are needed in the latter cases, subjecting the ULT solutions to larger heat losses. However, larger pipe diameters with the lower distribution temperature would still experience smaller heat losses than smaller pipe diameters with the higher distribution temperature in the case study, as explained in Section 4.3.2. Thus, even though the ULT solutions employ larger diameters in the piping, the heat loss in the MT solutions is larger.

Another factor that has a significant influence on the total heat loss, is the total pipe length of the DHN. Of all three scenarios, scenario 2 holds the smallest DHN. This is explained by the fact that its heat source is assumed to be present in the middle of the case study area. Subsequently, scenario 1 employs a little bit more piping, due to the location of the heat source on the edge of the case study area. Finally, scenario 3 uses a significantly longer DHN than the previous two scenarios. This is expected due to the distinction of the DHN into two separate DHNs operating at different temperatures. These differences in pipe length explain why scenario 3 experiences relatively the most heat losses inside the DHN.

5.1.2. Storage facility

Each scenario is expanded with an additional scenario, which implements a storage facility at the location of the HTS. This storage facility employs a buffer TTES and an ATES system for daily and seasonal storage, respectively. Table 5.2 gives an overview of the found results for the main parameters of these storage units for each scenario. Because scenario 3 is divided into a ULT and MT-part connected to different heat sources, two separate storage facilities are employed.

Table 5.2: Comparison of the main parameters of the storage units for the different DH scenarios for the case study

Storage unit	parameter	S1b	S2b	S3b (ULT-part)	S3b (MT-part)	Unit
Buffer TTES	Maximum power	2.13	1.44	1.28	0.67	MW
	Storage capacity	15.30	12.24	8.54	5.11	MWh
	Tank volume	401.38	764.20	515.41	131.89	m^3
ATES system	Maximum power	1.81	1.44	0.96	0.65	MW
	Storage capacity	2393.30	1909.60	1235.80	894.74	MWh
	Average COP of the HP	3.28	21.49	20.52	3.37	-

In the storage facility, the buffer TTES is responsible for the daily storage. Because the consumer heat demand has a high fluctuation throughout the day, the buffer TTES must be able to deliver and collect high peak loads. Subsequently, the buffer TTES does not often store the same amount of heat for longer than 24 hrs, resulting in a relatively small storage volume subjected to high (dis)charging loads. The hourly (dis)charging profiles as well as the storage capacity profiles of the buffer TTES systems in the case study, which illustrate this behavior, can be seen in Appendix B.

The found parameters of the buffer TTES for the different scenarios can be seen in Table 5.2. Here, it is evident that the buffer TTES of scenario 1 contains the highest (dis)charging loads and storage capacity. However, this does not result in the largest tank volume because of the higher temperature difference in the DHN. The buffer TTES of scenario 2 is subjected to lower (dis)charging loads and a lower storage capacity because part of the consumer heat demand is met by decentralized HPs. However, because the temperature difference in the DHN of scenario 2 is low, a larger volume must be stored in the storage tank to meet the required storage capacity. The same is applicable for the two different parts of scenario 3, respective to the distribution temperatures of the DHNs.

Additionally to the buffer TTES, an ATES system facilitates seasonal storage in the storage facility. These ATES systems operate on a much more constant basis than the buffer TTES system, while the (dis)charging behavior slowly changes between delivering and collecting heat. This is illustrated by the (dis)charging profiles for the ATES systems in Appendix B. For this reason, a large amount of heat can be accumulated in an ATES, resulting in the enormous storage capacities shown in Table 5.2.

From these results, it can be seen that scenario 1 employs the largest ATES system, followed by scenario 2. Scenario 3 employs two separate ATES systems due to the location of the heat sources and the different distribution temperatures of the DHNs. The difference between the size of the ATES systems of scenarios 1 and 2 is explained by the fact that the heat demand covered by the DHN is lower for scenario 2 than for scenario 1. The same is applicable for the two DHNs of scenario 3. The next parameter given in Table 5.2 is the average COP of the HP of the respective ATES systems. For each scenario, different COPs are found because of their dependency on the distribution temperature of the DHNs. The COP influences the amount of electricity that is consumed by the HP to upgrade the extracted heat to the required temperature. Thus, by comparing the different COPs of the ATES systems, it is found that the HPs of the ATES systems of scenario 2 and the ULT-part of scenario 3 consume much less electricity than that for scenario 1 and the MT-part of scenario 3.

5.1.3. Heat sources

Of the two employed heat sources in the case study, different parameters appear for each scenario. Table 5.3 gives an overview of the found results for the main parameters of these heat sources.

Table 5.3: Comparison of the main parameters of the heat sources for the different DH scenarios for the case study

Heat source	Parameter	S1a	S1b	S2a	S2b	S3a	S3b	Unit
MT heat source	Total supplied heat	11.78	11.44	-	-	4.28	4.16	GWh
	Maximum delivered power	3.77	1.35	-	-	1.31	0.49	MW
ULT heat source	Total supplied heat	-	-	8.69	9.05	6.05	6.28	GWh
	Maximum delivered power	-	-	2.92	1.14	2.02	0.79	MW

As shown in the table, scenario 1 is totally dependent on the MT heat source, due to the distribution temperature of the DHN. Also, it can be seen that for scenario 1a, high peak loads must be delivered by the heat source. Alternatively, in the case of scenario 1b, where a storage facility is added, the maximum delivered power is brought down to roughly a third of the original value. The same can be stated for scenarios 2 and 3, which employ either only the ULT heat source or a combination of both the ULT and the MT heat source. Additionally, the total supplied heat by the respective heat sources is lower for the scenarios with storage facilities than for the scenarios without. This difference can be attributed to two characteristics of the storage facility. The first one is a significant heat loss occurring in each ATES system, which results in a higher amount of heat that must be supplied by the respective heat sources. Subsequently, the ATES systems employ

HPs which convert electricity into a fraction of the delivered heat from the ATES during discharge. This lowers the total amount of heat that must be delivered by the heat source, which is stored in the ATES system. The amount of additional heat supplied by the HPs is dependent on its COP, which in turn is dependent on the distribution temperatures of the DHNs. From the results, it can be seen that for MTDH, the added heat from the HP outweighs the heat losses in the ATES system. This means that more heat is extracted from the ATES system than is put in, due to the electricity consumption of the HP. This is evident due to the lower amount of heat that must be supplied by the MT heat source. Alternatively, the heat losses in the ATES system outweigh the added heat from the HP in the case of ULTDH, resulting in a higher total amount of supplied heat by the heat source.

5.2. Expenses

With the found parameters of the different scenarios, discussed and shown in Section 5.1 and Appendix A, the total expenses of the scenarios are determined in terms of CAPEX and OPEX. An overview of these results is provided by Table 5.4. As can be seen here, the cheapest options for a DHN do not employ any storage. The cheapest option for a DHN in the case study is the MTDH scenario 1a. The combined ULT/MTDH scenario 3a is the second cheapest option, followed by the ULTDH scenario 2a. This can be explained by the fact that the ULTDH scenarios employ consumer HPs and thus require an additional investment as well as consume more electricity, resulting in a higher CAPEX and OPEX. Subsequently, the DHN scenarios which contain storage facilities follow. These storage facilities also require an additional investment as well as consume more electricity, resulting in a higher CAPEX and OPEX again. At last, the all-electric scenario, which employs air-to-water HPs at consumer level, is the most expensive option. This is due to the fact that every household is employed with an individual HP and that the scenario consumes a large amount of electricity, charged at the higher consumer rate. The CAPEX and OPEX values shown below do not include any type of profit for the DHN operator. Depending on the selling price and amount of delivered heat by the DHN and the differences in expenses, it can be concluded that a cheaper scenario is able to result in more profit for the DHN operator. A full review of the CAPEX and OPEX values of the components of each scenario can be seen in Appendix C.

Table 5.4: CAPEX and OPEX values for the different scenarios of the case study

Scenario	Heat supply	Storage facility	CAPEX [€]	OPEX [€/year]
1a	MTDH	no	10,927,124	637,814
1b	MTDH	yes	12,918,202	741,317
2a	ULTDH	no	11,962,907	996,460
2b	ULTDH	yes	13,835,858	1,072,581
3a	Combined ULT/MTDH	no	11,890,313	888,267
3b	Combined ULT/MTDH	yes	13,866,698	976,616
4	Air-to-water HPs	-	14,261,504	1,065,918

5.3. KPIs

After obtaining the results from the different scenarios, the chosen KPIs are determined. This section provides an overview of the results of the different KPIs. First, the LCOE and the CO_2 emissions of the case study scenarios will be provided and discussed. Thereafter, the loads of the different HTS of the scenarios will be introduced, giving more insight into the impact of the scenarios on the surrounding infrastructure of the case study area.

5.3.1. LCOE

The first KPI, the LCOE, can be determined with the CAPEX and OPEX of the different scenarios of the case study. As explained in Section 4.9, the discount rate for the case study is assumed to be 3.5% and the lifetime of the scenarios is assumed to be 30 yr. By calculating the LCOE for the different scenarios, the results in Table 5.5 are found. Here, the LCOE for the different scenarios is shown, as well as the relative LCOE savings of each scenario compared to the reference scenario. Subsequently, Figures 5.1 and 5.2 give a visualization of these LCOEs and their savings relative to the reference scenario. The difference in the LCOEs of the scenarios

results from its respective CAPEX and OPEX. Here, the CAPEX varies due to the different components employed in the scenarios. The difference in OPEX of the scenarios results not only from the different employed components but is also for a large part dependent on the type of energy consumed in the scenario, where for all the bought heat 0.035 €/kWh is charged and for electricity either 0.18 €/kWh or 0.072 €/kWh, depending on the consumer.

From these results, it can be seen that the reference scenario is by far the most expensive scenario of the case study. This can be explained by the fact that each household has to invest in an individual air-to-water HP and is responsible for the acquisition of their electricity, which is more expensive for residential consumers than for commercial parties. Additionally, the ULTDH scenarios are more expensive due to the employment of water-to-water HPs and the scenarios which have storage facilities employed require more investment.

Table 5.5: The LCOE of different scenarios and their relative LCOE savings compared to scenario 4

Scenario	Heat supply	Storage facility	LCOE [€/kWh]	relative LCOE savings
1a	MTDH	no	0.128	42%
1b	MTDH	yes	0.149	33%
2a	ULTDH	no	0.183	18%
2b	ULTDH	yes	0.200	10%
3a	Combined ULT/MTDH	no	0.169	24%
3b	Combined ULT/MTDH	yes	0.187	16%
4	Air-to-water HPs	-	0.223	0%

Figure 5.1: LCOE per scenario in €/kWh

Figure 5.2: LCOE savings per scenario in % relative to reference scenario 4

5.3.2. CO_2 emission
The second KPI which is assessed is the CO_2 emission of the scenarios. The yearly CO_2 emissions [t/y] for the different scenarios are calculated according to the yearly consumption for the different types of energy carriers and their respective emission factors. The results of each scenario are shown in Table 5.6, together with their relative savings compared to the reference scenario. Figures 5.3 and 5.4 illustrate tese results.

The root cause of the difference between the emission of the scenarios is the different emission factors for the types of used energy. Of these types, electricity contains by far the highest emission per delivered unit of energy. The used heat from the two heat sources in the scenarios has a much lower emission per delivered unit of energy. Here, the waste heat from the ULT heat source has a little lower emission factor than the heat from the MT heat source, origination from a biomass/waste incineration plant.

The results show that scenario 4 has the most CO_2 emissions per year. This is because this scenario only consumes electricity as a source for the air-to-water HPs. Scenarios 2a and b also consume quite some electricity, due to the consumer HPs, as well as a large amount of heat from the ULT source, resulting in a quite high yearly CO_2 emission. Alternatively, scenarios 1a and b only consume heat from the MT heat source and avoid a large consumption of electricity, resulting in the lowest yearly emission. Subsequently, scenarios 3a and b consist of a combination of the heating solutions of scenarios 1 and 2, resulting in lower employment of HPs and consumption of both electricity and heat from the two heat sources. Therefore, scenario 3 is subjected to a somewhat average yearly CO_2 emission compared to scenarios 1 and 2. Furthermore, higher yearly CO_2 emissions are related to the scenarios which employ storage facilities, which is again explained by the increased usage of electricity. This is especially the case for scenario 1b, which suffers a 40% increase in CO_2 emissions compared to scenario 1a. In future scenarios, it is most likely that ULTDH would become less CO_2 intense than biomass-powered MTDH when there is a higher share of renewable electricity in the Netherlands.

Table 5.6: The CO_2 emissions of different scenarios in t/y and their relative CO_2 savings compared to scenario 4

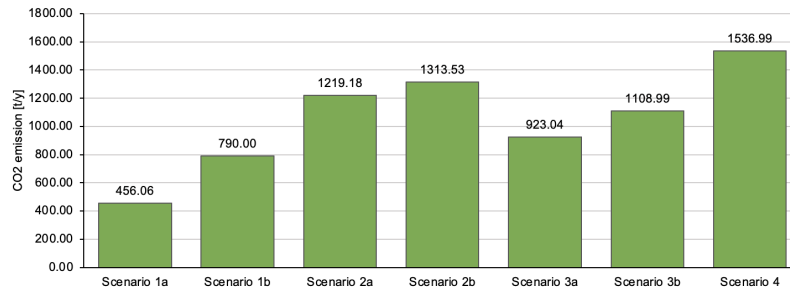| Scenario	Heat supply	Storage systems	Yearly CO_2 emission [t/y]	Relative CO_2 emission savings
1a	MTDH	no	456.06	70%
1b	MTDH	yes	790.00	49%
2a	ULTDH	no	1219.18	21%
2b	ULTDH	yes	1313.53	15 %
3a	Combined ULT/MTDH	no	923.04	40%
3b	Combined ULT/MTDH	yes	1108.99	28%
4	Air-to-water HPs	-	1536.99	0%

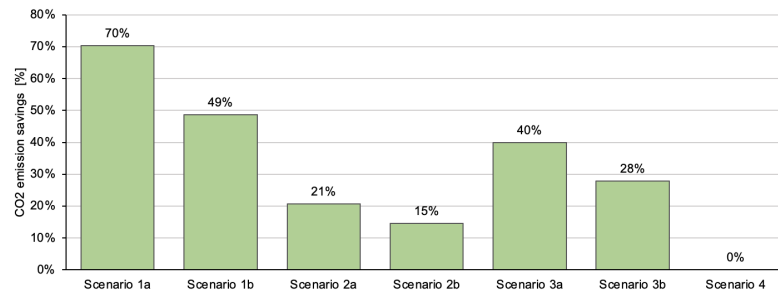Figure 5.3: CO_2 emission per scenario in t/y

Figure 5.4: CO_2 savings per scenario in % relative to reference scenario 4

5.3.3. HTS load

The final KPI which is assessed is the peak load of the HTS of each scenario. This KPI gives insight into the impact of each scenario on the infrastructure of the heat sources. The peak load of each HTS is examined individually and compared with the highest HTS peak load per heat source. Because the reference scenario does not employ an HTS, it has been left out of the scope of this KPI. Table 5.7 shows the HTS peak loads on both the MT and the ULT heat source. The table also contains the magnitude of the load in the percentage of the highest HTS load on each heat source. Figures 5.5 and 5.6 illustrate the found results of Table 5.7.

As can be seen from these results, scenario 1a employs by far the highest HTS load related to the MT heat source and scenario 2a employs by far the highest HTS load related to the ULT heat source. Scenario 3a employs somewhat lower loads on the HTS related to the two heat sources because the consumer demand is split between the two. From scenarios 1b, 2b and 3b it can be seen that implementing a storage facility into the scenario causes a huge drop in the HTS load. This is especially beneficial for the ULT heat source, which is not assumed to be able to deliver the high peak loads proposed by scenarios 2a and 3a. Although the MT heat source is assumed to be able to deliver the high HTS loads from scenario 1a, it may be considered to be advantageous to have lower HTS loads due to the resulting lower impact on the MT heat source. This is because the heat source is able to deliver to more DHNs nearby, without having to change its infrastructure. Also, it might occur that in the future other, more renewable, heat sources are connected to the MT heat net, which might require the implementation of storage systems.

Table 5.7: The HTS peak load for the two MT and ULT heat sources for different scenarios in MW and their magnitude relative to the highest respective HTS peak load in %

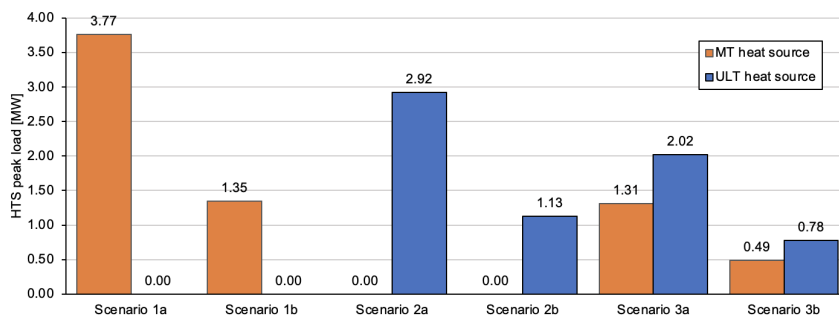| Scenario	MT HTS peak load [MW]	Relative MT HTS peak load	ULT HTS peak load [MW]	Relative ULT HTS peak load
1a	3.77	100%	0	0%
1b	1.35	36%	0	0%
2a	0	0%	2.92	100%
2b	0	0%	1.14	39%
3a	1.31	35%	2.02	69%
3b	0.49	13%	0.78	27%

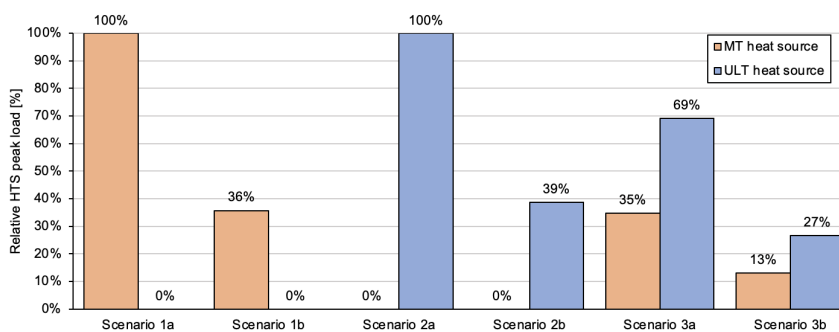Figure 5.5: HTS peak load per heat source and scenario in MW

Figure 5.6: HTS peak load per heat source and scenario in % relative to the highest respective peak loads

6

Conclusions and recommendations

In this chapter, the conclusions of this research are presented by answering the research questions. The results of the case study will be discussed and recommendations for future research will be mentioned.

6.1. Conclusions

The main objective of this research was to assess the influence of TES systems on the feasibility of DH for residential heating applications. To do so, a case study of an area in Heerhugowaard has been conducted, which assesses this feasibility on the hand of a newly constructed thermodynamic model based on the state of the art of DH and TES. The model simulates different DHN scenarios for the case study area, for which it performs hourly calculations for a year. Subsequently, the model assesses the influence of the combined use of a TTES and ATES system for each scenario. Finally, the results from this model are used to assess various KPIs regarding the feasibility of the DHNs.

Characteristics and modeling methods of DH

DH can be seen as a thermal distribution network of pipes filled with a heat transfer fluid, which is often water. In this network, mass flow is being controlled by pumps and valves, while extraction or supply of heat is maintained by the use of agents, such as consumers, sources and storage systems. The influence of these agents is highly related to the distribution temperature and pressures of the DHN as well as the energy efficiency of the employed techniques. The modeling of DH is based on the hydraulic and thermal equilibria of the system. This can either be done in physical or black-box models. Black-box models approach the whole system as one unit, where the different aspects of components are not considered, resulting in fast and easy modeling. Alternatively, physical models approach each component of the system independently, resulting in a higher accuracy but also a higher complexity. To decrease this workload, numerical approaches are often used.

Characteristics and modeling methods of TES

TES systems are used to store energy in thermal form and can be distinguished in three mechanisms: chemical storage, latent heat storage and sensible heat storage. Sensible storage systems are usually simpler, cheaper and more reliable than latent and chemical storage mechanisms. Also, more research must be conducted in chemical and latent heat storage technology, before they can be used for reliable and feasible storage applications. Therefore, the case study only investigates the use of sensible heat storage.

The amount of energy stored in a sensible TES system is for a large part dependent on the storage medium. According to the available research, water is the most promising storage medium, because of its high volumetric heat capacity, low thermal diffusivity and low cost. While multiple configurations for sensible heat storage exist, the most promising configuration for short-term storage is considered to be TTES, which has good operating characteristics while being subjected to a limited size. The most promising configuration for

long-term storage is considered to be ATES, which is a more complicated system but is able to store a large amount of heat for longer periods while having relatively low construction costs.

Modeling of TES tends to be complicated due to its many components and temperature-dependent behavior. For this kind of modeling, a wide range of tools can be employed, resulting from relatively simple and fast models to more sophisticated and complex models. When designing a model for TES, a trade-off must be made between simplicity and detail of result. Depending on the requirements of the model, the modeling of TES systems can be done on component level, TES level and system level. Various approaches are used for modeling on these levels and combining them. Depending on these levels, various parameters must be taken into account for producing a correct model. For this study, a simplified analytical model is designed, which provides a fast result for some known specific conditions.

Implementation of TES in DH in dense urban areas
Pairing TES with DH comes with numerous benefits and drawbacks which have to be taken into close consideration. According to the treated literature, it can be concluded that the implementation of TES in DH could benefit the overall system, especially when implementing RES. However, this might lead to a more complex DHN, especially for low temperature DH, where components like (booster) HPs must be installed. Therefore, a trade-off between the benefits and drawbacks of pairing TES with DH has to be made for each situation.

Influence of TES integrated DHNs on the LCOE
The LCOEs of the case study scenarios employing TES are 10-16% higher than that of the respective scenarios without TES. This is due to the fact that TES requires a relatively large additional investment and electricity consumption. Subsequently, the LCOE of ULTDH is around 43% higher than the LCOE of MTDH. This is again due to additional investments and electricity consumption, this time appointed to the employment of end-user HPs. However, depending on the availability of certain heat sources, it can be essential to implement TES and/or end-user HPs. Nonetheless, every case study scenario employing DH has a 10-42% lower LCOE than the all-electric scenario which employs individual air-to-water HPs.

Influence of TES integrated DHNs on CO_2 emissions
The CO_2 emissions of the case study scenarios are closely related to the different types of used energy. Due to the high CO_2 emissions of electricity, its use must either be minimized or the electricity must be generated more sustainably. By implementing TES in the DH scenarios, their yearly CO_2 emission has raised by 8-73% in regard to the same DH scenario without TES, depending on the extra electricity consumption and the employed heat sources of the respective scenario. Subsequently, two types of heat sources have been investigated in this research. Of those sources, ULT waste heat is considered to have lower CO_2 emissions than MT heat from biomass and waste incineration plants. However, when ULT waste heat is employed, additional consumption of electricity is required to boost the supply temperature to the required level for end-users. Also, the MT heat from the biomass and waste incineration plant in the case study is accompanied by relatively low CO_2 emissions. In regard to these comments, it is apparent that ULTDH is subjected to a 66-167% higher yearly CO_2 emission than MTDH, depending on the implementation of TES and as shown by the results. Additionally, it has been shown that every case study scenario employing DH has a 15-70% lower yearly CO_2 emission than the all-electric scenario. From the scenarios, MTDH heating is considered to be the most sustainable option of the explored heat sources in the case study as of today, in regard to CO_2 emissions. However, it must be taken into regard that ULTDH and the all-electric scenario might become less CO_2 intense than biomass-powered MTDH in the future, due to a growing share of renewable electricity in the Netherlands.

Influence of TES integrated DHNs on the infrastructure of the case study area
The heat used in the case study originates from two different heat sources: a biomass/waste incineration plant and a collective waste heat net. To reduce the impact of the DH on the already existing heat sources, the peak loads should be minimized. The implementation of TES can drastically lower the peak load by 61-64%, as shown by the results. In the case of the collective waste heat net, it is considered to be necessary to

implement TES, due to the high possibility of discrepancy between supply and demand. Alternatively, the biomass/waste incineration plant can handle the proposed peak loads. In practice, keeping in mind that DHNs are likely to grow in the near future with more areas added, it would be beneficial to implement TES to lower the impact of new areas added to the network and ultimately allow more users to be connected to one heat source.

After accounting for the sub-research objectives, the main objective of this research can be assessed, which is formulated as follows:

> ***"What is the influence of TES systems on the feasibility of new DH projects for residential heating applications?"***

According to the found results, the influence of TES systems on the feasibility of new DH projects for residential heating applications is considered to be substantial, especially in regard to financial perspective and sustainability. The implementation of TES is able to lower the peak loads at the source level by two-thirds, compared to the initial peak loads without TES. This reduction can be most beneficial for the heat source in terms of the potential growth of consumers and the discrepancy between supply and demand. This advantage comes at the cost of a significant additional investment and electricity consumption, which results in a 10-16% higher LCOE and an 8-73% higher yearly CO_2 emission, depending on the characteristics of the DHN and heat source of the respective scenario. Subsequently, the grid electricity mix plays a large role in the CO_2 emission of each scenario and might reduce the yearly CO_2 emissions significantly, depending on the share of renewable electricity.

When designing new DH projects, it is key to consider different heat sources available in the area. With the characteristics of these sources, a trade-off can be made between the (dis)advantages of the implementation of TES in regard to the heat sources. Especially in the case of DH coupled with renewable sources, TES might be a promising enhancement.

6.2. Recommendations

The research shows the impact of TES systems on the feasibility of new DH projects for residential applications and implies a case study in which this is assessed. The following recommendations are given for further studies.

Heat sources

The model is based on two existing heat sources in the case study area, with invariable characteristics. The impact of the heat sources on the KPIs in this research is therefore considered to be limited. Further research should include variable characteristics of various heat sources to assess the influence on TES. This should especially be promising for RES.

CO_2 emissions

The CO_2 emissions included in this research focus on the production of heat and electricity. The (in)direct emissions of the construction and decommissioning of the DH infrastructure have not been taken into regard in this study, but can be included in further research. Also, the CO_2 emission of electricity used in this research is considered to remain constant for the following years. However, by following the guidelines of the climate agreement, the generation of electricity should become more and more sustainable over the coming years. Because the CO_2 emissions of the consumed electricity are of significant influence in regard to the sustainability of DH projects, future research should include reliable predictions for the generation of renewable electricity.

Modeling of TES

In this research, a simplified analytical model is designed for TES. This provided fast results for either known or assumed conditions of the case study area. For more detailed results, further research could focus on more complex modeling of TES, including the modeling of its specific characteristics. Examples of such characteristics are the thermal capacity, geometry and insulation of the storage unit itself, positions of in- and outlet ports, stratification, storage media properties and surrounding conditions.

Control mechanisms

The model assumes perfectly predicted behavior of the DHN and its TES. In practice, such systems would work with predictive control mechanisms. For the sake of the operational side of the DHN and its TES, future research should include these control mechanisms and their translation in such models.

Meteorological data

The results of the model are based on the meteorological data of the case study area for one respective year, which is assumed to give a reasonable prediction for the coming years. Future research should include more variable and accurate predictions of meteorological data for a better representation of the performance indicators in the near future.

Commercial buildings

Because the scope of this research is on the residential application of DH, the model assumes the space heating demand of commercial buildings to be the same as for residential buildings. Also, the DHW demand for commercial buildings is assumed to be negligible compared to residential buildings. For the implementation of commercial consumer behavior in DHNs, future research should focus on this kind of heat demand.

Optimisation

The focus of this research lies on the comparison of the available techniques in the case study area. Therefore, no optimization of operational aspects or KPIs has been conducted. Future research can focus on finding optimal parameters for distribution characteristics of DH, such as optimal temperature and pressure, and/or for TES, such as optimal sizes and (dis)charging behavior.

Payback period and subsidies

This research only focuses on the total costs of new DH projects, with or without TES. An interesting addition would be the payback period compared to the current energy market. Because of the need for more sustainable residential heating applications, it is likely for such projects to receive subsidies for funding. In this research, optional subsidies have not been included. However, future research might include what influence subsidies have on the financial aspects, such as the payback period, of new DH projects.

A

Model parameters

A.1. Scenario 1: MTDH

An overview of the model parameters and results of scenarios 1a and 1b can be seen in Table A.1. The first three sections regarding the heat net, circulation pump and source are applicable for both scenarios, while the latter sections only apply for scenario 1b.

Table A.1: Overview of the model parameters and results for scenario 1a and 1b

Scenario	Model section	Model parameter / result	Value	Unit
1a/b	Heat net	Total pipe length	5320	m
		Total heat demand at consumers covered by DHN	10.35	GWh
		Total heat demand at the HTS	11.78	GWh
		Total heat losses in net	1.43	GWh
			12.15	%
	Circulation pump	Maximum volume flow	108.08	m^3/h
		Maximum head	3.78	bar
		Max epower	18.99	kW
		Total annual electric demand	27.43	MWh
	Source	Total heat demand scenario 1a	11.78	GWh
		Total heat demand scenario 1b	11.44	GWh
		Max power of HTS scenario 1a	3.77	MW
		Max power of HTS scenario 1b	1.35	MW
1b	Buffer TTES	Max abs power	2.13	MW
		Storage capacity	15.30	MWh
		Volume	401.38	m^3
		Height	5	m
		Radius	5.05	m
		Surface area	319.36	m^2
	ATES	Porosity	0.3	-
		ΔT between wells	10	K
		Thermal recovery	80	%
		average COP of the HP	3.28	-
		Max abs power	1.81	MW
		Storage capacity	2.39	GWh
		Water volume	210.000	m^3
		Total volume	701.000	m^3
		Length of the ATES	40	m
		Radius of the ATES	74.71	m
		Annual electricity demand of well pump and HP	0.89	GWh

A.2. Scenario 2: ULTDH

An overview of the model parameters and results of scenarios 2a and 2b can be seen in Table A.2. The first three sections regarding the heat net, circulation pump and source are applicable for both scenarios, while the latter sections only apply for scenario 2b. Because part of the consumer heat demand is covered by the HPs, the total heat demand at consumers covered by the DHN is lower than for scenario 1.

Table A.2: Overview of the model parameters and results for scenario 2a and 2b

Scenario	Model section	Model parameter / result	Value	Unit
2a/b	Heat net	Total pipe length	5000	m
		Total heat demand at consumers covered by DHN	7.98	GWh
		Total heat demand at the HTS	8.69	GWh
		Total electricity demand by HPs	2.37	GWh
		Total heat losses in net	0.71	GWh
			8.19	%
	Circulation pump	Maximum volume flow	190.12	m^3/h
		Maximum head	3.73	bar
		Max epower	32.95	kW
		Total annual electric demand	4.64	MWh
	Source	Total heat demand scenario 2a	8.69	GWh
		Total heat demand scenario 2b	9.05	GWh
		Max power of HTS scenario 2a	2.92	MW
		Max power of HTS scenario 2b	1.14	MW
2b	Buffer TTES	Max abs power	1.44	MW
		Storage capacity	12.24	MWh
		Volume	764.20	m^3
		Height	5	m
		Radius	6.98	m
		Surface area	525.01	m^2
	ATES	Porosity	0.3	-
		ΔT between wells	10	K
		Thermal recovery	80	%
		Average COP of the HP	26.86	-
		Max abs power	1.44	MW
		Storage capacity	1.91	GWh
		Water volume	165,000	m^3
		Total volume	550,000	m^3
		Length of the ATES	40	m
		Radius of the ATES	66.16	m
		Annual electricity demand of well pump and HP	0.21	GWh

A.3. Scenario 3: combined ULT- and MTDH

An overview of the model parameters and results of scenarios 3a and 3b can be seen in Table A.3. The first three sections regarding the heat net, circulation pump and source are applicable for both scenarios, while the latter sections only apply for scenario 3b. Because part of the case study area is covered by ULTDH and another part by the MTDH, a distinction is made between the components of the ULT- and MTDH part.

Table A.3: Overview of the model parameters and results for scenario 3a and 3b, for both the ULT- and MTDH part

Scenario	Model section	Model parameter / result	Value for the ULT-part	Value for the MT-part	Unit
3a/b	Heat net	Total pipe length	4500	1620	m
		Total heat demand at consumers covered by DHN	5.45	3.43	GWh
		Total heat demand at the HTS	6.05	4.28	GWh
		Total electricity demand by HPs	1.41	-	GWh
		Total heat losses in net	0.59	0.79	GWh
			9.85	18.62	%
	Circulation pump	Maximum volume flow	130.78	36.77	m^3/h
		Maximum head	3.84	2.14	bar
		Max epower	23.22	3.64	kW
		Total annual electric demand	32.34	6.11	MWh
	Source	Total heat demand scenario 3a	6.05	4.28	GWh
		Total heat demand scenario 3b	6.28	4.16	GWh
		Max power of HTS scenario 3a	2.02	1.31	MW
		Max power of HTS scenario 3b	0.79	0.49	MW
3b	Buffer TTES/PTES	Max power	1.28	0.67	MW
		Capacity	8.54	5.11	MWh
		Volume	515.41	131.89	m^3
		Height	5	5	m
		Radius	5.73	2.90	m
		Surface area	386.27	142.84	m^2
	ATES	Porosity	0.3	0.3	-
		ΔT between wells	10	10	K
		Thermal recovery	80	80	%
		Average COP of the HP	20.52	3.37	-
		Max power	0.96	0.65	MW
		Capacity	1.24	0.89	GWh
		Water volume	107,000	77,300	m^3
		Total volume	356,000	258,000	m^3
		Length of the ATES	40	40	m
		Radius of the ATES	53.23	45.29	m
		Annual electricity demand of well pump and HP	0.14	0.33	GWh

A.4. Scenario 4: all-electric

Scenario 4 is created as an all-electric scenario for reference, in which the heat demand is met by individual air to water HPs. Because no DHN is present, the scenario is much more simple and includes fewer components. For this scenario, it is assumed that every household in the case study has its own air-to-water HP with an HP boiler. An overview of the model parameters and results of scenario 4 can be seen in Table A.4. Here, the total heat demand met by the HPs is shown as well as the consumed electricity.

Table A.4: Overview of the model parameters and results for scenario 4

Scenario	Model section	Model parameter / result	Value	Unit
4	HPs	Total heat demand at consumers	10.35	GWh
		Total electricity demand by HPs	3.94	GWh

B

Hourly energy profiles

This appendix presents the power profiles and storage capacity profiles of the different scenarios, obtained by the Simulink and Matlab model. For each scenario that includes DH, a section is created which displays three figures regarding the power of the heat source, the power and storage capacity of the buffer TTES and the power and storage capacity of the ATES system.

The first figure in each section shows the supplied heat by the heat source for two separate cases. Case (a) shows the supplied heat when no storage is implemented in the respective DH scenario and case (b) shows the supplied heat when a buffer TTES and ATES system are employed in the respective DH scenario. The given power profiles show the power of delivered heat in MW on the y-axis for a given time during one year on the x-axis.

Subsequently, the second figure shows both the power profile and the storage capacity profile for the buffer TTES employed in the respective DH scenario. The top graph depicts the power profile of the buffer TTES, which describes its (dis)charging behavior with the power in MW on the y-axis for a given time during one year on the x-axis. Here, positive values indicate energy is delivered and negative values indicate energy is stored for later use. The bottom graph depicts the storage capacity profile of the buffer TTES, which shows the amount of stored heat in MWh on the y-axis for a given time during one year on the x-axis.

At last, the third figure shows both the power profile and the storage capacity profile for the ATES system employed in the respective DH scenario, in the same way as for the buffer TTES. The top graph depicts the power profile of the ATES system, which describes its (dis)charging behavior with the power in MW on the y-axis for a given time during one year on the x-axis. Here, positive values indicate energy is delivered and negative values indicate energy is stored for later use. The bottom graph depicts the storage capacity profile of the ATES system, which shows the amount of stored heat in MWh on the y-axis for a given time during one year on the x-axis.

Due to the distinction into an MT- and a ULTDH part in scenario 3, above mentioned figures are shown separately in a subsection for each respective part.

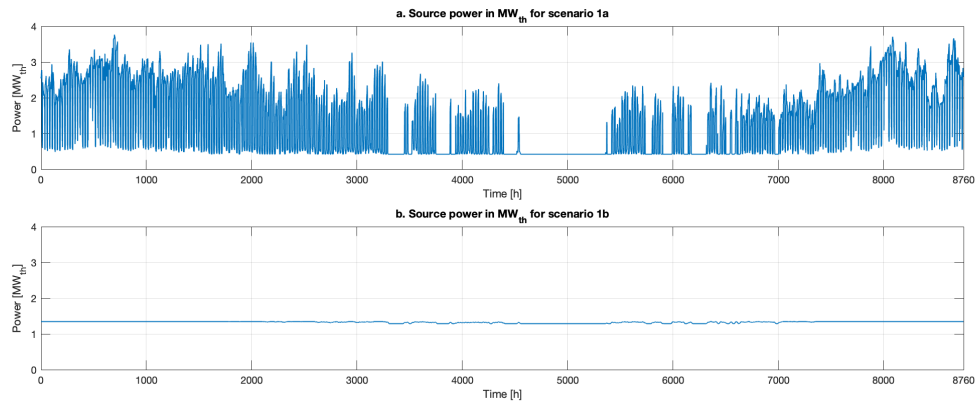## B.1. Scenario 1: MTDH

Figure B.1: Power profile at the MT heat source for scenario 1a (a) and scenario 1b (b) during one year
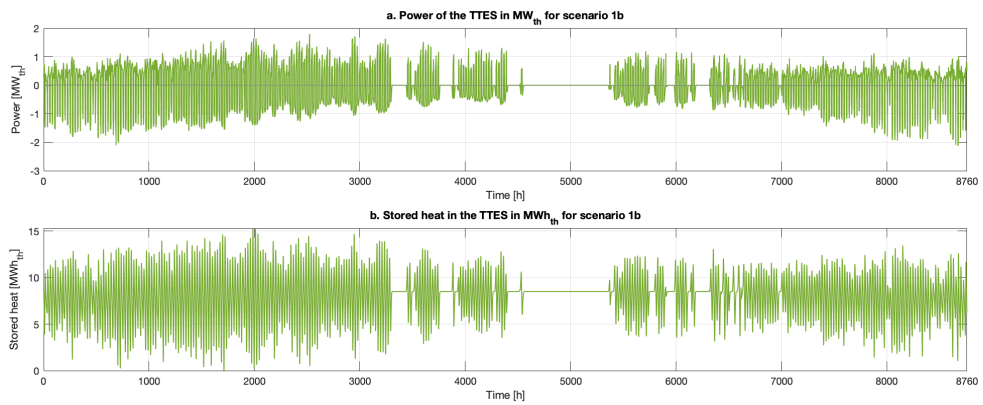

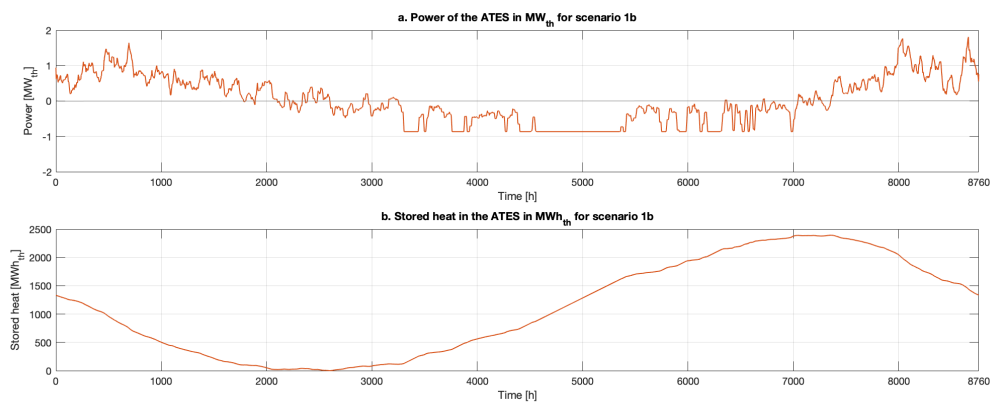Figure B.2: Power (a) and storage capacity profile (b) of the buffer TTES for scenario 1b during one year

Figure B.3: Power (a) and storage capacity profile (b) of the ATES system for scenario 1b during one year
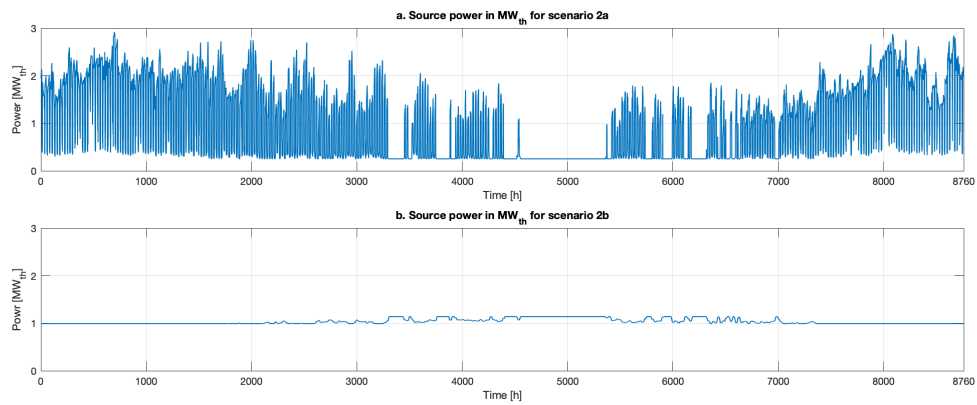
B.2. Scenario 2: ULTDH

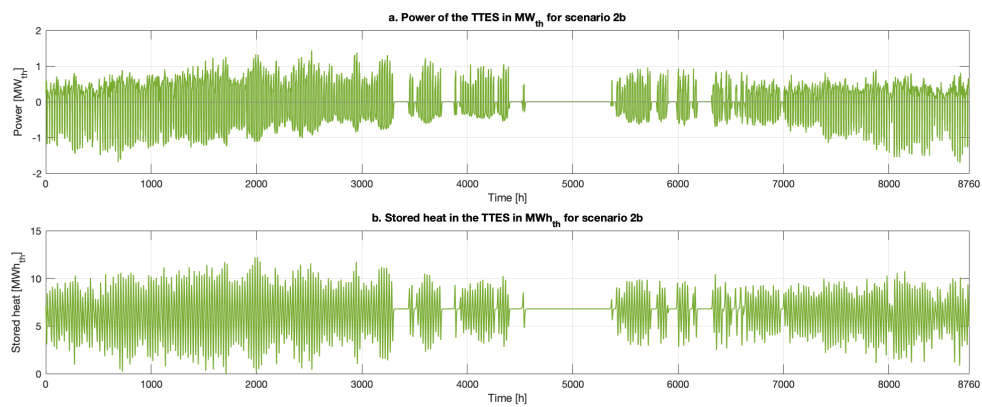Figure B.4: Power profile at the ULT heat source for scenario 2a (a) and scenario 2b (b) during one year

Figure B.5: Power (a) and storage capacity profile (b) of the buffer TTES for scenario 2b during one year
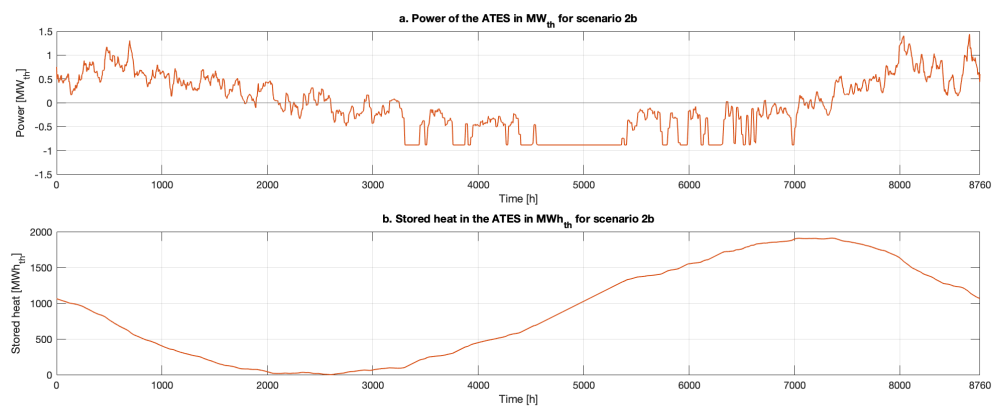

Figure B.6: Power (a) and storage capacity profile (b) of the ATES system for scenario 2b during one year

B.3. Scenario 3: combined ULT- and MTDH
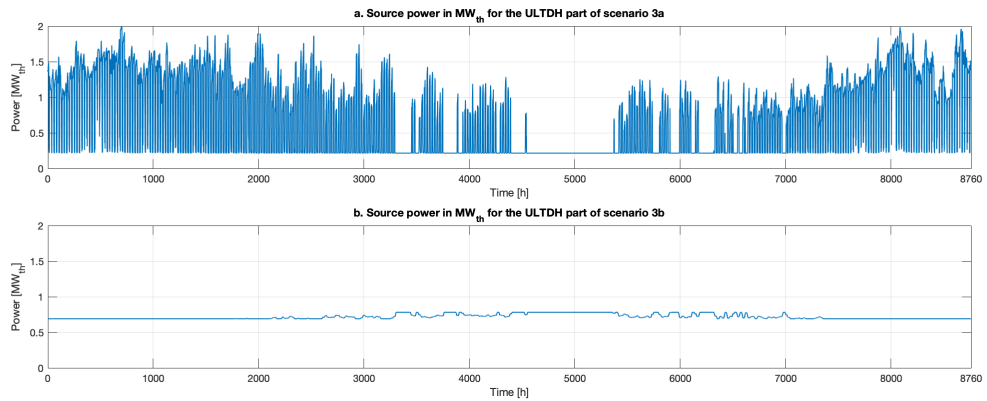## B.3.1. Scenario 3: ULTDH part

Figure B.7: Power profile at the ULT heat source for the ULTDH part of scenario 3a (a) and scenario 3b (b) during one year
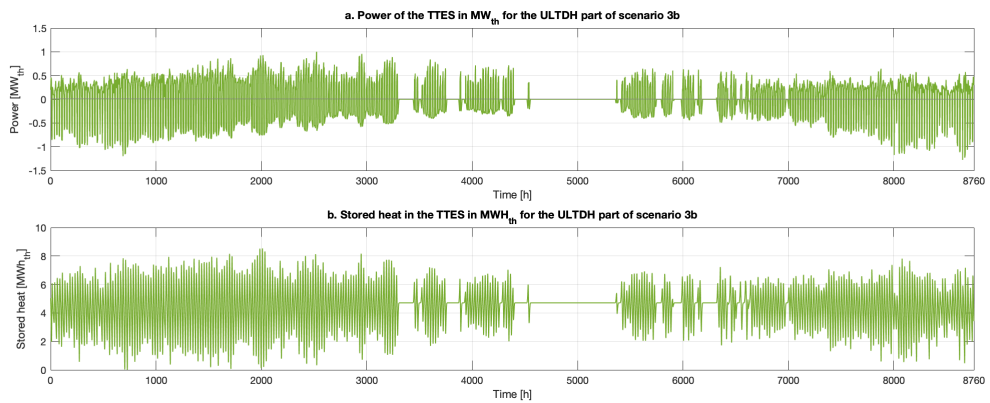

Figure B.8: Power (a) and storage capacity profile (b) of the buffer TTES for the ULTDH part of scenario 3b during one year

Figure B.9: Power (a) and storage capacity profile (b) of the ATES system for the ULTDH part of scenario 3b during one year

B.3.2. Scenario 3: MTDH part

Figure B.10: Power profile at the MT heat source for the MTDH part of scenario 3a (a) and scenario 3b (b) during one year

Figure B.11: Power (a) and storage capacity profile (b) of the buffer TTES for the MTDH part of scenario 3b during one year
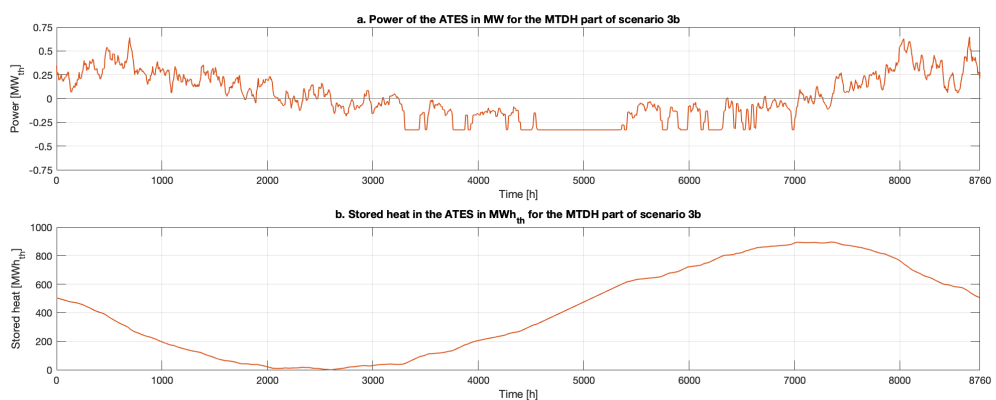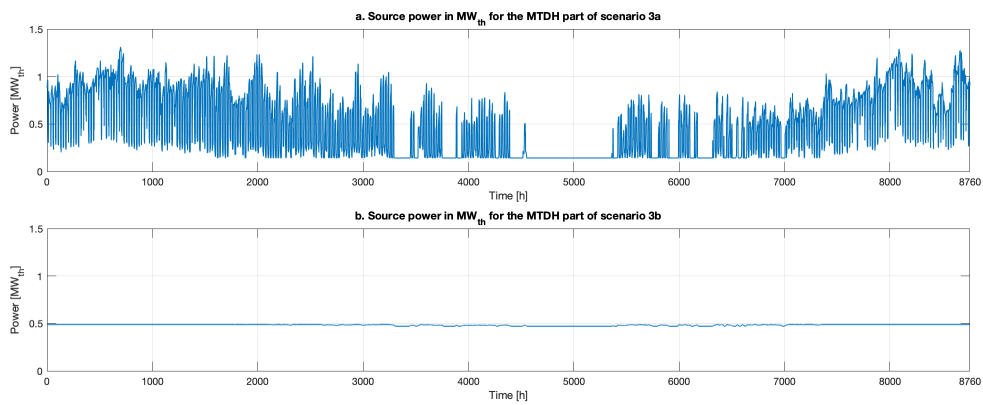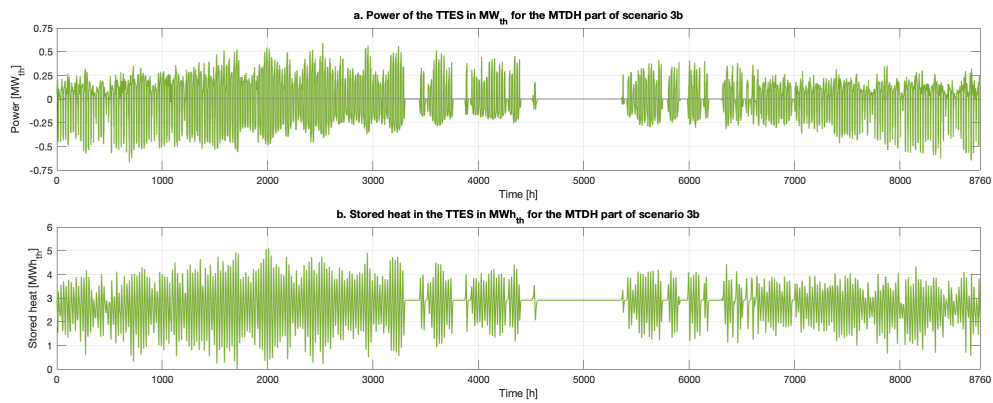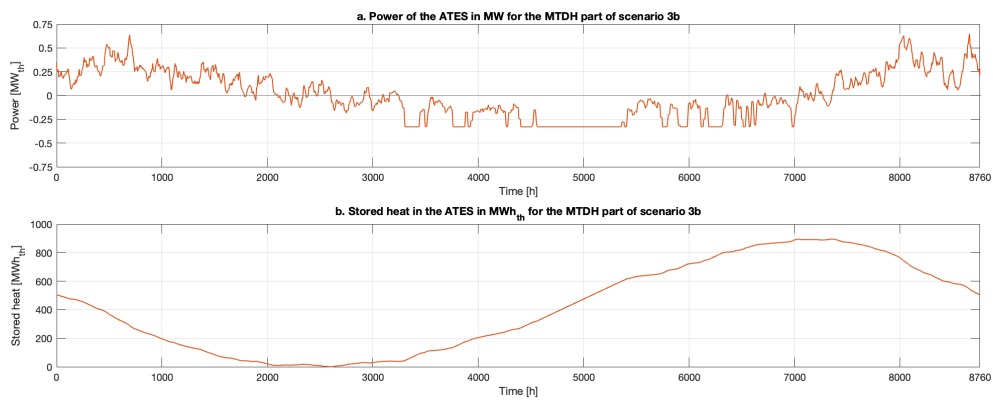

Figure B.12: Power (a) and storage capacity profile (b) of the ATES system for the MTDH part of scenario 3b during one year

C

Total expenses

This appendix presents the CAPEX and OPEX of all the components of the case study scenarios as well as its total values, obtained by the Simulink and Matlab model.

C.1. Scenario 1: MTDH

Table C.1: specific CAPEX, OPEX and lifetimes for scenario 1a

Component	Part	CAPEX [€]	OPEX [€/yr.]	Lifetime [yr.]
HTS	-	498,863 €	9,977 €	30
Circulation pump	-	12,817 €	2,295 €	15
Pipelines	-	3,795,374 €	75,907 €	30
Substations	-	486,270 €	14,588 €	30
Supply sets	Set + inhouse connections (per appartement)	2,890.344 €	57,807 €	15
	Set + inhouse connections (per detached home)	112,500 €	2,250 €	15
	Building connection	172,800 €	3,456 €	30
Water tanks	Individual DHW water tank	2,958,000 €	59,160 €	15
Heat consumption	Heat consumed at source	-	412,370 €	-
Total		10,927,124 €	637,814 €	

Table C.2: specific CAPEX, OPEX and lifetimes for scenario 1b

Component	Part	CAPEX [€]	OPEX [€/yr.]	Lifetime [yr.]
HTS	-	178,213 €	3,564 €	30
Circulation pump	-	12,817 €	2,295 €	15
ATES	-	2,049,257 €	115,255 €	30
Buffer TTES	-	262,471 €	6,562 €	30
Pipelines	-	3,795,374 €	75,907 €	30
Substations	-	486,270 €	14,588 €	30
Supply sets	Set + inhouse connections (per appartement)	2,890.344 €	57,807 €	15
	Set + inhouse connections (per detached home)	112,500 €	2,250 €	15
	Building connection	172,800 €	3,456 €	30
Water tanks	Individual DHW water tank	2,958,000 €	59,160 €	15
Heat consumption	Heat consumed at source	-	400,470 €	-
Total		12,918,202 €	741,317 €	

C.2. Scenario 2: ULTDH

Table C.3: CAPEX, OPEX and lifetime for scenario 2a

Component	Part	CAPEX [€]	OPEX [€/yr.]	Lifetime [yr.]
HTS	-	387,165 €	7,743 €	30
Circulation pump	-	15,448 €	3,727 €	15
Pipelines	-	3,525,867 €	70,517 €	30
Substations	-	380,430 €	7,609 €	30
Supply sets	Set + inhouse connections (per apartment)	2,890.344 €	57,807 €	15
	Set + inhouse connections (per detached home)	112,500 €	2,250 €	15
	Building connection	172,800 €	3,456 €	30
HPs	Water-to-water HP systems inc. boilers	4,478,197 €	539,275 €	15
Heat consumption	Heat consumed at source	-	304,073 €	-
Total		11,962,907 €	996,460 €	

Table C.4: CAPEX, OPEX and lifetime for scenario 2b

Component	Part	CAPEX [€]	OPEX [€/yr.]	Lifetime [yr.]
HTS	-	150,918 €	3,018 €	30
Circulation pump	-	15,448 €	3,727 €	15
ATES	-	1,629,481 €	56,015 €	30
Buffer TTES	-	482,042 €	12,051 €	30
Pipelines	-	3,525,867 €	70,517 €	30
Substations	-	380,430 €	7,609 €	30
Supply sets	Set + inhouse connections (per apartment)	2,890.344 €	57,807 €	15
	Set + inhouse connections (per detached home)	112,500 €	2,250 €	15
	Building connection	172,800 €	3,456 €	30
HPs	Water-to-water HP systems inc. boilers	4,478,197 €	539,275 €	15
Heat consumption	Heat consumed at source	-	316,880 €	-
Total		13,836,858 €	1,072,581 €	

C.3. Scenario 3: combined ULT- and MTDH

Table C.5: Specific CAPEX, OPEX and lifetimes for scenario 3a

Component	Part	CAPEX [€]	OPEX [€/yr.]	Lifetime [yr.]
HTS	-	440,735 €	8,815 €	30
Circulation pumps	-	19,412 €	4,715 €	15
Pipelines	-	4,400,002 €	88,000 €	30
Substations	-	425,782 €	8,514 €	30
Supply sets	Set + inhouse connections (per apartment)	2,890,344 €	57,807 €	15
	Set + inhouse connections (per detached home)	112,500 €	2,250 €	15
	Building connections	172,800 €	3,456 €	30
HPs	Water-to-water HP systems inc. boilers	3,428,838 €	340,313 €	15
Water tanks	Individual DHW water tank	645,000 €	12,900 €	15
Heat consumption	Heat consumed at source	-	361,498 €	-
Total		11,890,313 €	888,267 €	

Table C.6: Specific CAPEX, OPEX and lifetimes for scenario 3b

Component	Part	CAPEX [€]	OPEX [€/yr.]	Lifetime [yr.]
HTS	-	168,871 €	3,377 €	30
Circulation pump	-	19,412 €	4,715 €	15
ATES	-	1,820,527 €	79,114 €	30
Buffer TTES	-	428,503 €	10,713 €	30
Pipelines	-	4,400,002 €	88,000 €	30
Substations	-	425,782 €	8,514 €	30
Supply sets	Set + inhouse connections (per appartement)	2,890,344 €	57,807 €	15
	Set + inhouse connections (per detached home)	112,500 €	2,250 €	15
	Building connections	172,800 €	3,456 €	30
HPs	Water-to-water HP systems inc. boilers	3,428,838 €	340,313 €	15
Water tanks	Individual DHW water tank	645,000 €	12,900 €	15
Heat consumption	Heat consumed at source	-	368,498 €	-
Total		13,866,698 €	976,616 €	

C.4. Scenario 4: all-electric

Table C.7: Speficic CAPEX, OPEX and lifetimes for scenario 4

Component	Part	CAPEX [€]	OPEX [€/yr.]	Lifetime [yr.]
HPs	Air-to-water HP systems inc. boilers	14,261,504 €	356,538 €	15
	Electricity consumption	-	709,380 €	-
Total		14,261,504 €	1,065,918 €	

Bibliography

[1] Engineering Toolbox, 2001. URL https://www.engineeringtoolbox.com/.

[2] Ahmed, K., Pylsy, P., and Kurnitski, J. Hourly consumption profiles of domestic hot water for different occupant groups in dwellings. *Solar Energy*, 137:516–530, 2016. ISSN 0038092X. doi: 10.1016/j.solener. 2016.08.033.

[3] Arsene, C. T., Bargiela, A., and Al-Dabass, D. Modelling and simulation of water systems based on loop equations. *International Journal of Simulation: Systems, Science and Technology*, 5(1-2):61–72, 2004. ISSN 1473804X.

[4] Bakr, M., van Oostrom, N., and Sommer, W. Efficiency of and interference among multiple Aquifer Thermal Energy Storage systems; A Dutch case study. *Renewable Energy*, 60:53–62, 2013. ISSN 09601481. doi: 10.1016/j.renene.2013.04.004. URL http://dx.doi.org/10.1016/j.renene.2013.04.004.

[5] Bhave, P. R. *Analysis of Flow in Water Distribution Networks*. Taylor & Francis, 1991.

[6] Bloemendal, M. and Hartog, N. Analysis of the impact of storage conditions on the thermal recovery efficiency of low-temperature ATES systems. *Geothermics*, 71(October 2017):306–319, 2018. ISSN 03756505. doi: 10.1016/j.geothermics.2017.10.009. URL http://dx.doi.org/10.1016/j.geothermics.2017. 10.009.

[7] Boiler-info. HR ketel. URL https://www.boiler-info.nl/hr-ketel/.

[8] Bott, C., Dressel, I., and Bayer, P. State-of-technology review of water-based closed seasonal thermal energy storage systems. *Renewable and Sustainable Energy Reviews*, 113(June), 2019. ISSN 18790690. doi: 10.1016/j.rser.2019.06.048.

[9] Cabeza, L. F. *Thermal energy storage*, volume 3. Elsevier Ltd., 2012. ISBN 9780080878737. doi: 10.1016/ B978-0-08-087872-0.00307-3. URL http://dx.doi.org/10.1016/B978-0-08-087872-0.00307-3.

[10] Cabeza, L. F., Martorell, I., Miró, L., Fernández, A. I., and Barreneche, C. *Introduction to thermal energy storage (TES) systems*. Woodhead Publishing Limited, 2015. ISBN 9781782420965. doi: 10.1533/ 9781782420965.1. URL http://dx.doi.org/10.1533/9781782420965.1.

[11] CBS. Aardgas en elektriciteit, gemiddelde prijzen van eindverbruikers, 2021. URL https://opendata. cbs.nl/statline/#/CBS/nl/dataset/81309NED/line?ts=1615994888633&fromstatweb=true.

[12] CE Delft. Ketenemissies Warmtelevering - Directe en indirecte CO2-emissies van warmtetechnieken. 2016. URL www.ce.nl.

[13] CE Delft. Functioneel ontwerp Vesta MAIS 3.0. pages 1–127, 2017. URL https://www.pbl.nl/sites/ default/files/downloads/pbl-2017-functioneel-ontwerp-vesta-3.0_3196.pdf.

[14] CE Delft. overzicht aanpassingen Vesta MAIS. 2019. URL https://www.expertisecentrumwarmte. nl/themas/bibliotheek/1428415.aspx.

[15] CE Delft. Functioneel ontwerp Vesta MAIS 4.0. 2019. URL https://www.pbl.nl/sites/default/ files/downloads/pbl-2019-ce-delft-functioneel-ontwerp-vesta-4.0_4085.pdf.

[16] Colla, M., Ioannou, A., and Falcone, G. Critical review of competitiveness indicators for energy projects. *Renewable and Sustainable Energy Reviews*, 125(March), 2020. ISSN 18790690. doi: 10.1016/j.rser.2020. 109794.

[17] Colmenar-Santos, A., Borge-Díez, D., and Rosales-Asensio, E. *District heating and cooling networks in the European Union*. 2017. ISBN 9783319579528. doi: 10.1007/978-3-319-57952-8.

[18] Cruickshank, A. and Baldwin, C. *Sensible Thermal Energy Storage: Diurnal and Seasonal.* Elsevier Inc., 2016. ISBN 9780128034408. doi: 10.1016/B978-0-12-803440-8.00015-4. URL http://dx.doi.org/10.1016/B978-0-12-803440-8/00015-4.

[19] Cruickshank, C. A. and Harrison, S. J. Thermal response of a series- and parallel-connected solar energy storage to multi-day charge sequences. *Solar Energy*, 85(1):180–187, 2011. ISSN 0038092X. doi: 10.1016/j.solener.2010.09.010. URL http://dx.doi.org/10.1016/j.solener.2010.09.010.

[20] Dahash, A., Ochs, F., Janetti, M. B., and Streicher, W. Advances in seasonal thermal energy storage for solar district heating applications: A critical review on large-scale hot-water tank and pit thermal energy storage systems. *Applied Energy*, 239(February):296–315, 2019. ISSN 03062619. doi: 10.1016/j.apenergy.2019.01.189.

[21] EU Science Hub. Photovoltaic Geographical Information System (PVGIS). URL https://re.jrc.ec.europa.eu/pvg_tools/en.

[22] European Environment Agency. Greenhouse gas emission intensity of electricity generation, 2020. URL https://www.eea.europa.eu/data-and-maps/daviz/co2-emission-intensity-6#tab-googlechartid_googlechartid_chart_111_filters=%7B%22rowFilters%22%3A%7B%7D%3B%22columnFilters%22%3A%7B%22pre_config_date%22%3A%5B2018%5D%7D%3B%22sortFilter%22%3A%5B%22index_2018%22.

[23] Fleuchaus, P., Godschalk, B., Stober, I., and Blum, P. Worldwide application of aquifer thermal energy storage – A review. *Renewable and Sustainable Energy Reviews*, 94(July):861–876, 2018. ISSN 18790690. doi: 10.1016/j.rser.2018.06.057. URL https://doi.org/10.1016/j.rser.2018.06.057.

[24] Frerking, M. A. and Beauchamp, P. M. JPL technology readiness assessment guideline. *IEEE Aerospace Conference Proceedings*, 2016-June(May), 2016. ISSN 1095323X. doi: 10.1109/AERO.2016.7500924.

[25] Friedel, P., Jong, A., and Horstink, M. Energieprestaties van 5 warmtetechnieken bij woningen in de praktijk. page 92, 2014. URL https://www.rvo.nl/sites/default/files/Definitief_RapportPraktijkprestatiesvanwarmtetechniekenbijhuishoudens.pdf.

[26] Fröling. Energy tank with stratification baffles. URL https://woodboilers.com/tarm-biomass-wood-boilers-distributor-intelligently-engineered-wood-boiler-systems/tarm-biomass-products/thermal-storage-biomass-boiler-tanks/heat-storage-systems/.

[27] Guelpa, E. and Verda, V. Thermal energy storage in district heating and cooling systems: A review. *Applied Energy*, 252(June), 2019. ISSN 03062619. doi: 10.1016/j.apenergy.2019.113474.

[28] Hariri, A. S. and Ward, I. C. A review of thermal storage systems used in building applications. *Building and Environment*, 23(1):1–10, 1988. ISSN 03601323. doi: 10.1016/0360-1323(88)90011-X.

[29] Heat Pump Association UK. Types of Heat Pump. URL https://www.heatpumps.org.uk/consumers/heat-pump-technical-information/types-of-heat-pump/.

[30] HVC Energy B.V. Technische gegevens warmtelevering.

[31] HVC Energy B.V. Warmte etiket 2019. 2019.

[32] HVC Groep. Warmtenet Heerhugowaard. URL https://www.hvcgroep.nl/warmtenet-heerhugowaard.

[33] Infante Ferreira, C. Personal communication with C. Infante Ferreira on 23-03-2021.

[34] International Energy Agency. Energy efficiency indicators: Highlights. *Energy efficiency indicators*, 2019. doi: 10.1787/9789264268692-en.

[35] Kennisinstituut voor Installatietechniek. *ISSO-publicatie 7 Grondleidingen voor warmte- en koudetransport.* 2012. ISBN 9789050442329.

[36] KNMI. Uurgegevens van het weer in Nederland, . URL http://projects.knmi.nl/klimatologie/uurgegevens/selectie.cgi.

[37] KNMI. Daggegevens van het weer in Nederland, . URL `http://projects.knmi.nl/klimatologie/daggegevens/selectie.cgi`.

[38] Kodi Energie Besparende Technieken, ZON Energie Ontwikkelingsbedrijf, Gemeente Heerhugowaard, and Hogeschool Inholland. Het Waerdse Energie Circuit. URL `https://www.waerdse-energie.nl/#top`.

[39] Kuiper Compagnons. Stationsgebied Heerhugowaard. URL `https://www.kuipercompagnons.nl/nl/projecten/stationsgebied_heerhugowaard/`.

[40] Li, G. Sensible heat thermal storage energy and exergy performance evaluations. *Renewable and Sustainable Energy Reviews*, 53:897–923, 2016. ISSN 18790690. doi: 10.1016/j.rser.2015.09.006. URL `http://dx.doi.org/10.1016/j.rser.2015.09.006`.

[41] Liander. Kleinverbruiksdata per jaar. URL `https://www.liander.nl/partners/datadiensten/open-data/data`.

[42] Lund, H., Werner, S., Wiltshire, R., Svendsen, S., Thorsen, J. E., Hvelplund, F., and Mathiesen, B. V. 4th Generation District Heating (4GDH). Integrating smart thermal grids into future sustainable energy systems. *Energy*, 68:1–11, 2014. ISSN 03605442. doi: 10.1016/j.energy.2014.02.089. URL `http://dx.doi.org/10.1016/j.energy.2014.02.089`.

[43] Meteotest. Meteonorm. URL `https://meteonorm.com/en/`.

[44] Mills, A. F. *Basic Heat and Mass Transfer: Pearson New International Edition.* Pearson Education Limited, 2014. ISBN 1292042486, 9781292042480.

[45] Ministerie van Binnenlandse Zaken en Koninkrijksrelaties. Bouwbesluit Online 2012, 2020. URL `https://rijksoverheid.bouwbesluit.com/Inhoud/docs/wet/bb2012`.

[46] Moosavian, N. and Jaefarzadeh, M. R. International Journal of Engineering Hydraulic Analysis of Water Supply Networks Using a Modified Hardy Cross. 27(9):1331–1338, 2014.

[47] NASA. Technology Readiness Level Demistified, 2010. URL `https://www.nasa.gov/topics/aeronautics/features/trl_demystified.html`.

[48] Nielsen, B. Methods for Analyzing Pipe Networks. *Hydraulic Engineering*, 115(2):139–157, 1989.

[49] Nijssen, J. M. L. Stromings- of impulspompen. *Cost Engineering Process Industry: Handboek CE*, (april): 1–14, 2002. URL `https://www.dace.nl/kennisbank/17695282`.

[50] Nordell, B. Large-scale Utilisation of Renewable Energy Requires Energy Storage. *Int. Conf. for Renewable Energies and Sustainable Development (ICRESD_07)*, pages 21–24, 2007.

[51] Office of the Deputy Prime Minister. The Building Regulations 2006 L1B Conservation of fuel and power in existing buildings. *Changes*, (April):35, 2006. URL `www.thebuildingregs.com`.

[52] Pilkington Solar International GmbH. Survey of Thermal Storage for Parabolic Trough Power Plants Period of Performance: September 13, 1999ñJune 12, 2000: Survey of Thermal Storage for Parabolic Trough Power Plants Period of Performance. *Nrel*, (September):61, 2000. URL `http://www.nrel.gov/csp/troughnet/pdfs/27925.pdf`.

[53] Pinel, P., Cruickshank, C. A., Beausoleil-Morrison, I., and Wills, A. A review of available methods for seasonal storage of solar thermal energy in residential applications. *Renewable and Sustainable Energy Reviews*, 15(7):3341–3359, 2011. ISSN 13640321. doi: 10.1016/j.rser.2011.04.013. URL `http://dx.doi.org/10.1016/j.rser.2011.04.013`.

[54] Planbureau voor de Leefomgeving. Startanalyse aardgasvrije buurten. Technical report, 2020.

[55] Rijksdienst voor Ondernemend Nederland. Voorbeeldwoningen 2011 Bestaande bouw.

[56] Royal Haskoning DHV. Basis ontwerp warmtenet: Benedenbuurt Wageningen. Technical report, 2019.

[57] Sarbu, I., Mirza, M., and Crasmareanu, E. A review of modelling and optimisation techniques for district heating systems. *International Journal of Energy Research*, 43(13):6572–6598, 2019. ISSN 1099114X. doi: 10.1002/er.4600.

[58] Sommer, T., Sulzer, M., Wetter, M., Sotnikov, A., Mennel, S., and Stettler, C. The reservoir network: A new network topology for district heating and cooling. *Energy*, 199:117418, 2020. ISSN 03605442. doi: 10.1016/j.energy.2020.117418. URL https://doi.org/10.1016/j.energy.2020.117418.

[59] Sommer, W., Valstar, J., Leusbrock, I., Grotenhuis, T., and Rijnaarts, H. Optimization and spatial pattern of large-scale aquifer thermal energy storage. *Applied Energy*, 137:322–337, 2015. ISSN 03062619. doi: 10.1016/j.apenergy.2014.10.019. URL http://dx.doi.org/10.1016/j.apenergy.2014.10.019.

[60] Sørensen, P. A., Nielsen, J. E., Battisti, R., Schmidt, T., and Trier, D. Solar district heating guidelines: Collection of fact sheets. *Solar Distric Heating*, (August):152, 2012. URL http://solar-district-heating.eu/Portals/0/Factsheets/SDH-WP3-D31-D32_August2012.pdf.

[61] Streicher, W., Heinz, A., Bony, J., Citherlet, S., Cabeza, L., Schultz, J. M., and Furbo, S. 279 - Results of IEA SHC Task 32 : Subtask C : Phase Change Materials. *Eurosun 2008*, 2008.

[62] Talebi, B., Mirzaei, P. A., Bastani, A., and Haghighat, F. A review of district heating systems: Modeling and optimization. *Frontiers in Built Environment*, 2(October 2016):1–14, 2016. ISSN 22973362. doi: 10.3389/fbuil.2016.00022.

[63] The Institute of Plumbing. Plumbing Engineering Services Design Guide. 2002.

[64] The MathWorks Inc. MATLAB, 2020.

[65] Thermaflex. Flexalen Product Guide. (April), 2018.

[66] Thermaflex. Technical Data Sheet: Flexalen ® 600. Technical report, 2018.

[67] van Melle, T., Menkveld, M., Oude Lohuis, J., de Smidt, R., and Terlouw, W. De systeemkosten van warmte voor woningen, 2015.

[68] van Miltenburg, R. Integration of decentralized solar collectors in Dutch district heating grids (MSc thesis). 2016.

[69] Viessmann. VITOCAL Ontwerphandleiding water/water-warmtepompen. pages 1–204, 2019.

[70] Viessmann. VITOCAL Ontwerphandleiding lucht/water-warmtepompen. 2019.

[71] Viessmann. Prijslijst 2020 NL Decentrale energieoplossingen voor woningen. 2020.

[72] White, F. M. *Fluid Mechanics*. McGraw Hill, 7th edition, 2011.

[73] Zhang, Y. and Wang, R. Sorption thermal energy storage: Concept, process, applications and perspectives. *Energy Storage Materials*, 27(February):352–369, 2020. ISSN 24058297. doi: 10.1016/j.ensm.2020.02.024. URL https://doi.org/10.1016/j.ensm.2020.02.024.